A novel function of DPP9

in DNA damage repair via BRCA2 regulation

Dissertation
for the award of the degree
“Doctor rerum naturalium” (Dr. rer. nat.)
of the Georg-August-Universität Göttingen

within the doctoral program *Molecular Biology of Cells*
of the Georg-August University School of Science (GAUSS)

submitted by

Maria Silva-Garcia

from Astorga, Spain

Göttingen 2018

Members of the Thesis Committee

Dr. Ruth Geiss-Friedlander (1st reviewer)
Department of Molecular Biology
University Medical Center Göttingen

Prof. Dr. Ivo Feußner (2nd reviewer)
Department of Plant Biochemistry
Faculty of Biology. Georg-August-University, Göttingen

Prof. Dr. Henning Urlaub
Department of Bionalytical Mass Spectrometry
Max Planck Institute for Biophysical Chemistry

Further members of the Examination Board

Prof. Dr. Blanche Schwappach-Pignataro
Department of Molecular Biology
University Medical Center Göttingen

Prof. Dr. Matthias Dobbelstein
Institute of Molecular Oncology
University Medical Center Göttingen

Prof. Dr. Michael Thumm
Department of Cellular Biochemistry
University Medical Center Göttingen

Date of oral examination: 26th November 2018

Declaration

Herewith I declare that I prepared the Ph.D. dissertation ‘’A novel function of DPP9 in DNA damage repair via BRCA2 regulation” on my own and with no other sources and aids than quoted.

Göttingen, September 2018

Acknowledgments

I would like to thank all the people that have supported and motivated me during all these years.

First, I would like to thank my supervisor, Dr. Ruth Geiss-Friedlander for providing me with such an exciting project and the lab members, specially Ulrike Moller and my former lab colleague Dr. Daniela Justa-Schuch, who helped me during the first two years of my Ph.D. time. I would also like to thank all the collaborators who helped me during this work.

I would like to thank the members of my thesis committee, Prof. Dr. Ivo Feußner and Prof. Dr. Henning Urlaub for supervising me during my Ph.D. work and the further members of my examination board, Prof. Dr. Blanche Schwappach-Pignataro, Prof. Dr. Matthias Dobbelstein and Prof. Dr. Michael Tumm, for their time and support.

I would like to give a big thank you to Prof. Dr. Markus Bohnsack for his help as the head of the Ph.D. program of Molecular Biology of cells at the GGNB, as well as, to Prof. Dr. Blanche Schwappach-Pignataro for her help and support.

I am very grateful to my former and current colleagues in the Molecular Biology Department. I would like to thank Dr. Ahmed Warda for his strong support and help during this work, as well as to my friends Elena Álvarez and Fabiola Llavona for being such beautiful people in my life.

I am being blessed with a lovely family which strength made me reach so far. My brother, Dr. Javier Silva García, who besides from being the best influenced I could have had since I was a child, has been there for me every day of my life. My father, Antonio Silva Fernández, a man full of knowledge, who gives me all his support in life and during my studies. My grandparents, Amando García and María Martínez, hard workers, who have given me their love and their strength every day of my life. I have been blessed with the most beautiful and lovely aunts Paula García, Montse García, and Amparo García and my uncle Ángel Rodríguez, who take care of me and love me for all those years.

Last and the most important in my life, **Adelina García Martínez**, my mum, my best friend, and my reference in life. She raised me in love, knowledge and respect. She will always be the most special and loved person of my life. She made me a strong woman and taught me the most important thing in life, to love. Te quiero Mamá.

Table of Contents

List of Abbreviations

53BP1: p53 binding protein 1

aa: Amino acid

AK2: Adenilate Kinase 2

AP site: Apurinic/apyrimydinic sites

APE1: DNA-(apurinic or apyrimidinic site) lyase or AP endonuclease 1

ATM: Ataxia Telangiectasia-Mutated

ATR: Ataxia Telangiectasia and Rad3-related

BER: Base Excision Repair

BRCA1: Breast Cancer type 1 protein

BRCA2: Breast Cancer type 2 protein

CDK1: Cyclin Dependent Kinase 1

CDK2: Cyclin Dependent Kinase 2

Chk1: Checkpoint kinase 1

Chk2: Checkpoint kinase 2 or Serine/threonine-protein kinase Chk2

CHX: Cycloheximide

CK2: Casein kinase 2

CTD: C-terminal domain

CtIP: C-terminal binding protein 1 (CtBP1) interacting protein. DNA endonuclease RBBP8

DDR: DNA Damage Repair

DNA-PKcs: DNA-dependent protein kinase catalytic subunit

DPP4: Dipeptidyl peptidase 4

DPP8: Dipeptidyl peptidase 8

DPP9: Dipeptidyl peptidase 9

DSB: Double-Strand Break

DSS1: Deleted in split hand/split foot protein 1 or 26S proteasome complex subunit SEM1

EGF: Epidermal growth factor

ER: Estrogen receptor

ERCC1: DNA excision repair protein ERCC-1

EXO1: Exonuclease 1

FAP: Fibroblast activating protein

FDA: Food and Drug Association

FLNA: Filamin A

H: Hours

H2AX: variant of histone 2A

H4: Histone 4

HAUSP: Herpes-virus associated ubiquitin-specific protease

HERC2: E3 ubiquitin-protein ligase HERC2 or HECT domain and RCC1-like domain-containing protein 2

HR: Homologous Recombination

ICL: Interstrand crosslink

MDC1: Mediator of DNA damage checkpoint protein 1

Min: Minutes

MLH1: DNA mismatch repair protein Mlh1

MMC: Mitomycin C

MMR: Mismatch Repair

MSH3: DNA mismatch protein Msh3

MSH6: DNA mismatch protein Msh6

NER: Nucleotide Excision Repair

NHEJ: Non-Homologous End joining

NLS: Nuclear localization sequence

NPY: Neuropeptide Y

NSCLC: Non-small cell lung cancer

PALB2: Partner associated and localizer of BRCA2

PARP: Poly (ADP-ribose) polymerase 1

PCNA: Proliferating cell nuclear antigen

PCR: Polymerase chain reaction

PIKK: class-IV phosphoinositide 3-kinase (PI3K)-related kinase family

PIN1: Peptidylprolyl cis/trans isomerase

PLA: Proximity Ligation Assay

PMS2: Mismatch repair endonuclease PMS2

PN: Proteostasis network

PNKP: Polynucleotide kinase-3'-phosphate

Pol: Polymerase

PR: Progesterone Receptor

pRp: Deoxyribose phosphate residue

PTM: Post Translational Modifications

RAD50: DNA repair protein RAD50

RAD51: DNA repair protein RAD51, recombinase

RAP80: BRCA1-A complex subunit RAP80 or Receptor-associated protein 80

RNF168: E3 ubiquitin-protein ligase RNF168 or RING-type E3 ubiquitin transferase RNF168: E3 ubiquitin protein ligase RNF168 or RING finger protein 168

RNF8: E3 ubiquitin-protein ligase RNF8 or RING finger protein 8

RPA: Replication Protein A

SDS-PAGE: sodium dodecyl sulfate polyacrylamide gel electrophoresis

Sec: seconds

SPR: Surface Plamon Resonance

SSB: Single-Strand Break

SUBA: SUMO binding arm

SUMO: Small ubiquitin-like modifier

TLS: Translesion Polymerase System

TOPORS: E3 ubiquitin-protein ligase Topors or Topoisomerase I-binding arginine/serine-rich protein or E3 SUMO1 protein ligase.

UBA: Ubiquitin-like modifier-activating enzyme 1

UBC13: UBE2N Ubiquitin-conjugating enzyme E2 N

WB: Western Blot

XPA: DNA repair protein complementing XP-A cells

XPB: General transcription and DNA repair factor IIH helicase subunit XPB

XPF: DNA repair endonuclease XPF

XRCC1: X-ray repair cross-complementing protein 1

XRCC4: X-ray repair cross-complementing protein 4

Abstract

Eukaryotic cells are constantly exposed to exogenous and endogenous agents that induce mutational stresses in their genome, which can lead to genetic lesions, such as chromosome loss, translocations or deletions. The most harmful type of DNA damage is the double-strand breaks (DSBs). Efficient repair of DNA DSBs is an essential process for maintaining genome integrity and defects in the repair of such breaks are a major cause for tumorigenesis.

The dipeptidyl peptidase 9 (DPP9) protein has been associated in the last years with several cancers. Disruption of DPP9 basal levels is a common feature in tumor and inflamed cells, however, little is known about the role of DPP9 during cancer development. Here we present a new function of DPP9, which involves the enzymatic activity of DPP9 in the regulation of the DNA damage repair. Firstly, we found that DPP9 binds to chromatin and this increases upon DSBs induction. Moreover, the localization of DPP9 in the chromatin was found in close proximity to the DSBs sites where the repair machinery is recruited. In addition, we found that DPP9 senses DNA damage and deficiency of DPP9 in cells results in poor survival.

Here, we identified a new interacting partner of DPP9, the Breast Cancer type 2 protein (BRCA2), a key player in the repair of DSBs. We found DPP9 and BRCA2 are in close proximity and that this interaction increases after DNA damage induction. We also showed that the enzymatic activity of DPP9 regulates BRCA2 protein turnover, stabilizing the protein in cells lacking DPP9 activity. In addition, we applied microscopy analysis to follow the localization and the interactome of BRCA2, which was disrupted upon DPP9 silencing. Consequently, the function of BRCA2 was affected as seen in the lower loading of RAD51 to the ssDNA, which is an essential process to complete the repair.

Taken together, our results found a new role of DPP9 in DNA damage repair, by controlling the stability, localization and the interactome of BRCA2 protein. Moreover, we proved that defects in DPP9 can lead to deficient DNA damage repair and reduce cell survival, which open a possible explanation for the reported connection of DPP9 in cancer development.

1. Introduction

1.1. Overview of DNA damage and its cellular responses in eukaryotes

Eukaryotic cells are constantly exposed to exogenous and endogenous agents that threaten their genomes. Mutational stresses can lead to a wide variety of genetic lesions, such as chromosome loss, translocations or deletions, which may lead to cell death (reviewed in Gumeni *et al*., 2017). DNA lesions trigger a multitude of mechanistically-different responses that are collectively known as the DNA damage response (DDR), which recognizes, signals and repairs these damages (reviewed in Summers *et al*., 2011; Shiloh and Ziv, 2013). DDR processes are tightly controlled by numerous proteins that undergo through many post-translational modifications such as phosphorylation, ubiquitination, sumoylation, methylation or acetylation (reviewed in Gumeni *et al*., 2017). Key regulators of the DDR include the Ataxia-telangiectasia-mutated (ATM; Savitsky *et al*., 1995), Ataxia telangiectasia and Rad3-related (ATR; Cimprich *et al*., 1996) and DNA-dependent protein kinase catalytic subunit (DNA-PKcs; Blunt *et al*., 1995), which all belong to the class-IV phosphoinositide 3-kinase (PI3K)-related kinase (PIKK) family and are involved in cellular responses to various stresses (reviewed in Bakkenist and Kastan, 2004). ATM and ATR act upon different types of DNA lesions but mainly upon double-strand breaks (DSBs) and their responses are mediated by the phosphorylation of various targets including checkpoint kinase 2 (Chk2), partner and localizer of BRCA2 (PALB2), DNA repair protein RAD50, cellular tumor antigen p53 and meiotic recombination 11 protein (MRE11; reviewed in Shiloh and Ziv, 2013).

Depending on the type of DNA damage, cells have evolved different mechanisms to resolve such lesions. Among these, four general types of repair can be distinguished: the repair of single-strand breaks (SSB) or modifies bases by base excision repair (BER; reviewed in Moor *et al*., 2018), the repair of DNA mismatches by mismatch DNA repair (MMR; reviewed in Yamamoto and Imai., 2015), the repair of bulky lesions by nucleotide excision repair (NER; reviewed in Gillet and Schärer, 2006) and the repair of DSBs by either homologous recombination (HR) or by non-homologous end joining (NHEJ; reviewed in Chang *et al*., 2017).

1.1.1. Single-strand breaks and modified bases repair

Modified nitrogenous bases and apurinic/apyrimidinic sites are the most abundant types of DNA damage and, together with single-strand DNA breaks (SSBs), are resolved by a process known as base excision repair (BER; reviewed in Moor *et al*., 2018). Although BER responses can slightly differ depending on the type of damage, they share a similar mechanism: (1) recognition of the damage and excision of the base, (2) removal of the deoxyribose phosphatase residue, (3) synthesis of the correct nucleotide and (4) ligation of the DNA (Liu *et al*., 2005).

BER is a coordinated process that starts with the DNA glycosylase-mediated recognition and removal of damaged bases, leaving deoxyribose phosphatase residues (Figure 1A). Poly ADP-ribose polymerases (PARPs) scaffold the binding to endonucleases, such as DNA-(apurinic or apyrimidinic site) lyase (APE1) and polynucleotide kinase-3'-phosphate (PNKP), which cleave the deoxyribose phosphatase residue resulting in a SSB in the DNA (reviewed in Moor and Lavrik, 2018). Filling the gap is performed by polymerase (Pol) β, which in some cases requires the action of Pol δ and ε. Binding of these polymerases is stabilized by the scaffold protein x-ray cross-complementing protein 1 (XRCC1). Finally, DNA ligase III joins the ends of the DNA and resolves the damage (Liu *et al*., 2005, Lebedeva *et al*., 2005). Interestingly, post-translational modifications play a major role in the regulation of these processes, for example, XRCC1 is activated by phosphorylation via the action of two kinases casein kinase 2 (CK2) and Chk2, which are previously phosphorylated by ATM/ATR (Parson *et al*., 2010). Following its phosphorylation, XRCC1 is ubiquitinated by the carboxyl terminus Hsc70 interacting protein (CHIP) and degraded, explaining the low steady state levels of the protein (Parson *et al*., 2008). To avoid degradation, ubiquitination of XRCC1 can be suppressed by polyADP-ribosylation (also known as parylation) by PARP1 protein (Wei *et al*., 2013) and the subsequent sumoylation by a SUMO1-protein E3 ligase named TOPORS, which increases the binding of Pol β to the DNA nicks, thereby improving the efficiency of the repair (Hu *et al*., 2018).

1.1.2. DNA mismatches repair

DNA base mismatches and insertion-deletion loops are corrected by a highly conserved mechanism known as mismatch DNA repair (MMR). MMR plays a major role in the S phase, during DNA replication and meiosis in eukaryotes (Liu *et al*., 2017). Within the total genome there are specific sites defined as microsatellites that are more sensitive to present such damages. Microsatellites are short sequences that display tandemly-repeated nucleotides between which polymerases commonly slip and introduce errors (reviewed in

Yamamoto and Imai., 2015; Baretti and Le 2018). Despite the exonucleolytic proofreading function of several high-fidelity DNA polymerases, which allows correction of such errors and lowers the error rate from 10^{-4} to 10^{-7} per introduced nucleotide, these errors remain in many cases unrepaired, making the MMR system an essential tool for correcting those errors (reviewed in Kunkel and Erie, 2015). In eukaryotes, MMR starts with the recognition of the damage by the MutSα (MSH6-MSH2 in humans) or MutSβ (MSH3-MSH2 in humans) ATPase complexes (Bjornson *et al*., 2003; Figure 1B). These complexes then recruit the MutLα (MLH1-PMS2 in humans) complex, which introduces a cleavage site or a nick in the damaged DNA. After the nick formation, the newly-synthesized DNA is eliminated by exonuclease 1 (EXO1), forming a gap in the strand. Finally, Pol δ fills the gap and DNA ligase I ligates the DNA resolving the remaining nick (Liu *et al*., 2017). Mutations in *MLH1*, *MSH2*, *MSH6*, *PMS2* or *PMS1* genes are implicated in Lynch syndrome, an autosomal dominant disorder that presents a high risk of endometrial and colorectal cancers among others (reviewed in Baretti and Le, 2018).

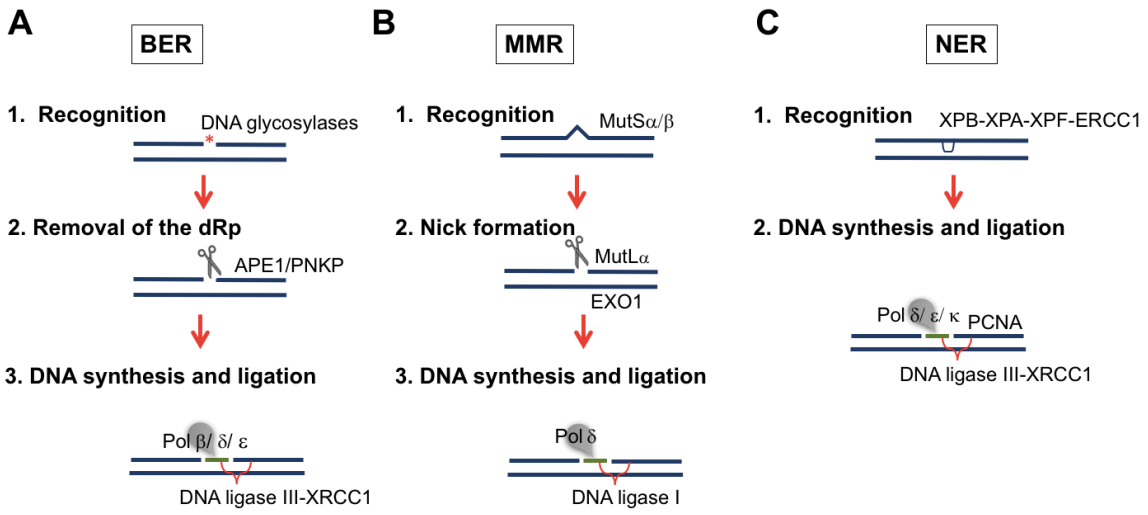

Figure 1. Types of DNA repair of single-strands of DNA.
(A) Base excision repair (BER) involves DNA glycosylases and endonucleases (APE1 and PNKP) for removal of the deoxyribose phosphatase residue (dRp). Synthesis is taken place by pol β, δ and ε. The ligation is done by DNA ligase III and the cofactor XRCC1 (reviewed in Moor *et al*., 2018).
(B) Repair of DNA mismatches by mismatch DNA Repair (MMR) involves two different complexes, first MutSα that recognize the damage and MutLα that performs the nick in the DNA. Final synthesis is done by pol δ and ligation by DNA ligase (reviewed in Yamamoto and Imai., 2015).
(C) Bulky lesions are repaired by nucleotide excision repair (NER). First, bulky lesions are recognized by XPB-XPA-XPF-ERCC1 following by the filling of the gap by pol δ, ε and pol κ and ligated by the DNA ligase III and XRCC1 cofactor (reviewed in Gillet and Schärer, 2006).

1.1.3. Bulky lesion crosslinks repair

Bulky lesion crosslinks include UV photoproducts and DNA adducts that are repaired by an accurate mechanism known as nucleotide excision repair (NER; reviewed in Gillet and Schärer, 2006).

NER is a non-mutagenic and versatile DNA repair system that involves the recognition of the lesion by a protein complex, containing XPB, XPA, XPF and the DNA excision repair protein ERCC-1 (ERCC1), followed by polymerases-mediated (Figure 1C), which is aided by cofactors such as proliferating cell nuclear antigen (PCNA; reviewed in Gillet and Shärer, 2006). It was previously thought that only Pol δ and Pol ε (high-fidelity B family DNA polymerases) are involved in NER (reviewed in Wood and Shivji 1997), however, Pol κ (an error prone family Y DNA polymerase) was recently shown to also increase the efficiency of NER in mice (Ogi and Lehmann, 2006) and in humans (Ogi e*t al*., 2010). Besides polymerases, which are regarded as the key regulators of NER, important players include PCNA, which upon its ubiquitination recruits the polymerases to the DNA damaged sites (Hoege *et al*., 2002). After their binding, the three polymerases fill the DNA gaps (around 30 nucleotides) and similar to BER it is finally resolved by XRCC1/ligase III complex (Parson e*t al*., 2010).

Alternatively, cells can undergo another type of repair, called translesion synthesis (TLS) to solve these lesions. However, in TLS a DNA lesion is bypassed by polymerases (majority from the polymerase Y family) introducing mutations in the genome. Some studies have defined TLS as DNA damage tolerance, instead of repair, since it promotes replication across damage sites (reviewed in Waters *et al*., 2009).

1.1.4. Double-Strand Breaks

Double-Strand Breaks (DSBs) represent the most harmful type of DNA damage. Mammalian cells are estimated to present around 10 DSBs per cell per day (reviewed in Lieber and Karanjawala, 2004). DSBs can be formed either by one single DSB in both strands simultaneously or by two SSBs form in an intermediate proximity. In both scenarios those lesions result in DSBs (reviewed in Ranjha *et al*.,2018). Inefficient repair can lead to mutations, loss of large chromosomal regions and genome instability. Cells presenting these anomalies in DDR are more sensitive to radiation and chemicals, which reduces their viability. To resolve DSBs, cells evolved two different mechanisms; non-homologous-end-joining (NHEJ) and homologous recombination repair (HR; reviewed in Chang *et al*., 2017) (Figure 2). Interestingly, these pathways are regulated by the cell cycle. HR is active in cells in late S phase or G2 phase, since it requires the duplicated DNA, whereas NHEJ is active

throughout the cell cycle with more activity in the phases G0, G1 and early S phase (Orthwein *et al*., 2015; Goldberg *et al*., 2003; reviewed in Shrivastav *et al*., 2007). To control the choice of repair, there is a complex network of cell cycle proteins and regulators, which activation or inactivation is regulated by post-translational modifications. In fact, DSBs repair starts with the activation of ATM and ATR, which phosphorylate the mediator of DNA damage Checkpoint1 (MDC1), promoting its binding to the DNA (Goldberg *et al*., 2003). MDC1 recruits the ubiquitin E3 ligase complex RNF8/HERC2/UB2N and the ubiquitin activating enzyme UBA1. These proteins induce the binding of an E3 ligase, RNF168, which ubiquitinates proteins such as histone 2AX (H2AX; Moudry *et al*., 2012). H2AX is a variant of H2A (reviewed in Fernandez-Capetillo *et al*., 2004) which is ubiquitinated in lysine 15 (H2AXK15) and then is phosphorylated by ATM and ATR kinases (γH2AX; Rogakou *et al*., 1998; reviewed in Turinetto and Giachino, 2015). H2AX together with the modified histone 4 (H4), H4k20diME (H4 lysine 20 dimethylation) are recognized by regulators of the DDR such as the p53 binding protein 1 (53BP1; Fradet-Turcotte *et al*., 2013).

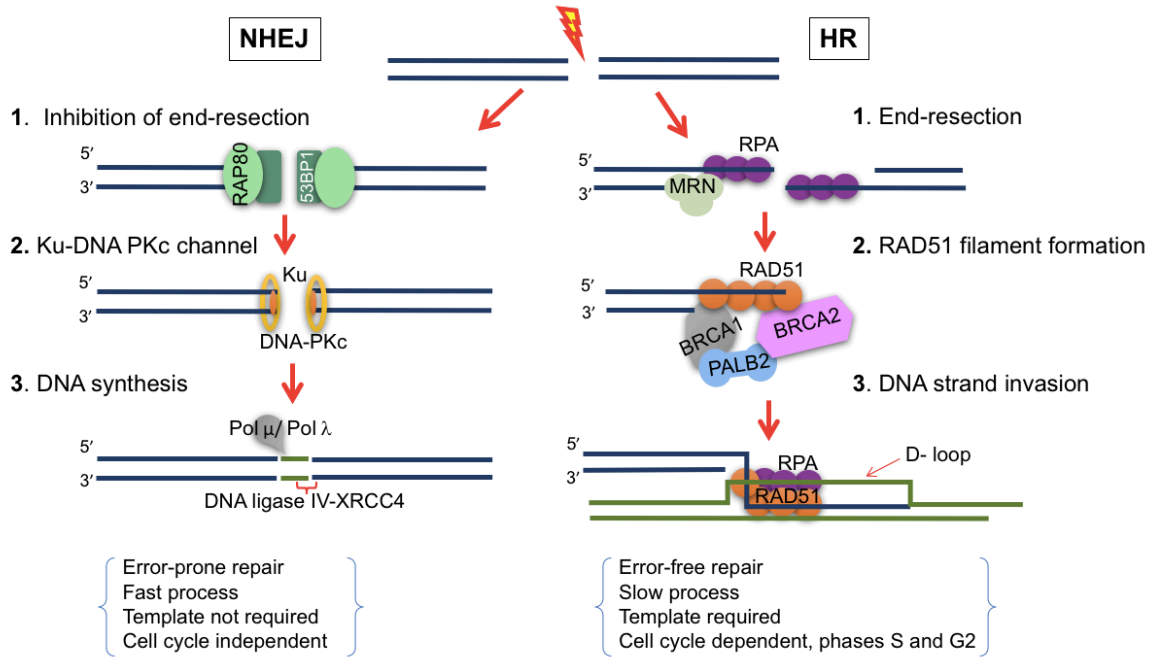

Figure 2. Two main pathways of DSBs repair. Left: NHEJ involves the action of RAP80 and 53BP1 which block end-resection and enables the recruitment of Ku-DNA PKc complex to form a channel. This is followed by the binding of polymerases capable of DNA, template-independent, synthesis and the DNA ligase IV which ligates the DNA. Right: HR repair involves the replication protein A (RPA; in purple) which mediates the protection of the ssDNA after end-resection and it is followed by the recruitment of BRCA1-PALB2-BRCA2 complex, which loads RAD51 (orange) into the ssDNA (in blue) forming filaments which are observed as foci by microscopy. RAD51 filaments allow the invasion into the homologous strand (in green), forming the D-loop. DNA synthesis is performed by polymerases which require of this homologous strand and then the repair is completed.

Before starting the repair of the DSB, cells have to choose between HR or NHEJ repairs. The pathway choice is controlled by proteins such as 53BP1 or RAP80, which inhibit end-

resection process (Figure 2). End-resection is the first step of HR repair and involves the cleavage of nucleotides in one strand of the DNA, thereby 53BP1 and RAP80 promote NHEJ repair (Bunting *et al*., 2010). The mechanism of action is regulated by post-translational modifications, where RAP80 preserves the poly-ubiquitin chains of 53BP1, which are necessary for its binding to chromatin. The binding of RAP80 to the chromatin is in itself dependent on its sumoylation by PIAS1 and PIAS4 (Lombardi *et al*., 2017) and ubiquitination by RNF8 and RNF168 (Wang and Elledge, 2007). Localization assays showed that, during HR, both 53BP1 and RAP80 are re-localized from the core of the DSB site into the periphery of the lesion, allowing the proteins involved in HR to bind the damaged sites, emphasising that removal of these proteins from the DSBs is required for HR repair (Kakarougkas *et al*., 2013).

1.1.5. NHEJ

NHEJ repair is an error prone mechanism, nonetheless, this process is more frequent than HR since it is cell cycle independent (Bunting *et al*., 2010; reviewed in Chang *et al*., 2017). NHEJ starts with the recognition of the DSB by the Ku70/80 (Ku) complex, which binds to the DNA-ends of the DSB with high affinity (Ramsden and Gellert, 1998). The binding of Ku promotes the recruitment of DNA-protein kinase catalytic subunit (DNA-PKcs), a member of the PIKK family, forming the DNA-PK complex, which acts as a channel that encloses and protects the DNA from degradation (Weterings and Chen, 2007). Once DNA-PKcs is bound to the DSBs sites, it is autophosphorylated, promoting its disassociation from the damaged sites as well as the phosphorylation of replication protein A (RPA), H2AX or the endonuclease Artemis, which signal for recruitment of the repair machinery (reviewed in Summers *et al*., 2011). Afterwards, Pol μ and Pol λ (members of the polymerase X family) bind the Ku complex by the BRCT domain in their N-terminal ends, mediating DNA repair (Moon *et al*., 2014: Bebenek *et al.,* 2014). Pol μ and Pol λ do not require a template for DNA synthesis, increasing the error rate. Finally, DNA-ends are ligated by the DNA ligase IV in the presence of the cofactor XRCC4 (Chang *et al*., 2016). In some cases, NHEJ undergoes a small end-resection in the 5' or 3' overhangs of around 4 nucleotides called microhomology. This process requires the use of nucleases such as Artemis, MRN complex or the C-terminal binding protein 1 interacting protein (CtIP) among others (reviewed in Ranjha *et al*., 2018). Recently, an alternative similar pathway to NHEJ has been proposed, called alternative-end joining pathway (a-EJ), which differs from NHEJ in the end-resection process. Whereas NHEJ involves only few nucleotides (< 4), in a-EJ the microhomology formation ranges from 2-20 nucleotides and it requires the function of Pol θ (Chang *et al*., 2016).

1.1.6. Homologous Recombination repair

HR utilizes homologous sequences in the genome for the repair of the break, thereby providing an error-free mechanism of DNA repair. Since HR requires the presence of a homologous DNA, cells need to be in their late S phase or G2 phase of the cell cycle (Orthwein *et al*., 2015). Generally, HR starts the end-resection of the DNA, which consists of degradation of the 5' ends leaving 3' ssDNA tails coated with RPA protein. This is followed by the formation of RAD51 nucleoprotein filaments, DNA strand invasion and, finally, DNA synthesis (reviewed in Shrivastav *et al*., 2007; Ranjha *et al*., 2018).

1.1.6.1. End-resection

Nucleases bind to the DNA breaks and cleave the 5' ends, consequently leaving 3' ssDNA tails or also known as overhangs. End-resection can be divided into the short-range end-resection (start of the cleavage) and the long-range end-resection (extension of nucleotides cleavage; reviewed in Ranjha *et al*., 2018). Short-range end-resection involves the MRN (MRE11-RAD50-NBS) complex, where the endonuclease and exonuclease activities reside in MRE11 protein and energy is provided by RAD50, which has ATPase activity (Cannavo and Cejka, 2014; Mimitou and Symington, 2010; Zhu *et a*l., 2008; reviewed in Ranjha *et a*l., 2018). Additionally, the MRN complex also requires the presence of a cofactor, CtIP, which is previously activated in a cyclin-dependent kinase (CDK) manner (Cannavo and Cejka 2014; Huertas *et al*., 2008). Long-range end-resection involves different exonucleases, EXO1 or DNA2 (Gravel *et al*., 2008), which catalyse DNA cleavage in the 5' → 3' direction, forming extended ssDNA overhangs (reviewed in Ranjha *et al*., 2018). Consistently, EXO1 has been recently shown to be negatively regulated by DNA helicase B (HELB) to promote NHEJ repair during G1 phase cells (Tkáč *et al*., 2016). Upon resection, RPA, which contains three subunits, RPA1-RPA2-RPA3, coats and protects the exposed ssDNA (Zhao *et al*., 2015). The kinases ATM and ATR phosphorylate downstream regulators that are needed for the final binding of the recombinase RAD51, which is involved in the strand invasion step (reviewed in Ranjha *et al*., 2018).

1.1.6.2. RAD51 nucleation

The displacement of RPA allows RAD51 to bind to the ssDNA, forming a filament known as the presynaptic filament. This process is mainly mediated by Breast Cancer type 2 protein (BRCA2), which binds RAD51 via its eight BCR repeats and an additional region in its C-terminal end (Figure 3; reviewed in San Filippo *et al*., 2008). BRCA2 promotes binding of RAD51 to ssDNA overhangs by inhibiting RAD51 binding to the dsDNA and its ATPase activity (Jensen *et al*., 2010). Additionally, the displacement of RPA by BRCA2 is facilitated by the direct binding partner of BRCA2, DSS1, a small multifunctional and conserved eukaryotic protein (Zhao *et al.*, 2015; Kragelund *et al*., 2016).

The recruitment of BRCA2 to the DSBs sites requires of the Partner Localizer of BRCA2, also known as PALB2 and of BRCA1 protein. BRCA1 is the first protein to bind the ssDNA, followed by PALB2-BRCA2 (Xia *et al*., 2006). Similar to BRCA2, additional proteins termed as RAD51 paralogs have been described to facilitate RAD51 binding and RPA displacement, however, unlike RAD51, they do not present own DNA strand exchange activity (see section 1.2.2.; Sigurdsson, 2001).

1.1.6.3. DNA homology search

The exact mechanism by which the homologous DNA is recognized by the presynaptic filament remains unknown. However, it has been suggested that it occurs randomly through trying multiple and temporary contact sites with different DNA duplexes (reviewed in Renkawitz *et al*., 2014). Upon DNA recognition, RPA is suggested to re-bind to the ssDNA to stabilize the newly formed displacement-loop or D-loop structure (Figure 2), which involves the separation of the two strands and the invasion into the homologous DNA (Eggler *et al*., 2002). Interestingly, it was recently shown that the E3 ligase RFWD3 is involved in the removal of RPA and RAD51 from the ssDNA and that RPA and RAD51 simultaneously bind to the ssDNA (Feeney *et al*., 2017; Inano *et al*., 2017). The binding of RPA and RAD51 to the ssDNA overhangs has raised some controversy in the field, regarding the precise order of events. Some studies argue that both proteins bind sequentially, which fits with the end-resection process where RPA is suggested to bind first and RAD51 substitutes it to form the presynaptic filament. Other studies have found both proteins are binding at the same time to the ssDNA, which could be explained by the last step of HR, which involves the D-loop formation (Feeney *et al*., 2017; Inano *et al*., 2017).

Finally, the DNA synthesis involves various polymerases; Pol δ, η, κ or Pol ε. Although the exact roles of these polymerases are unknown, it has been hypothesized that Pol η, which is recruited with the help of PALB2 and BRCA2, initiates a short DNA

extension that is subsequently followed by Pol δ for a longer synthesis of the DNA (Buisson *et al*., 2014). These polymerases also require helicases to maintain the D-loop and topoisomerases to maintain DNA integrity (reviewed in Ranjha *et al*., 2018).

Defects in proteins involved in DSBs repair may lead to chromosome instability, which is a leading cause for multiple types of cancer. One example is BRCA2, which has emerged as one of the main targets for cancer treatment.

1.2. BRCA2

The human *BRCA2* encodes a large 384 kDa protein, which primarily functions in controlling the genome integrity by facilitating HR upon DNA damage. Besides recruiting RAD51 to the DNA damaged sites in HR (Yang *et al*., 2002; Zhao *et al*., 2015), BRCA2 plays other roles, such as inhibiting NHEJ (Han *et al*., 2017), regulating RAD51 activation by Plk1 (Yata *et al*., 2012), maintaining telomere stability (Zimmer *et al*., 2016) or stimulating Pol η together with PALB2 to start DNA synthesis after the D-loop formation (Buisson *et al*., 2014). Moreover, BRCA2 has also been implicated in regulating transcriptional activation (Shin and Verma, 2003; Rajagopalan *et al*., 2010) and controlling mitosis (Couch *et al*., 2012).

BRCA2 is also involved in the Fanconi Anemia (FA) pathway (Gallmeier and Ken, 2007; Knies *et al*., 2017; Nalepa and Clapp, 2018). The FA pathway coordinates the mechanism by which cells resolves DNA interstrand cross-links (ICL). The pathway includes the initial binding of the FA complex to the ICL, creating a DSB, followed by resolving the DSB via the classical HR pathway, which involves BRCA2 (Gallmeier and Ken, 2007; Nalepa and Clapp, 2018).

FA is a rare and genetic disorder that occurs when any of the 21 known FA genes present biallelic mutations. Those genes are named with the prefix *FANC,* in the case of *BRCA2* is also named as *FANCD1*. Failure in FA genes causes progressive bone marrow failure, developmental abnormalities and cancer predisposition (Gallmeier and Ken, 2007; Knies *et al*., 2017; Nalepa and Clapp, 2018).

1.2.1. The roles of BRCA2 in transcription activation and mitosis

The third exon of *BRCA2* encodes a transcription activating domain, which is suggested to target different proteins, including transcription factors. For example cells depleted of exon 3 of *BRCA2*, corresponding to amino acids (aa) from 23 to 105, or cells deficient in BRCA2 protein display impaired transcription of the androgen receptor (Shin and Verma, 2003). This domain of BRCA2 was also described to bind the oncogene EMSY, which has been suggested to regulate BRCA2 transcriptional function and it is amplified in multiple types of cancer (Figure 3; Hughes-Davies *et al*., 2003). However, no clear relation of EMSY and the functions of BRCA2 in HR has been reported (Jelinic *et al*., 2017). Moreover, BRCA2 binds p53, a key tumor suppressor that regulates the transcription of multiple target genes with various biological functions. Interestingly, overexpression of BRCA2 was shown to inhibit the transcriptional activity of p53, thereby reducing the expression of its target genes p21 and Bax (Rajagopalan *et al*., 2010).

In mitosis, BRCA2 is recruited to the mid-body by Filamin A (FLNA) protein and acts as a scaffold to recruit proteins involved in the cytokinesis process (Couch *et al.*, 2012). However, the exact role of BRCA2 during cell division remains to be investigated.

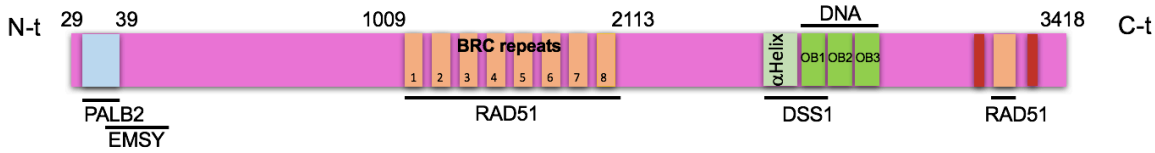

Figure 3. Domain organization of BRCA2 and its interaction partners.
BRCA2 protein is formed by 3418 amino acids (aa). The N-terminal region binds to PALB2 (indicated in light blue; Xia *et al*., 2006; Oliver *et al*., 2009 corrected in 2017) and EMSY (Hughes-Davies *et al*., 2003). Eight central BRC repeats (indicated in orange) are responsible for binding RAD51 (Chen *et al*., 1999). The C-terminal domain (CTD) presents a helical domain and the three DNA binding domains OB1, OB2 and OB3 (indicated in light and dark green). Binding of BRCA2 to DSS1 occurs through the helical domain and the adjacent OB1 domain (Jensen *et al*., 2010). In the CTD, there are two NLS (indicated in red) that are separated by a region (indicated in orange) where RAD51 is known to bind, besides the BRC repeats.

1.2.2. Mechanism of BRCA2 function in HR

The main function of BRCA2 during HR is to load RAD51 protein into the ssDNA tails. For that BRCA2 needs to be recruited to DSBs, a step that requires the prior formation of a complex with its interaction partner PALB2 (Xia *et al.*, 2006). PALB2 and BRCA2 interacts via a highly conserved motif in the N-terminus of BRCA2 (aa 21-39) and a WD40-repeat domain at the C-terminus of PALB2 (Figure 3; Oliver *et al*., 2009 corrected in 2017).

The BRCA2-PALB2 complex is recruited to the DSBs sites by BRCA1, which acts upstream to PALB2, and through PALB2, recruits BRCA2 to the DSBs sites (Zhang *et al.*, 2009).

The interaction between PALB2 and BRCA1 is mediated by hydrophobic bonds between two coiled-coil motifs at the N-terminus of PALB2 (aa 9-42) and in BRCA1 (aa 1393-1424; Zhang *et al.*, 2009). The interaction of PALB2-BRCA1 has been shown to compete with the formation of a PALB2-PALB2 dimer, which inactivates the function of PALB2 in HR (Buisson and Masson, 2012). Upon DSBs, PALB2 is phosphorylated in an ATM/ATR dependent manner on three residues at its N-terminal end, which promotes RAD51 filament formation and maintains genome stability (Ahlskog *et al.*, 2016).

PALB2 has been reported to bind D-loop regions of DNA with a higher efficiency than ssDNA. PALB2, similar to BRCA2, binds RAD51 (Buisson *et al*., 2010) and it has been shown to be able to load RAD51 into ssDNA *in vitro*, without the requirement of BRCA2. However, in cells, the loading of RAD51 requires the prior removal of RPA, which is

controlled by the activity of the BRCA2-DSS1 complex. Therefore, BRCA2 deficient cells have lower RAD51 filament formation, compared to WT cells (Buisson *et al*., 2010).

The binding of BRCA2 to DSS1 enables the exchange of RPA with RAD51 in the ssDNA (Jensen *et al*., 2010). First, DSS1 directly interacts with RPA, attenuating the ssDNA binding affinity of RPA, which facilitates the loading of RAD51 by BRCA2 (Zhao *et al*., 2015). Besides the BRCA2-DSS1 complex, additional factors may be involved in the removal of RPA from the ssDNA since. For example, the inactivation of BRCA2 was shown to cause premature removal of RPA2, a subunit of RPA, leading to activation of the NHEJ repair (Han *et al*., 2017).

1.2.3. BRCA2 in cancer

Mutations in *BRCA2* have been reported to be a common feature of several cancers. For example, around 5 to 10% of in familiar breast cancer cases follow mendelian inheritance patterns and up to 30% of these cases carry mutations in *BRCA1* or *BRCA2* genes (Economopoulou *et al*., 2014). In addition, sporadic breast cancer, which is caused by somatic mutations, can also involve mutations in *BRCA2*. Importantly, one of the most aggressive breast cancer types is the triple negative breast cancer, in which the cause is not due to any the following proteins, estrogen receptor (ER), progesterone receptor (PR) or HER2 protein but to mutations in other proteins, such as BRCA2 (Telli *et al*., 2018). Treatment of triple negative breast cancer involves the use of chemotherapy and radiotherapy as well as new treatments using PARP inhibitors. Interestingly, *BRCA2*-mutated cancer cells are hypersensitive to reduction of PARP activity which has been shown to function in multiple DNA repair pathways, including SSBs repair. Such synthetic lethality allowed PARP inhibitors to emerge as potential treatments for BRCA2-mutated cancers by causing their programmed cell death, apoptosis (Makvandi *et al*., 2016). In line with this, the PARP1 inhibitor, olaparib, has been recently approved by the Food and Drug Association (FDA) for the treatment of *BRCA2*-mutated ovarian and breast cancers.

Together, this highlights the complexity of regulation of DNA repair in cells, which requires a tight control of expression, localization and stability of the involved factors. Therefore, cells have developed several mechanisms to ensure the proper regulation of the process for example, by maintaining the integrity of the entire set of proteins or proteome.

1.3. The proteostasis network

Generally, homeostasis of the proteome is critical for cellular function. An elaborate mechanism that is generally referred to as the proteostasis network (PN) ensures the integrity of the proteome and involves processes such as protein synthesis, folding or degradation (reviewed in Gumeni *et al*., 2017). The degradation of proteins is managed by two main mechanisms, the autophagy-lysosome and the Ubiquitin Proteasome System (UPS; reviewed in Gumeni *et al*., 2017; Mofers *et al*., 2017). Key players of all of these processes are the proteases, which, upon cleavage of the different substrates, regulate several functions in the cell.

1.3.1. The Ubiquitin Proteasome System

The ubiquitin proteasome system (UPS) is a highly regulated mechanism that is crucial for proper cell function. The system consists of two main steps, ubiquitination of the targeted substrates, followed by degradation of the substrates by the proteasome (reviewed in Mofers *et al*., 2017; Gumeni *et al*., 2017).

Ubiquitin is a highly conserved 76 amino acid protein that can form chains (poly-ubiquitin chains) via 7 internal lysine residues that allow the formation of isopeptide bonds with other ubiquitin molecules. Additionally, ubiquitin can also form chains by conjugation of the first methionine of one molecule to the last glycine in the C-terminal end of another ubiquitin molecule (Kee and Huang, 2016). The conjugation of ubiquitin into the substrates requires the action of 3 enzymes, E1 (ubiquitin activating enzyme), E2 (ubiquitin conjugating) and E3 (ubiquitin ligase) (reviewed in Mofers *et al*., 2017; Gumeni *et al*., 2017; Gilberto and Peter, 2017). E1 forms a high-energy thioester bond with ubiquitin in an ATP-dependent manner. The activated ubiquitin is then transferred to E2, which recruits a compatible E3 ligase. The E3 ubiquitin ligase selectively binds to the protein substrates targeted for degradation and catalyzes the transfer of the poly-ubiquitin chains (reviewed in Gilberto and Peter, 2017; Mofers *et al*., 2017).

E3 ligases are classified into three classes known as: Really Interesting New Gene (RING)-type E3 ligases, homologous to the E6AP carboxyl terminus (HECT)-type E3 and RING-in-between-RNG (RBR) E3 ligases. RING-type E3 directly promotes the transfer of ubiquitin to the substrate, whereas, HECT-type and RBR-type require of an intermediate, a covalent E3-ubiquitin conjugate, to transfer the ubiquitin to the substrate (reviewed in Dove and Klevit, 2017; Gilberto and Peter, 2017). Ubiquitination is a reversible process as the ligated ubiquitin can be cleaved by deubiquitinases (DUBs), which are a type of cysteine proteases that can influence different cellular pathways, including the DDR (reviewed in Lopez-Otín and Matrisian, 2007; Kee and Huang, 2016).

After their poly-ubiquitination, the ubiquitin-tagged protein substrates can be specifically recognized by the proteasome. The proteasome is a cylindrical complex formed of three subunits, two regulatory subunits known as 19S subunit and the core 20S subunit. Recognition takes places in the 19S subunit of the proteasome, which is also responsible for the removal and recycling of the ubiquitin chains by the action of a DUB known as POH1. Interestingly, POH1 has been associated with DDR as it antagonizes the action of RNF8, an E3 ligase required for NHEJ, thereby promoting HR repair (Kee and Huang, 2016; reviewed in Mofers *et al*., 2017). Finally, protein degradation takes place in the 20S subunit of the proteasome, which consists of two heptameric α subunits placed over two heptameric β subunits, forming the proteolytic chamber (reviewed in Mofers *et al*., 2017).

1.3.2. The N-end rule pathway

The N-end rule pathway attributes the half-life of a protein to the identity of the residues in the N-terminal end (reviewed in Varshavsky, 1997). The degradation signals in a protein, also known as degrons, define the stability of a protein. The first characterized degron was found in the N-terminal end of a protein (Bachmair *et al*., 1986) and, therefore, it was named as N-degron (Varshavsky, 1991). The residues in the N-terminal end of a protein have been classified in different orders depending on their stability, and they are arranged in the known N-end rule pathway (reviewed in Varshavsky, 1997). In eukaryotes, the N-degron requires of two important residues, a destabilizing residue that is recognized by an E3 ligase and an internal lysine that gets poly-ubiquitinated by the E3 ligase that has bound previously. The E3 ligases that are capable to recognize N-degrons are called N-recognins (reviewed in Varshavsky, 2011). Residues can be grouped depending on their stabilization degree into primary, secondary or tertiary. Primary residues such as lysine, arginine, histidine, leucine, phenylalanine, tyrosine, isoleucine and tryptophan are highly destabilizing and they can be directly recognized by an E3 ligase. In contrast, secondary and tertiary residues require a preliminary modification for their recognition (reviewed in Varshavsky, 2011).

The N-end rule pathway consists of two branches, the Acetyl/N-end rule (Ac/N-end rule) and the Arginine/N-end rule (Arg/N-end rule). The Ac/N-end rule involves the co-translational acetylation of residues (either methionine or alanine, valine, serine, threonine or cysteine) on the N-terminus of nascent proteins. On the other hand, the Arg/N-end rule N-degrons are directly recognized by E3 ligases (arginine (Arg), lysine (Lys), histidine (His), leucine (Leu), phenylalanine (Phe), tyrosine (Tyr), tryptophan (Trp), isoleucine (Ile)) or after the modification by Arg-transferases, which add Arg residues into the amino acids (aspartate, glutamate, asparagine, glutamine or cysteine; reviewed in Varshavsky, 2011;

Lucas and Ciulli, 2016; Park *et al*., 2015). A novel N-end rule pathway that involves proteins containing proline in the end has been recently proposed. Chen and colleagues suggested that the proline in the N-terminus is recognized for protein degradation, despite that prolines are considered to be stabilizing residues (Chen *et al*., 2017). This is the first time to introduce prolines as possible destabilizing residues, however, this study did not test the stability of such proteins in the absence of the Met-Pro. This could imply the presence of other proteases that cleave the Met-Pro before the recognition of the N-degron by an E3 ligase, and expose the third amino acid in the protein.

1.3.3. Proteases

Proteases are enzymes which mainly cleave peptide bonds in the targeted substrates leading to changes in their function (reviewed in López-Otín and Matrisian, 2007). Early discoveries in the proteases field defined proteases as destructive enzymes that catalyze the degradation of their protein substrates in order to generate amino acids. However, this concept started to change in 1976 when proteases were described as enzymes that cleave zymogens or also known as inactive protein precursors, to produce new active protein products (Neurath and Walsh, 1976; reviewed in López-Otín and Bond, 2008).

1.3.3.1. Classes of proteases

Proteases can hydrolyze different types of bonds in their target substrates in a specific manner leading to changes in their function. Such protein modifications consequently lead to cellular changes, influencing cell behavior and survival (Rawlings *et al*., 2017; reviewed in Lopez-Otín and Matrisian, 2007). Despite most proteolytic enzymes cleave peptide bonds, some proteases display slight differences in the cleavage reaction. Examples include DUBs, which cleave isopeptide bonds and γ–glutamyl hydrolases and glutamate carboxypeptidases, which target γ –glutamyl bonds (reviewed in López-Otín and Bond, 2008). Early classifications divided the proteases into two major groups: the endopeptidases, which cleave internal peptide bonds, and the exopeptidases, which cleave at the N-terminal or C-terminal ends of their protein substrate. New classifications have emerged dividing the proteolytic enzymes into five classes according to the mechanism of cleavage, which are metalloproteases, aspartic, cysteine, serine and threonine proteases. Whereas the first two classes receive the electron necessary for the hydrolysis from active water molecules, the other three classes have their own nucleophiles within the amino acids of their active site (Figure 4; reviewed in López-Otín and Bond, 2008). Alternatively, proteases can be classified based on their cellular localization into extracellular and

intracellular proteases. Examples for extracellular proteases include the Matrix Metalloproteinases (MMP), ADAMTs family, cathepsins or two members of the DPP4 family, DPPIV and FAP. As intracellular proteases, some include caspases, DUBs, autophagins, and the other two members from the DPP4 family, DPP8 and DPP9 (reviewed in López-Otín and Matrisian, 2007).

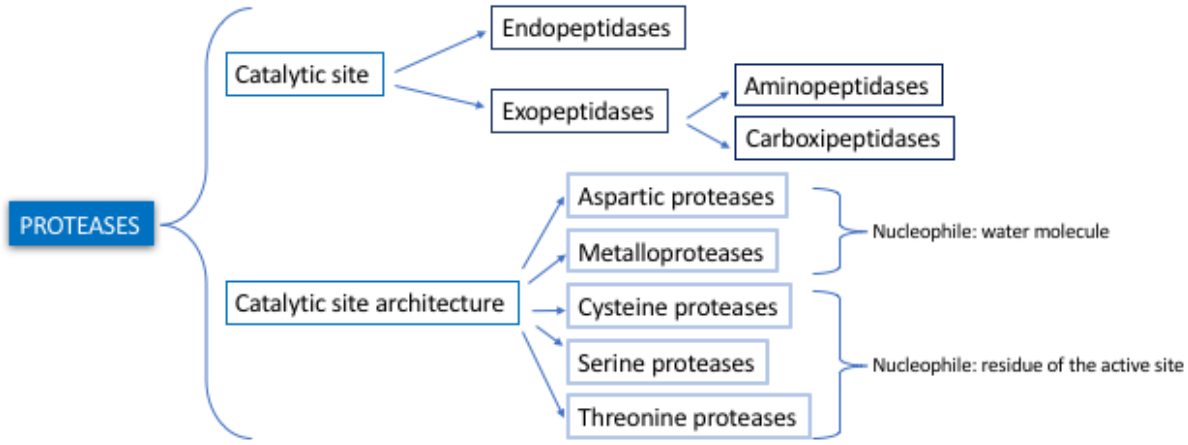

Figure 4: Two different classifications of proteases.
Early classification based on catalytic site, divides proteases into two groups: the endopeptidases and the exopeptidases. New classification of proteases is based on the mechanism of cleavage and it divides proteases into five groups in mammals: metalloproteases and aspartic proteases, which receive the electron necessary for the hydrolysis from active water molecules and cysteine, serine and threonine proteases, which have their own nucleophiles within the amino acids of their active sites (Rawlings *et al*., 2017; reviewed in López-Otín and Bond, 2008).

1.3.3.2. Functions of proteases

Several biological processes such as, DNA replication, angiogenesis, ovulation, immunity, autophagy, senescence or apoptosis, have been associated with proteases, which regulate the underlying mechanisms of these processes via the control of the localization, activity or the protein-protein interactions of their substrates (reviewed in López-Otín and Bond, 2008). Therefore, it is not surprising that defective protease activity is associated with several disorders such as, inflammatory, cardiovascular and neurodegenerative diseases as well as cancer (reviewed in Turk *et al*., 2006; reviewed in Lopez-Otín and Matrisian, 2007). The first report of a link between proteases and cancer was in 1946, when the degradation of the extracellular matrix by proteases was related to the tumor invasion into the surrounding tissues (Fisher, 1946).

Nowadays, several proteases have been connected not only to the later stages of the tumor but also to the general tumor progression. Examples include are caspase 8 and caspase 10, which act as metastatic suppressors or autophagins to promote autophagy of tumor cells (reviewed in Lopez-Otín and Matrisian, 2007). Similarly, a DUB called herpes-virus associated ubiquitin-specific protease (HAUSP) acts as a tumor suppressor by stabilizing the guardian of the genome p53 (Li *et al*., 2002). Moreover, in the last years, several studies have linked to cancer the dipeptidyl peptidase 9 or DPP9, a member of the dipeptidyl peptidase 4 (DPP4) family (Lu *et al*., 2011; Tang *et al*., 2017; Smebye *et al*., 2017).

1.4. The Dipeptidyl peptidase 4 (DPP4) protein family

The DPP4 family of proteases is classified as an S9 serine subfamily of the prolyl oligopeptidase family (reviewed in Yu *et al*., 2010; Gall and Gorrell, 2017). Proteases of the DPP4 family are aminopeptidases characterized by the hydrolysis of a post-proline dipeptides (Figure 5) by a catalytic triad, which is formed by a serine, an aspartate and a histidine. In some cases, DPP4 proteases also cleave post-alanine peptides but with less affinity than to proline-containing substrates (Yu *et al*., 2009; Waumans *et al*., 2015). Only a few proteases are able to cleave post-proline bonds due to the rigid structure of prolines imposed by their pyrrolidine ring, highlighting the importance of the DPP4 family (Figure 5). Such rigid structure confers stability to the proteins and therefore, upon proline cleavage, these substrates are degraded (Tinoco *et al*., 2010; reviewed in Gorrell *et al*., 2005; Gall and Gorrell, 2017).

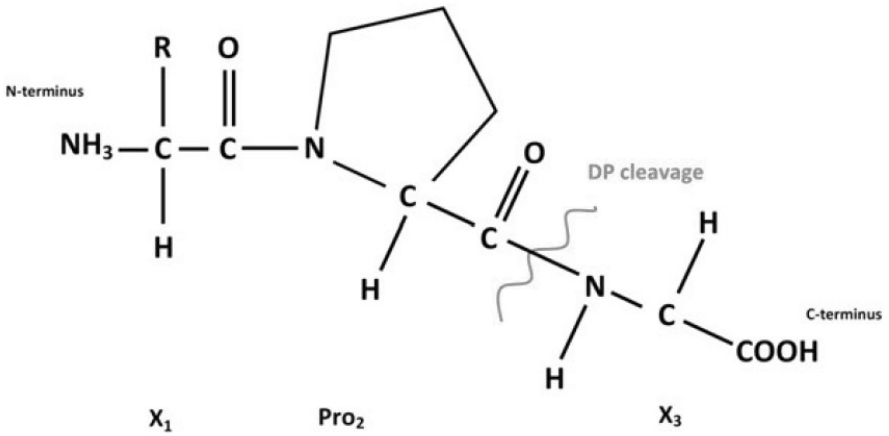

Figure 5. Peptide cleavage of the DPP4 family
The DPP4 proteases cleave dipeptides after a proline (Pro) in the second position. The three binding residues are shown, a residue bound to proline in second position followed by a third unknown residue (X_1-Pro_2-X_3). The dipeptide cleavage takes place after the proline, forming two products, X_1-Pro_2 and X_3-rest of the substrate (modified from Gall and Gorrell, 2017).

The DPP4 protein family consists of six members but only four of them display enzymatic activity. The catalytically active members are DPP4, the Fibroblast Activating protein (FAP), DPP8 and DPP9, whereas, the catalytically inactive members are DPP6 (also known as DPL1 or DPX) and DPP10 (also known as DPL2 or DPY), which lack the catalytic serine and other key residues for the enzymatic activity (reviewed in Yu *et al*., 2010). DPP4, FAP, DPP8 and DPP9 are structurally conserved and present similar protease activities (Ross *et al*., 2018). However, the localization and expression of these proteins are different from each other, conferring different functions for each protein (reviewed in Yu *et al*., 2010; Gorrell 2015).

1.4.1. DPP4

The exopeptidase DPP4 is the most studied member of the DPP4 protein family. DPP4 mainly localizes to the plasma membrane of cells, however, it can be also present in a soluble form in the plasma (reviewed in Gall and Gorrell, 2017; Mulvihill, 2018). The post-proline catalytic activity of DPP4 resides in the α/β hydrolase domain (aa 507-766) in its C-terminal end. Additionally, DPP4 displays two α helical hydrophobic domains (aa 1-22) in the N-terminal end which mediates the insertion into the plasma membrane and a β propeller (aa 56-497; reviewed in Ojeda-Montes *et al*., 2018).

DPP4 is expressed in epithelial cells (in the liver, gut, kidney and uterus), endothelial capillaries, acinar cells of mucous and salivary glands and pancreas, as well as immune organs (thymus, spleen and lymph node). In its soluble form DPP4 is expressed in serum, seminal fluid, saliva, kidney liver and bile (reviewed in Gall and Gorrell, 2017).

DPP4 has been shown to have roles in lymphocyte activation, cell migration, apoptosis and cleavage of bioactive peptides (reviewed in Gall and Gorrell, 2017). Substrates of DPP4 include cytokines, chemokines, the neuropeptide Y (NPY) and the incretins, glucagon-like peptidase 1 (GLP-1) and glucose-dependent insulinotropic (GIP), which regulate glucose homeostasis by inducing the release of insulin from the pancreas (Choi *et al*., 2015). Moreover, cytochrome c, peroxiredoxin and cathepsin β among others have been reported to be DPP4 substrates, suggesting the involvement of DPP4 in additional cellular pathways (Tinoco *et al*., 2010).

1.4.1.1. DPP4 in type 2 diabetes mellitus and DPP4 inhibitors

One important function of DPP4 is to control insulin secretion by cleaving the incretins, GLP-1 and GIP (Choi *et al*., 2015). After food intake, GLP-1 and GIP are secreted in the gut and induce insulin secretion from the pancreatic β cells. Therefore, DPP4 inhibition stabilizes GLP-1 and GIP and increases the release of insulin, which is necessary for glucose homeostasis after food intake (Chen and Jiaang, 2011; Ojeda-Montes *et al*., 2018). In fact, DPP4 inhibitors represent an important class of antihyperglycemics used for the treatment of Type 2 Diabetes Mellitus (T2DM).

The development of DPP4 selective inhibitors has been a challenge for the pharmaceutical industry due to the structural similarity between DPP4 and other members of the family. To date, there are eleven DPP4 inhibitors approved by the FDA for T2DM treatment (Ojeda-Montes *et al*., 2018). The first DPP4 inhibitor for T2DM in the market was sitagliptin (approved in 2006) followed by vildagliptin (approved in 2008) and saxagliptin (approved in 2011).

The half maximal inhibitory concentration (IC_{50}) is used to measure the potency of an inhibitor towards a substrate. Sitagliptin, which is a B-alanine based inhibitor, has an IC_{50} of 18 nM towards DPP4 and more than 100 μM with DPP9, making it quite selective (Chen and Jiaang, 2011). In contrast, vildagliptin, even though is a very stable drug, inhibits DPP4 with an IC_{50} of 3 nM and an IC_{50} 66 nM for DPP9, thereby creating a cross-inhibition which is dangerous for the patients (Chen and Jiaang, 2011). Alogliptin, gemigliptin or the latest FDA approved amarigliptin are some of the other DPP4 inhibitors in the market. Interestingly, sitagliptin was proposed as a possible treatment strategy in patients with breast cancer (Choi *et al*., 2015), since in women with T2DM there is a modesty association with postmenopausal breast cancer.

1.4.2. FAP

FAP or also known as seprase, has 52% sequence identity with DPP4 and as DPP4, is localized into the plasma membrane or present as a soluble form. It is the only member of the DPP4 family with endopeptidase activity in addition to the exopeptidase activity, which is shared with the rest of the members (reviewed in Gall and Gorrell, 2017). The normal levels of FAP in adult cells are low, however, they highly increase in inflamed organs, in damaged tissues during tissue remodeling, which includes scar formation or wound healing and in malignant tumors (reviewed in Yu *et al*., 2010). Nonetheless, as a protease, not many substrates have been characterized for FAP, some are the α-antiplasmin, which is involved in blood clotting, and the type I collagen, both are cleaved by the endopeptidase activity of the soluble FAP. This gelatinase activity of FAP has been connected to the degradation of the extracellular matrix (reviewed in Yu *et al*., 2010).

1.4.3. DPP8

DPP8 has been studied in parallel with DPP9 since both localize intracellularly and share biochemical properties. *DPP8* gene is located on human chromosome 15q22 (reviewed in Gall and Gorrell, 2017). Bioinformatics analysis have revealed four different isoforms of DPP8 (Abbott and Gorrell, 2012).

DPP8 shares with DPP9 60% homology in the amino acid sequence (Geiss-Friedlander *et al*., 2009) and the structure of both proteases also share conformational features (Ross *et al*., 2018). DPP8 and DPP9 are cytosolic amino di-peptidases (Geiss-Friedlander *et al*., 2009). Despite the combined studies of DPP8 and DPP9, in the last year DPP9 has gained more attention. In the following section, 1.4.4., DPP9 is described in detail together with the known properties of DPP8 from the studies of both proteases.

1.4.4. DPP9

DPP9 is a ubiquitously expressed protein that has been related to several processes such as macrophage M1 activation, pre-adipocyte differentiation, cell adhesion, cell migration or cell death among others (Matheeussen *et al*., 2013; Han *et al*., 2015; Zhang *et al*., 2015). *DPP9* gene locates on human chromosome 19p13.3 (Olsen and Wagtman, 2002). DPP9 is the main cytosolic peptidase of peptides containing a proline in second position in the N-terminus (Geiss-Friedlander *et al*., 2009) and likewise the rest of the members of the DPP4 family, requires dimerization to be enzymatically active (reviewed in Gall and Gorrell, 2017).

Two isoforms of DPP9 were identified on mRNA with two possible translation initiation sites, a short form, DPP9-S with 863 amino acids, and a long form, DPP9- L with 971 amino acids (Justa-Schuch *et al*., 2014). DPP9-L has a nuclear localization signal (NLS) in the N-terminal domain, which localizes the protein into the nucleus (Justa-Schuch *et al*., 2014). DPP9 is ubiquitously expressed with higher levels in liver, heart and skeletal muscle (Olsen and Wagtman, 2002; reviewed in Gall and Gorrell, 2017). The active site of DPP9 resides in serine 730, histidine 840 and aspartate 708 in humans (Ross *et al*., 2018) and mutations in those residues showed deficient DPP9 enzymatic activity. DPP9 *in vivo* studies have shown that mice expressing an inactive form of DPP9, $DPP9^{S729A/S729A}$, died within 8 to 24 hours after birth, highlighting the importance of DPP9 function in the organism (Gall *et al*., 2013). However, the precise cause for this neonatal mortality in mice is unknown. One recent study, which also generated such mice, suggested that $DPP9^{S729A/S729A}$ impairs muscle tongue formation, leading to sucking defects during feeding and thereby final death due to fasting (Kim *et al*., 2017).

1.4.4.1. DPP9 substrates

Little is known about the natural substrates targeted by DPP9. The first suggested DPP9 substrate was the NPY, a known substrate of DPP4, since despite DPP4 inhibition the NPY remained cleaved in cells (Frerker *et al*., 2007). However, NPY has not been directly proved to be a natural substrate of DPP9. The first known natural substrate of DPP9 is the $RU1_{34-42}$ antigenic peptide described by Geiss-Friedlander (Geiss-Friedlander *et al*., 2009). Moreover, in this study DPP9 was shown to be the only member of the DPP4 family able to cleave the $RU1_{34-42}$ antigenic peptide in cells, thus giving the property of rate limiting peptidase of proline containing peptides (Geiss-Friedlander *et al*., 2009). Afterwards, a screen was done to look for putative substrates of DPP9 by using Terminal Amine Isotope Labeling of substrates (TAILs), which found calreticulim and adenilate kinase 2 (AK2) as possible DPP9 substrates *in vitro* (Wilson *et al*., 2013). A second screen performed using two-dimensional gel electrophoresis identified 24 candidates found in the previous screen

(Zhang *et al*., 2015). Nonetheless, *in vivo* studies are needed to confirm those possible substrates. Only one more natural substrate, besides RU1 antigenic peptide, has been found for DPP9, the spleen tyrosine kinase (Syk). Syk and DPP9 study was also performed by the Geiss-Friedlander group where we found DPP9 as a negative regulator of Syk in B cell signaling (see point 1.4.4.5.; Justa-Schuch *et al*., 2016).

1.4.4.2. DPP9 in cell adhesion and cell migration

DPP9 has been associated with cell migration and cell adhesion processes, in which silencing or overexpression of DPP9 was found to reduce cell adhesion, cell migration and cell survival (Yu *et al*., 2006; Zhang *et al*., 2015). DPP9 localization manifested a re-distribution near to the plasma membrane after stimulation with Phorbol-12-myristate-13-acetate or epidermal growth factor (EGF), which induce cell migration and cell adhesion processes (Zhang *et al*., 2015). First studies attributed the role of DPP9 in cell adhesion to an extra-enzymatic function (Yu *et al*., 2006). Nonetheless, in this last study, the silencing or inactivation of DPP9 reduced the expression of Integrin β1 and Talin and low phosphorylation of focal adhesion kinase (FAK) and of Paxillin (regulators of cell adhesion and migration processes; Zhang *et al*., 2015) involving the enzymatic activity of DPP9 in cell adhesion and cell migration function.

1.4.4.3. The regulation of the enzymatic activity of DPP9

DPP9 has a SUMO1 binding domain, named SUMO Biding arm (SUBA) close to the active site that regulates the enzymatic activity of DPP9 in an allosteric manner (Pilla *et al*., 2012). Sumoylation is a process similar to ubiquitination where the conjugated molecule is SUMO instead of ubiquitin. In humans, there are three functional isoforms of SUMO; SUMO1, SUMO2 and SUMO3. SUMO2 and SUMO3 present a high degree of similarity in contrast to SUMO1 that only shares 47% of sequence homology. SUMO presents a SIM-interacting groove where most proteins bind to the molecule (reviewed in Geiss-Friedlander and Melchior, 2007; reviewed in Flotho and Melchior., 2013). In DPP9, the binding to SUMO1 occurs in an opposite area in the structure define as E67-interacting loop (EIL) that covers 61-75 residues. Mutation in SUMO1 E67 position to alanine shows reduced binding to DPP9 and did not increase DPP9 activity as it was the case for SUMO1-DPP9 binding (Pilla *et al*., 2012). A DPP9 inhibitor was developed from the first eight amino acids of the EIL of SUMO1 (SLRFLFEG) where the second Phe was mutated into Tyr, increasing 170 times the inhibitory effect. The final inhibitor SLRFLYEG shows more specificity for DPP8 and DPP9 compared to DPP4 protein in cells, thus showing the relevance for targeting

those proteins (Pilla *et al*., 2013). Recently, a structural study has revealed that the SLRFLYEG inhibitor surprisingly binds to the active site of DPP9 (Ross *et al*., 2018).

1.4.4.4. DPP9 structure

DPP9 shares many conformational similarities with DPP8. Both proteins, likewise DPP4, have two main domains, the β propeller and the α/β hydrolase domain (Ross *et al*., 2018). In DPP8/9 the α/β hydrolase domain presents five α helices and eight β strands where the first α helix has different orientation compared to DPP4. A major difference between DPP4 and DPP8/9 is the active site, which is more voluminous in DPP8/9 compared to DPP4. One reason is a sequence exchange in DPP8/9, where H450/424 presents a displacement of seven angstroms in an opposite orientation compared to the corresponding residue, F357, in DPP4. In addition, Q673/648 in DPP8/9 is a binding site for the SLRFLYEG inhibitor, meanwhile in DPP4 the corresponding residue C551 does not bind. Apart from the difference in sequence there is also a second reason for the increased of the size of the active site, the presence of an extra loop in H525/500 DPP8/9 compared to DPP4 (Ross *et al*., 2018). Those differences in substrate binding give specificity for targeting different proteins in the cell and helps in the development of selective inhibitors of these proteases.

1.4.4.5. The roles of DPP9 in the immune system

Initial studies of the DPP4 family in the immune system used DPP4 inhibitors and related the phenotypes found to DPP4 protein. However, later studies proved that some of those inhibitors were not selective for DPP4 and argue that some of these findings were due to inhibition of DPP8/9 (Lankas *et al*., 2005; Reinhold *et al*., 2009). One of the first studies showed that DPP4 inhibitors inhibit T cell activation, where DPP4 was highly expressed (Tanaka *et al*., 1997). However, later studies have showed that DPP4 levels (or CD26) do not always increased during T cell activation, as seen in leukemia cell lines, but not in B cells or macrophages, which raised the question of the selectivity of the DPP4 inhibitors (Lankas *et al*., 2005). In 2009, a possible role of DPP8/9 in T cell activation was suggested (Reinhold *et al*., 2009), which was confirmed afterwards in B cells (Raji cells) where DPP9 was upregulated leading to an increased in cell death (Chowdhury *et al*., 2013).

The enzymatic activity of DPP9 in the immune system was proven by the cleavage of RU1 antigenic peptide (Geiss-Friedlander *et al*., 2009). Antigenic peptides are formed after proteasome degradation followed in some cases by peptidase activity. The $RU1_{34-42}$ antigenic peptide is formed after proteasome activity that forms $RU1_{29-42}$ peptide, which is

then cleaved by two peptidases. First acts the tripeptidyl peptidase II (TPPII), leading to $RU1_{32-42}$ followed by the puromycin sensitive aminopeptidase (PSA), which produces the final active form $RU1_{34-42}$ (Lévy *et al*., 2002). DPP9 cleaves the active $RU1_{34-42}$, impairing its presentation to cytotoxic T lymphocytes (CTL). In contrast, DPP9 silencing maintains the mature form of RU1, $RU1_{34-42}$ antigen, increasing its presentation to CTL cells which promotes the production of interferon gamma (Geiss-Friedlander *et al*., 2009).

Additionally, the Spleen Tyrosine Kinase (Syk) in its active form was shown to be cleaved by DPP9 in B cells, regulating B cell signaling. DPP9 requires the interaction with FLNA to cleave the methionine alanine (Met-Ala) in the N-terminus of Syk, which upon the cleavage exposes the third amino acid, a serine (Justa-Schuch *et al*., 2016). Serine, in principle, is not a destabilizing residue, however, Ac/N-degrons are formed upon acetylation, and here it was suggested that the serine gets acetylated and recognized by the E3 ligase of Syk. Inhibition of DPP9 resulted in Syk stabilization and accumulation of the phosphorylated form of Syk in tyrosine 323 (Justa-Schuch *et al*., 2016), which is a post-translational modification needed for Cbl recognition (Lupher *et al*., 1998). Silencing of DPP9 decreased the binding of Cbl to the phosphorylated Syk in tyrosine 323, suggesting that the cleavage of the Met-Ala of Syk is necessary for degradation (Justa-Schuch *et al*., 2016). All together this study showed that DPP9 acts upstream of Cbl, which poly-ubiquitinates and targets Syk to the proteasome where it is degraded. This was the first time to show a direct connection of DPP9 and the N-end rule pathway (Justa-Schuch *et al*., 2016).

1.4.4.6. DPP9 and cell death

In the last years DPP9 has been connected to cell death by pyroptosis (Okondo *et al*., 2016; Johnson *et al*., 2018). Pyroptosis defines a type of cell death that involves a highly inflammatory response, generally induced by intracellular pathogens, infections or viruses, which via caspase-1 activation involves the formation of a complex of proteins named as inflammasome. DPP9 inhibition by a non-selective inhibitor for proline cleaving enzymes, ValBoroPro, led to an increased in pyroptosis in cells in a non-canonical caspase-1 manner (Okondo *et al*., 2016) and lately this inhibition has been related to activation of NLRP1b, an essential protein in the inflammasome formation (Johnson *et al*., 2018).

However, ValBoroPro is not only targeting DPP9 but also other prolyl-peptidases, so further studies with more selective inhibitors of DPP9, such as SLRFLYEG, should be done in the same line to validate those results. It is important to note that in addition to these studies a later approach showed a direct interaction between DPP9 and NLRP1b via the FIIND domain in NLRP1b. FIIND is involved in the auto-proteolysis of NLRP1b needed for its activation and the binding to DPP9 resulted in inactivation of NLRP1b. In Zhong study,

they proved that DPP9 inactive mutant, silenced DPP9 or inhibition of DPP9 resulted in NLRP1 activation and cell death (Zhong *et al*., 2018). As inhibitors resulted in similar effects, NLRP1 could be a substrate of DPP9, but further studies are needed in order to understand the role of DPP9 in pyroptosis.

Besides the involvement of DPP9 in pyroptosis, DPP9 has been indirectly related to cancer in various studies in the last years. Interestingly, the protein levels of DPP9 were found upregulated in cirrhotic liver (Chowdhury *et al*., 2013), inflamed lungs (Lu *et al*., 2011) and leukemia cells (Spagnuolo *et al*., 2013). This together with other studies points at DPP9 as a possible marker of cancer diagnosis and raises the question if DPP9 functions as a possible regulator of tumor progression and cell death.

1.5. Aim of this work

Dysregulation of cell death processes and DNA damage are common hallmarks of most cancers. Proper regulation of DNA damage repair is essential to maintain genome integrity. In the last years, DPP9 has been connected to cell death processes and more importantly, DPP9 has been associated to different cancers. Cells lacking DPP9 or inactivation of DPP9 are prone to present aberrant growth and develop cancer. However, little is known of the role of DPP9 in cell survival and in cancer. Therefore, the aim of this thesis was to understand the function of DPP9 in the DNA damage repair and understand the involvement of DPP9 in cell survival.

To approach this, first we aimed to understand the connection of DPP9 with cell survival by looking at cell survival of cells upon different conditions using colony formation assays and viability assays. Furthermore, we studied DPP9 in DNA damage repair by looking at γH2AX levels and the localization of DPP9 after DNA damage induction. As an enzyme, DPP9 targets different proteins in the cell. Only two natural substrates were known for DPP9 before this study, thereby we aimed to unravel possible substrates of DPP9 which are known to be involved in the DNA damage repair response. To approach this, we used microscopy assays such as immunofluorescence and proximity ligation assays, as well as, biochemical approaches.

Overall, these experiments should provide more insights in the involvement of DPP9 in cell survival and cancer and open new perspectives for using DPP9 inhibitors as therapeutic treatments.

2. Material and Methods

2.1. Material

2.1.1. Technical equipment

Equipment	Company
Agarose gel documentation Gel STICK touch	INTAS Science Imaging Instruments
Agarose gel running chamber	Home-made, Workshop, UMG
ÄKTA column HiLoad 26/60 Superdex 200 prep grade	GE Healthcare
ÄKTA column HiLoad 26/60 Superdex prep grade	GE Healthcare
ÄKTA purifier	Amersham Biosciences
Autoclave DX-200	Systec
BioPhotometer	Eppendorf
Cell culture hood Herasafe ^{TM} KS	Thermo Scientific
Cell culture incubator Heracell ^{TM} 150i	Thermo Scientific
Cell culture incubator Cytoperm 2	Hearaeus Instruments
Centrifuge 5424	Eppendorf
Centrifuge Allegra® X-15R with rotor SX4750	Beckman Coulter
Centrifuge Allegra® X-22 with rotor SX4250	Beckman Coulter
Centrifuge Avanti^{TM} J-30I with rotor JA30.50Ti	Beckman Coulter
Centrifuge Optima MAX-XP with rotor TLA 100.3	Beckman Coulter
Confocal Microscope LSM 510 meta	Zeiss
Developer machine CURIX60	Agfa
Incubator Shaker INNOVA 4430	New Brunswick Scientific
Mini Trans-Blot® Cell	BioRad
Odyssey® Sa Infrared Imaging System	LI-COR
Olympus CK40 Culture Microscope	Olympus
Spectrophotometer NanoDrop 2000c	Thermo Scientific
Thermocycler Tprofessional	Biometra
Thermomixer comfort	Eppendorf
Thermomixer compact	Eppendorf
UV sterilizer	Biometra
Vortexer MS2 Minishaker	IKA
Western blot incubation boxes	LI-COR

2.1.2. Consumables

Consumable	Company
Amersham Hybond ECL Nitrocellulose	GE Healthcare
Blotting Membrane	GE Healthcare
Amersham Protran 0.45 µm NC Nitrocellulose Blotting Membrane	GE Healthcare
Cell culture consumables	Sarstedt, Greiner bio-one
Cell culture plastic ware	Sarstedt, Greiner bio-one
Centrifuge Bottle Assembly, Polycarbonate 50 ml	Beckman Coulter
Centrifuge tube, thickwall, Polycarbonate 500 µ	Beckman Coulter
Microscope cover slips (10 mm, 12 mm Ø)	Paul Marienfeld GmbH & Co
Microscope slides (76x26 mm)	Paul Marienfeld GmbH & Co
Minisart RC 15, single use syringe filters (0.45 µm, 0.20 µm)	Sartorius Stedim Biotech
Minisart single use filter units (0.45 µm)	Sartorius Stedim Biotech
Parafilm “M”	Bemis Company, Inc.
Reaction tubes (1.5, 2 ml)	Sarstedt, Greiner bio-one
Whatman gel blotting paper	GE Healthcare

2.1.3. Software

Software	Company
Adobe Illustrator CS6	Adobe
Adobe Photoshop	Adobe
DuoLink software	Sigma-Aldrich
ImageStudio/ ImageStudio Lite 4.0.21	LI-COR
Lasergene 10.1.1 (3)	DNASTAR
LSM 510 Release Version 4.0 SP2	Zeiss
LSM Image Browser	Zeiss
Microsoft Office Home and Student 2016	Microsoft
NanoDrop 2000 Software	Thermo Scientific
Prism 7	Graphpad

2.1.4. Kits

Kits	Company
CloneJET PCR Cloning Kit	Thermo Scientific
NucleoBondTM Xtra Midi	Macherey-Nagel
NucleoSpin® Gel and PCR Clean-up	Macherey-Nagel
NucleoSpin® Plasmid	Macherey-Nagel
PLA probe Rabbit plus	Sigma-Aldrich
PLA probe Mouse plus	Sigma-Aldrich
PLA probe Mouse minus	Sigma-Aldrich
PLA probe Goat plus	Sigma-Aldrich
PLA reactive reagents	Sigma-Aldrich

2.1.5. Buffers, solutions, media

2.1.5.1. Buffers

Buffers	Composition
Coomassie fixing solution	40% ethanol, 10% acetic acid
Coomassie staining	5% aluminium sulfate-(14-18)-hydrate, 10% ethanol, 2% ortho-phosphoric acid, 0.02% CBB- G250
DNA loading buffer (6x)	0.2% bromophenol blue, 0.2% xylene cyanole, 60% glycerol, 60 mM EDTA
Laemmli running buffer (10x)	250 mM Tris, 1.92 M glycine, 0.5% SDS
PBS (10x)	1.37 M NaCl, 27 mM KCl, 100 mM Na_2HPO_4, 18 mM KH_2PO_4, pH 7.5
SDS sample buffer (4x)	200 mM Tris-HCl pH 6.8, 8% SDS, 40% glycerol, 0.02% bromophenol blue
SDS sample buffer (2x)	100 mM Tris-HCl pH 6.8, 4% SDS, 20% glycerol, 0.02% bromophenol blue
TAE buffer (50x)	2 M Tris, 50 mM EDTA, 5.71% acetic acid
TBS buffer (10X)	25 mM Tris-HCl pH 7.5, 138 mM NaCl, 2.7 mM KCl
Western blot transfer buffer (10x)	250 mM Tris, 1.93 M glycine, 0.2% SDS

2.1.5.2. Stock solutions

Solution	Composition
1,4-Dithiothreitol (DTT)	1 M in H_2O
Ammonium persulfate (APS)	10% APS (Sigma-Aldrich) in H_2O
Ampicillin	100 mg/ml in H_2O
Aprotinin	1 mg/ml in 20 mM HEPES pH 7.4
Kanamycin	60 mg/ml in H2O
Leupeptin/Pepstatin	1 mg/ml each, in DMSO
Phenylmethylsulfonyl fluoride (PMSF)	100 mM in 2-propanol

2.1.5.3. Bacterial media

Medium	Composition
LB	1% (w/v) bacto-tryptone, 0.5% (w/v) yeast extract, 1% (w/v) NaCl
LB agar plates	LB supplemented with 1.5% (w/v) bacto-agar
SOC	2% (w/v) tryptone, 0.5% (w/v) yeast extract, 10 mM NaCl, 2.5 mM KaCl, 10 mM $MgCl_2$, 10 mM $MgSO_4$, 0.36% (w/v) glucose, pH 7.0

2.1.5.4. Cell culture solvents

Solvent/Medium	Company/source
Calcium chloride buffer	250 mM $CaCl_2$
FBS superior (fetal bovine serum)	Biochrom
Gibco® DMEM (1x)	Gibco Life Technologies
Gibco® Opti-MEM® (1x)	Gibco Life Technologies
Gibco® Penicillin Streptomycin	Gibco Life Technologies
L-Glutamine 200 mM	Gibco Life Technologies
PBS (10x)	Gibco Life Technologies

2.1.6. Enzymes

Enzymes	Company/source
Pfu Ultra II polymerase	Aligent
Phusion High-Fidelity DNA polymerase	Thermo Scientific
Restriction enzymes (various)	Thermo Scientific
T4 DNA ligase	Thermo Scientific
Gibco® Trypsin/ EDTA 0.25% (1x)	Gibco Life Technologies

2.1.7. Chemicals and reagents.

Chemicals and reagents	Company/source
1G244 (in DMSO)	AK Scientific, Inc.
β-Mercaptoethanol	Roth
Acrylamide 4k Solution (30%)	AppliChem
Bovine Serum Albumin (BSA) (20mg/ml)	Thermo Scientific
BSA fraction V	AppliChem
CellTiter-Glo® Luminescent Cell Viability Assay	Promega
Cycloheximide (CHX)	Sigma-Aldrich
Dako Fluorescent Mounting Medium	Dako
DAPI (D9542)	Sigma-Aldrich
dNTP set 100mM solution	Thermo Scientific
Formaldehyde solution 37%	Millipore
GeneRuler 100 pb DNA ladder	Thermo Scientific
GeneRuler 1kb DNA ladder	Thermo Scientific
Lipofectamine RNAimax	Thermo Fisher
Mayer's Hemalum	Merck
Methanol	Roth
Mitomycin C (MMC)	Sigma-Aldrich
MG132 (in DMSO)	Sigma-Aldrich
Neocarzinostatin (NCS)	Sigma-Aldrich
NP-40	Applichem
Olaparib	Selleckchem
PagerRuler Unstained Protein Ladder	Thermo Scientific

PagerRuler Prestained Protein Ladder	Thermo Scientific
PagerRuler Plus Prestained Protein Ladder	Thermo Scientific
Powdered milk	Roth
Puromycin	Sigma-Aldrich
SafeView™ Classic (DNA stain)	Sigma-Aldrich

2.1.8. Antibodies

2.1.8.1. Primary Antibodies

Antibody/Species	Method	Company	Identifier	Dilution
BRCA1 Mouse	IF	Santa Cruz	Sc-6954	1:100
BRCA2 Mouse	IF-PLA	R&D	MAB2476	1:100
BRCA2 Rabbit	IF/ PLA	Santa Cruz	sc-8326	1:50
BRCA2 Rabbit	WB	Abcam	123491	1:500
BRCA2 Mouse	WB	Calbiochem	OP95	1:100
DPP9 Rabbit	WB	Abcam	AB42080	1:1000
DPP9 Goat	IF/ PLA	Self-made		1:20
Filamin A Rabbit	WB	Novus	nb-100-58812	1:1000
Filamin A Mouse	IF/PLA	Millipore	MAB1680	1:200
FLAG M2 Mouse	WB	Sigma-Aldrich	f1804	1:1000
H2AX-P Rabbit	IF/ PLA/WB	Cell Signaling Technology	#9718	1:100/ 1:100
H2AX-P Mouse	IF-PLA/WB	Abcam	Ab26350	1:50/ 1:100
H3 Rabbit	WB	Cell Signaling Technology	#9715	1:100
HA Rabbit	WB/ IF	Sigma-Aldrich	H6908	1:100
penta HIS Mouse	WB	Qiagen	34660	1:1000
PALB2 Rabbit	IF/ PLA	Bethyl/biomol	A301-246M	1:100
PALB2 Goat	IF/ PLA	Santa Cruz	sc-160647	1:100
Phalloidin 488	IF/ PLA	Abcam	Ab176753	1:600
RAD51 Rabbit	IF/WB	Abcam	ab63801	1:500/ 1:1000
RAP80 (D1T6Q) Rabbit	WB	Cell Signaling Technology	14466	1:100
RPA32/RPA2 Mouse	WB	Abcam	ab2175	1:100
Tubulin Mouse	WB	Santa Cruz	sc-32293	1:100
Vinculin Mouse	WB	Sigma-Aldrich	V9131	1:6000

2.1.8.2. Secondary Antibodies

Secondary Antibodies	Method	Company	Dilution
α-Mouse HRP	WB Films	Invitrogen	1:10000
α -Rabbit HRP	WB Films	Invitrogen	1:10000
α -Goat HRP	WB Films		1:10000
α -Mouse 680	WB Fluorescent LI-COR	LI-COR	1:5000
α -Rabbit 680	WB Fluorescent LI-COR	LI-COR	1:5000
α -Mouse 800	WB Fluorescent LI-COR	LI-COR	1:5000
α -Rabbit 800	WB Fluorescent LI-COR	LI-COR	1:5000
α -Goat AlexaFluor® 488 conjugated	IF	Invitrogen	1:500
α -Goat AlexaFluor® 594 conjugated	IF	Invitrogen	1:500
α -Goat AlexaFluor® 647 conjugated	IF	Invitrogen	1:500
α -Mouse AlexaFluor® 488 conjugated	IF	Invitrogen	1:500
α -Mouse AlexaFluor® 594 conjugated	IF	Invitrogen	1:500
α -Mouse AlexaFluor® 647 conjugated	IF	Invitrogen	1:500
α -Rabbit AlexaFluor® 488 conjugated	IF	Invitrogen	1:500
α -Rabbit AlexaFluor® 594 conjugated	IF	Invitrogen	1:500
α -Rabbit AlexaFluor® 647 conjugated	IF	Invitrogen	1:500

2.1.9. siRNAs

siRNA	Sequence 5'→3'	Company
DPP9	GGAUCAAUGUUCAUGACAUTT	Invitrogen
DPP9	GCCACCAGGUUUAUCCAATT	Invitrogen
BRCA2	GAAGAAUGCAGGUUUAAUA	Dharmacon
PALB2	GAAGUCACCUCACACAAAU	Dharmacon
FLNA	GCAGGAGGCUGGCGAGUAU	Dharmacon
RAD51	UAUCAUCGCCCAUGCAUCA	Dharmacon
FLNA	GCAGGAGGCUGGCGAGUAU	Dharmacon

2.1.10. Oligonucleotides

* Clon: cloning, Seq: sequencing, Mut: mutagenesis.

Use*	Oligonucleotides	Sequence
Clon	fwPALB2bamH1. 1-20	GGCGGATCCATGGACGAGCCTCCCGGGAA
Seq	rvPALB2.primer2. 326-307	GGGTTAAAGGACTCAGGCCC
Seq	fwPALB2primer3. 307-326	GGGCCTGAGTCCTTTAACCC
Seq	fwPALB2primer4.937-956	GGCCAACTGCCCACAAGTTC
Seq	fwPALB2primer5. 1563-1582	CCCAGCATCAGATCATTGTG
Seq	fwPALB2primer6. 2187-2206	CATCTTAGGTACTACTCCAG
Seq	fwPALB2primer7.3025 -3044	CCTGAGGAGACTATACTAAC
Clon	rvPALB2.not1.3561-3542	GGCGCGGCCGCTTATGAATAGTGGTATACAA
Clon	2rvPALB2not1. 3531-3561	GGCGCGGCCGCTTATGAATAGTGGTATACAA ATATATTTCC

2.1.11. Vectors and plasmids.

2.1.11.1. Vectors

Vector	Resistance	Company
pENTR3C	Kanamycin	Novagen

2.1.11.2. Plasmids

Plasmid	Resistance
pENTR3C PALB2	Kanamycin

2.1.12. Cell lines

2.1.12.1. Mammalian cell lines

Cell line	Characteristics
HeLa genscript	HeLa cell #SC1589
HeLa DPP9 KD genscript	HeLa cell #SC1589-3
MEF WT	Derived from healthy C57BL/6 mice with no clinical symptoms of infection. Goods were manufactured in the Centenary Institute, Australia (Gall *et al*., 2013)
MEF DPP9 ki	Derived from healthy C57BL/6 mice with no clinical symptoms of infection. Goods were manufactured in the Centenary Institute, Australia. DPP9 gki presents mutation in S729A (Gall *et al*., 2013)

2.1.12.2. Bacterial strains

Strain	Features
DH5α	F- Φ80lacZΔM15 Δ (lacZYA-argF) U169 recA1 endA1 hsdR17 (rK-,mK+) phoA supE44 λ- thi-1 gyrA96 relA1

2.1.12.3. Insect cells

Cell type	Characteristics
Sf9	#11496-015 Gibco Invitrogen

Baculovirus kit for Insect cells

Kit Name	Catalog number	Company
Gateway LR clonase II	#11791-023	Invitrogen
Ganciclovir	#12562-023	Invitrogen

2.2. Methods

2.2.1. Molecular biology techniques

2.2.1.1. Polymerase chain reaction (PCR)

Polymerase chain reaction (PCR) is used to amplify the DNA of interest from a template DNA. PCR requires the use of primers or small oligonucleotides (about 20 nucleotides), which sequence is complementary to the sequence of interest, a polymerase to amplify the DNA and dNTPs for the new amplified DNA. Forwards (fw) and reverse (rv) primers were designed using the Lasergene software containing restriction enzyme sequence motifs for cloning purposes. In the reverse primers, a stop codon was added for translation termination. In the case of PALB2 cDNA was used as template. The PCR mix used was: 5 µl of pfu Ultra Buffer 10X, 2 µl of dNTPs 10 mM, 2 µl of primer fw 10 µM, 2 µl of primer rv 10 µM, 1 µl of cDNA, 2 µl of DMSO (100%), 0.5 µl of pfu enzyme and nuclease free water to top up to 50 µl. The amplification time for PCR reactions was done using a T_m calculator (Thermo Scientific homepage). For PALB2 PCR was performed as follows: denaturing at 95°C for 2 min followed by 30 cycles (95°C for 30 sec, 45°C for 30 sec, 72°C for 4 min), and the final extension at 72°C for 10 min.

2.2.1.2. Agarose gel electrophoresis

To visualized the DNA, agarose gel-electrophoresis was performed. 1% agarose gels were casted in presence of SafeView™ classic DNA stain and dissolved in 1x TAE buffer. PCR products supplemented with 6 x DNA loading buffer were run in the gel for about 40 min at 120 V. As DNA size marker, either GenerRuler 100 bp or 1kb DNA ladder was used, depending on the size of the DNA of interest.

2.2.1.3. Restriction enzyme digestion

To perform the digestion of the vectors and the PCR products, different Restriction Enzymes (Thermo Scientific) were used. In the case of PCR products (50 µl) were digested with 1 unit of the respective restriction enzymes and the corresponding buffer (using the digestion tool in Thermo Scientific homepage). Samples were incubated for 2 h at 37°C, followed by the analysis in the agarose gel (as described above.) Bands corresponding with the size of interest were cut in a UV transilluminator followed by purification of the bands with NucleoSpin® Gel and PCR Clean-up (Macherey-Nagel).

2.2.1.4. Transformation of plasmid into competent cells

Transformation defines a process by which an organism acquires exogenous DNA, either in a natural or in an artificial manner. This assay allows to generate copies of our DNA of interested. To perform the assay, competent cells of *E.coli*, DH5α strain, were used. Cells were thawed on ice for about 20 min. The plasmid containing the DNA of interested was added to the cells (1 µl of plasmid per 100 µl of competent cells) followed by 20 min incubation on ice. After the incubation, cells were exposed to a heat shock at 42°C for 1 min and immediately taken to ice for another 1 min. The change of temperature allows the exogenous DNA to penetrate into the cells. Afterwards, cells were incubated with SOC medium (500µl per sample) on a Thermomixer (800 rpm) for 1 h shaking at 37°C. Finally, cells with the DNA were plated on LB-agar plates with the corresponding antibiotic and were kept in the incubator overnight at 37°C.

2.2.1.5. Isolation of plasmids

Isolation of plasmids was performed either with NucleoSpin® Plasmid kit (Macherey-Nagel) for small scale isolations or mini-preparations (mini-preps) and with NucleoBond™ Xtra Midi kit (Macherey-Nagel) in case of large scale purifications or midi-preparations (midi-preps). LB medium was used in both preparations.

For small scale plasmid isolation, 5 ml of LB medium with the corresponding antibiotic was inoculated with a single bacterial colony from a LB-agar plate. The culture was incubated overnight at 140 rpm and at 37C. Plasmid DNA was isolated from 2 ml of this overnight culture according to manufacturer's protocol. DNA elution was performed with 50 µl of Milli-Q water.

In the case of large scale plasmid isolation, 200 ml of LB medium with the corresponding antibiotic was inoculated with one bacterial clone or with 1 ml of previous incubated mini-prep and incubated overnight at 37°C in an Erlenmeyer flask at 140 rpm. The bacterial culture was pelleted at 5250 g for 20 min at 4°C (Allegra® X-15R with rotor, Beckman-Coulter) and purified according the manufacterer's protocol. DNA elution was performed with 200 µl of Milli-Q water.

NanoDrop (NanoDrop 2000c software, ThermoScientific) was used to measure plasmid concentrations and purity previously adjusted with Milli-Q water.

2.2.1.6. Ligation of DNA

After DNA digestion, the insert containing the DNA sequence of interest was linked into the corresponding vector. This process called ligation requires the use of a DNA ligase, in this case T4 DNA ligase. To establish the volumes of the mixture the tool Ligation calculator from UT Dallas website was used. The DNA sequences were ligated in a molecular ratio of 1:3 (vector: insert). The reaction was done at 16°C overnight and half of the mixture was transformed into *E.coli* DH5α.

2.2.1.7. Sequencing of DNA

All plasmids were sent for sequencing to GATC company. The samples were sent in standard Eppendorf tubes in a concentration between 50-80 ng/µl in a finale volume of 30 µl. For sequencing GATC-standard sequencing primers (such as T7 promoter or BGH reverse primer) and the custom-made primers specific for each DNA sequence were used. Analysis was done using SeqMan software of the Lasergene suite.

2.2.2. Biochemical techniques

2.2.2.1. Separation of proteins and detection

To separate proteins, sodium dodecyl sulfate polyacrylamide gel electrophoresis (SDS-PAGE) was used. This system was first described by Laemmli in 1970 and it is formed by a non-continuous gel made of two parts, named as the stacking gel and the resolving gel. The percentage of polyacrylamide in the resolving gel was chosen according to the size of the proteins of interest (from 6% to 15%). Gels were run in a chamber with Tris-HCl/Tris-glycine buffer. To prepare the samples, cells were lysed directly in the culture wells with SDS sample buffer 2x (100 mM Tris-HCl pH 6.8, 4% SDS, 20% glycerol, 0.02% bromophenol blue, 100 mM dithiothreitol (DTT); see table 2.1.5.1.).

For BRCA2 detection cells grown in 6 well plates were lysed in 100 µl of SDS Buffer 2x followed by 10 min denaturation at 65°C and 4 pulses of sonication at 1% intensity. Afterwards samples were loaded into SDS- polyacrylamide gels (6% gels for BRCA2 detection). The same was done for DPP9 protein.

For chromatin fractions samples were sonicated in waterbath sonicator from BioRad for 15 min. Before the loading, samples were treated with SDS sample buffer 4x (200 mM Tris-HCl pH 6.8, 8% SDS, 40% glycerol, 0.02% bromophenol blue, 100 mM DTT; see table 2.1.5.1.). Samples were separated either by using 15% SDS-PAGE gels to detect low molecular weight proteins (Histones, RAD51 and RPA2) or using 6% SDS-PAGE gels

for the detection of high molecular weight proteins (BRCA2, FLNA, DPP9). The run was performed in the cold room between 80-100 V for approximately 6 h in cold room.

Immunoblotting was performed to visualized the proteins, (see section 2.2.2.3.) and Coomassie staining in the case of purified proteins.

Coomassie staining is frequently used to visualize proteins directly in the gel and test the purity of the sample. After an initial fixing step using Coomassie fixing solution (see table 2.1.5.1.) for about 10 min on a shaker, the gel was incubated with Coomassie staining solution (see table 2.1.5.1.) for at least 1 h. Finally, the gel was washed and de-stained with the Coomassie fixing solution.

2.2.2.2. Protein transfer by western blot

Western Blotting (WB) is used to detect proteins in a membrane via HRP o or fluorophore-coupled secondary antibodies (see 2.2.2.3). The wet blot protocol was performed to transfer the proteins from the SDS-PAGE gels into the membranes (Hybond ECL nitrocellulose membrane, GE Healthcare). Whatman paper sheet was placed followed by the gel and the membrane and another whatman paper and all were assembled between two sponges and placed into the blotting chamber from BioRad. The blotting chamber was containing the WB buffer (1x supplemented with methanol 20%). The blotting voltage and time was adjusted to the percentage of the gel. For high percentage gels and low molecular weight proteins, blotting was done at 90 V for 90 min. The voltage and time were increased in the case of low percentage gels, 6%, and large molecular weight proteins, such as BRCA2, to100 V for 2 h in cold room.

2.2.2.3. Immunoblot analysis

Nitrocellulose membranes from the WB were first blocked to avoid unspecific bindings, with 4% milk powder in TBS 1x tween 0.1% for at least 1 h, followed by incubation of the primary antibodies performed overnight at 4°C. After primary incubation, membranes were washed with TBS 1x tween 0.1% buffer 3 times for about 10 min. Fluorophore-coupled secondary antibodies were used to visualize the proteins. For this, membranes were placed in black boxes to avoid light contact and incubated with the corresponding LI-COR antibody for 1 h. Afterwards, membranes were washed again 3 times for 10 min each with TBS 1x tween 0.1%, developed in the Odyssey Sa infrared Imaging System (LI-COR) and analysed with the software ImageStudio (version 4.0.21, LI-COR).

In the case of Horseradish-peroxidase (HRP) detection, membranes were washed as described above and incubated with HRP-coupled antibodies for 1 h. After incubation membranes were washed again (described above) and incubated with Immobilon™

Western chemiluminescent HRP Substrate (Millipore) for 2 min. Immediately to this, membranes were developed using Amersham Hyperfilm ECL (GE Healthcare) in an automated CURIX60 (Agfa) developing machine.

2.2.2.4. Purification of recombinant proteins

DPP9 was purified as previously described in (Pilla *et al*., 2012).

PALB2 was obtained from infected Sf9 insect cells (see point 2.2.3.1). The cell pellet from 1 liter of Sf9 expression culture was resuspended, on ice, in 40 ml Lysis Buffer (25 mM HEPES-NaOH pH 7.5, 400mM NaCl, 5 mM imidazole and 5mM β-mercaptoethanol, 1 ug/ml each of leupeptin, pepstatin and aprotinin and 1 mM DTT). Cells were lysed combining a thawing process and a brief sonication step. To remove cell debris and precipitated material, a high-speed centrifugation step (at 50000 x *g* for 60 min and at 4°C) was done. The supernatant arising from this step was incubated with nickel beads (4 ml of nickel beads, previously washed with lysis buffer per liter of culture) at 1000 rpm at 4ºC rotatory for 1 h. Afterwards the incubated product was centrifuged at 1000 rpm and washed twice with wash buffer (25 mM HEPES-NaOH pH 7.5, 50 mM NaCl, 5 mM imidazole and 5mM β-mercaptoethanol) supplemented with protease inhibitors (aprotinin 1µg/ml, leupeptin 1 µg/ml and pepstatin 1µg/ml) and 1 mM (DTT). Elution of proteins was done using a elution buffer (25 mM HEPES-NaOH pH 7.5, 50 mM NaCl, 250 mM imidazole and 5mM β-mercaptoethanol) supplemented with protease inhibitors (aprotinin 1µg/ml, leupeptin 1 µg/ml and pepstatin 1µg/ml) and 1 mM (DTT). Fractions were collected in 2 ml tubes and tested by a dot blot with poinceau staining in a nitrocellulose membrane. Positive fractions were transferred to a centricon 50 KD to concentrate the protein and centrifuged at 3000 g to get around 5 ml of sample. Sample was ultra-centrifugated at 70000 rpm for 30 min at 4ºC. The supernatant was then applied to a Superdex S200 (GE Healthcare, Little Chalfont, UK) size exclusion column equilibrated in: 10 mM HEPES-NaOH pH 7.5, 250 mM NaCl, 5 mM DTT, 1 mM EDTA. The concentration of the purified PALB2 protein obtained was 0,4 mg/ml. Recombinant PALB2 was shock-frozen on liquid N_2 and stored at -80ºC until required.

2.2.2.5. Surface Plasmon Resonance (SPR)

Surface Plasmon Resonance (SPR) allows us to measure direct binding of proteins *in vitro*. To perform the SPRs the Reichert SPR Biosensor (SR 7500 C, Reichert Instruments) was used. For that Ni^{2+} chelator chips (NiHC 1000m, Xantec Bioanalytics, Duesseldorf) were used. The surfaces of the chips were initially purged of contaminants injecting 0.5 M EDTA, pH 8.5, followed by equilibration steps and washing steps of the surface with the immobilization buffer (20 mM Hepes, 150 mM NaCl, pH 7.4, 0.005 % Tween 20). The flow rate of the buffer injection was 30 µl/min. The left channel of the chip surface or the ligand channel was charged with Ni^{2+} (0.3 M $NiSO_4$). His-tagged solution (200 nM) was used for affinity purified DPP9, which was injected at 30 µl/min. of flow rate. DPP9 was immobilized to a response between 2500 to 3500 µRIU. To control the run, the right channel was kept empty and used it as the first reference. Custom-made peptides containing the first 40 amino acids of the BRCA2 N-terminal end were used as the analytes. The peptides were injected over the chip surface at concentrations of: 16, 8, 4, 2, 1, 0.5, 0.25, and 0.125 µM in the different runs. All binding experiments were carried out at a flow rate of 40 µl/min in SPR running buffer (20 mM Hepes, 150 mM NaCl, pH 7.4, 0.005 % Tween 20, 0.05 mM EDTA). After each binding experiment the chip surface was washed (with EDTA 0.5 M, pH 8.5). Analisys was done measuring the response of each analyte sample was doubly referenced with the response obtained from the reference channel, right channel. The response obtained by injecting buffer was analyzed using Scrubber version 2.0c. Finally, Graph Pad Prism 6.0 was used to make the equilibrium binding study.

2.2.3. Cell biology techniques

2.2.3.1. Insect cells

LR recombination reaction was done with 10 µl of Baculo Direct Nterm DNA 300 ng vial, 1 µl of pENTR3C PALB2 (final concentration 260 ng/µl), 5 l TE Buffer pH 8 and 4 µl Clonase II enzyme mix. The recombinant reaction was incubated for 18 h at 25°C.

Transfection and infections were done as follows. Transfection of Mix A containing 8 µl of Cellfectin II reagent and 100 Ml of SF900II media, without antibiotics, was added to transfection Mix B containing the LR recombination reaction 10 µl and 100 Ml of SF900II media. The mixture was mixed without vortex, and incubated for 25 min at RT.

Sf9 cells were seeded at $0.8*10^6$ cells per 6-well plate (total volume 2 ml per well). The transfection mix was added dropwise to the insect cells and incubated for 5 h at 27°C. Afterwards the medium was replaced with SF900II with 10 % FCS and 100 µM Ganciclovir followed by incubation at 27°C for 72 h when signs of infection (big cells) were observed. Finally, cells were splitted and supernatant of infected cells was kept as P1.

Fresh Sf9 insect cells were again seeded in 6-well plates at $0.6*10^6$ cells per 6-well without antibiotics. To obtain P2 fraction, cells were infected with P1 in a dilution 1:10. Afterwards cells were spin down and supernatant kept as P2. This process was repeated once more to obtain fraction P3 using the P2 fraction in a dilution of 1:1000. Cells were harvested by centrifugation at 1000 *g* for 5 min, and the resulting cell pellet was stored at -20°C until day of purification.

2.2.3.2. Mammalian cell culture

For this study two different mammalian cell lines were used: HeLa cells and Mice Embryonic Fibroblasts (MEFs). HeLa cells WT and HeLa DPP9 stable knock down (DPP9 KD) were custom made for us by GenScript and were cultured as previously described in Justa-Schuch *et al*., 2016. Briefly, cells were cultured at 37°C and 5% CO_2 in Dulbecco's modified Eagle's medium which was supplemented with 10% fetal bovine serum, 2 mM L-glutamine, and antibiotics (100 U/ml penicillin and 100 µg/ml streptomycin). 1.5 µg/ml puromycin (Sigma-Aldrich, Germany) was added to the growth medium to maintain the selection pressure on the DPP9 KD cells. In the case of MEF WT and MEF DPP9 gki cells (Gall *et al*., 2013), Dulbecco's modified Eagle's medium supplemented with 10% fetal bovine serum, 2 mM L-glutamine, 100 U/ml penicillin and 100 µg/ml streptomycin was used and cells were incubated at 37°C and 5% CO_2.

2.2.3.3. Silencing

For silencing of DPP9, HeLa cells were transfected following the lipofectamine RNAimax manufacter's instructions. Cells at 50% of confluence ($0.6x10^6$ cells per well in 6 well plates) were transfected with a mix made of two solutions, one containing Gibco® Opti-MEM® (1x; 250 µl) incubated with 4 µl of lipofectamine RNAimax for 5 min and the other one with Gibco® Opti-MEM® (1x; 250 µl) and siRNA (5 µl of siRNA 20 nM), followed by 25 min incubation of the two solutions together. During this time, the medium from the cells was changed into a DMEM supplemented only with FBS and Glutamine. After the 25 min the solution, containing the siRNA oligonucleotides, was added to the wells and then cells were placed in the incubator at 37°C and 5% CO_2 for 4 h. After this time, cells were washed with PBS and cultured with DMEM supplemented with FBS Glutamine and

Penicillin/Streptavidine. For MMC treatment, cells were silenced as mentioned above and after 48 h of silencing, cells were treated with MMC. After 72 h from transfection, cells were harvested with Laemmli buffer and/or in the case of microscopy mples, coverslips were fixed with 4% formaldehyde for 10 min.

2.2.3.4. Cycloheximide chase assays

HeLa cells were seeded at $0.5x10^6$ density in 6 well plates and treated with MMC 300 nM (stock 1.5 mM diluted in Milli-Q water) the next day. After 24 h with MMC, cells were treated with 100 µg/ml cycloheximide (CHX) and in the case of proteasome inhibitor experiment, 100 µM MG132 were added 30 min before adding the CHX or DMSO as a mock. Then, cells were harvested at these time points: 0, 2, 4, 6 and 8 h, using Laemmli buffer 2x and DTT, according to the cell number, followed by liquid N_2. by shock-freeze.

2.2.3.5. Accumulation of DNA damage analysis

HeLa WT and DPP9 KD cells as well as MEF WT and DPP9 gki cells were treated for 24 h with MMC (300 nM) in 6 well plates. For controls (0 h) cells were harvested without MMC at the moment of the treatment. After 24 h treatment cells were washed with PBS and new DMEM medium was added without MMC to let the cells recovered. Samples were harvested with Laemmli buffer 2x at the following time points: 24, 26, 28 and 32 h of damage. To analyse DNA damage 15% gels were run follow by H2AX-P detection in LI-COR. Quantifications were done for γH2AX and H3 bands with Image Studio software and the ratio of γH2AX / H3 was represented in the graphs.

2.2.3.6. Chromatin fractionation

Chromatin fractionation allows to identify proteins binding to DNA. This assay was done with HeLa WT and HeLa DPP9 KD that were seeded in 6 well plates for one day until they reached 90% confluence. Afterwards cells were treated with MMC (300 nM) and harvest after 8 and 24 h. Chromatin fractionation was performed as previously described (Kari V *et al*., 2011). Briefly cells were re-suspended in lysis buffer (10 mM HEPES (pH 7.9), 10 mM KCl, 1.5 mM $MgCl_2$, 0.34 M sucrose, 10% glycerol, 0.1% Triton X-100, 1 mM DTT, and protease inhibitors) and centrifuged at 1500 *g* for 5 min, and the nuclear pellet was lysed in nuclear lysis buffer (3 mM EDTA, 0.2 mM EGTA, 1 mM DTT, and protease inhibitors) for 30 min on ice. Soluble chromatin fractions were separated by centrifuging at 1.700 *g* for 5 min (performed by Vijaya Kari). Chromatin fractions were analyzed by SDS–PAGE electrophoresis. Immunoblotting and antibody incubations were performed according to the standard protocol.

2.2.3.7. Colony Formation Assay

To calculate the respective surviving fractions (SF) after treatment with MMC (0, 5, 10, 20, 40 and 80 ng/ml) and γradiation (0, 1, 2, 4, 6 and 8 γG), a standard colony-forming assay was performed, as previously described (Rave-Frank M, *et al*., 2007). Briefly, the number of MEF cells seeded was 500, 500, 500, 500, 1000 and 1500 cells per well for the MMC treatment: 0, 5, 10, 20, 40 and 80 ng/ml respectively. The number of MEF cells seeded in γradiation was: 500, 500, 500, 1000, 1500 and 2000 respectively to the following doses: 0, 1, 2, 4, 6 and 8 γG. After seeding, cells were treated for 24 h with MMC follow by washing with PBS and incubation for 7 days or exposed to γG radiation and incubated for 7 days. After this time cells were fixed with 70% ethanol, and stained with Mayer's hemalaum (Cat#1.09249.0500, Merck). Non-irradiated cultures and not treated cells with MMC were used for normalization. Colonies with more than 50 cells were counted as survivors. The experiments were performed in triplicate, independently repeated three times, and calculated as the median.

2.2.3.8. Viability assay

To measure the viability of cells according to the metabolic activity, the ATP of cells was measured after DNA damage induction. For this, cells were seeded in white opaque-walled, solid bottom 96-well plates, to avoid light transmission and treated with Olaparib or MMC. Olaparib was added right after seeding and in the case of MMC was added after 18-24 h of seeding. In the olaparib experiment, mock cells were treated with DMSO, at a concentration corresponding to the highest concentration of the drugs added as a control. Remaining wells without cells were filled with PBS in order to obtain a value for background luminescence. Olaparib treatment was performed for 96h meanwhile MMC was done for 72 h. The concentrations used for MMC were 37.5, 75, 150, 300, 600, 1200, and 2400 nM. In the case of Olaparib, the concentrations used were 0.2, 0.5, 1, 5, 7.5, 10, 25, and 50 µM. The total volume of medium per well was 90 µl. To measure the luminescence, the CellTiter-Glo®Luminescence Cell Viability Assay (Promega) was used. 10 µl of CellTiter-Glo®Reagent was added to each well followed by 10 min incubation in dark and shaking in an orbital shaker. Subsequently, the luciferase signal was analysed on a LuminometerDLReadyTMCentro LB 960 reader.

2.2.3.9. Immunofluorescence

HeLa and MEF cells were seeded on coverslips in 24 well plates. Cells were fixed with 4% formaldehyde in PBS and permeabilized with 0.2% Triton-X-100 in PBS for 5 min. Afterwards, cells were washed with PBS 1x three times and blocked with 2% BSA in PBS

1x for 10 min. Both cell lines were incubated with primary antibodies for 90 min at 37°C, following by a PBS wash and a second incubation for 45 min at room temperature with the respective secondary antibodies in dilution 1:500. Finally, cells were washed twice with PBS 1x and once with Milli-Q water, and mounted in fluorescent mounting medium (DAKO) with DAPI. Images were taken using a LSM 510-Meta confocal microscope, oil immersion objective 63x/1.3 (Carl Zeiss MicroImaging, Inc. LSM image Browser software (Carl Zeiss MicroImaging, Inc.) was used to processed the images and image J Fiji software.

2.2.3.10. Proximity Ligation Assay

Proximity Ligation Assay (PLA) was performed using the DUOLINK In Situ PLA Kit from Sigma-Aldrich, according to the manufacturer's protocol. HeLa cells were seeded on coverslips, treated and fixed as described in Immunofluorescence (see section 2.2.3.9.). In the case of DPP9 inhibition studies, 1G244 (10 μM) inhibitor or DMSO as mock was added 30 min before fixation of the cells. HeLa cells were then incubated with primary antibodies, 90 min at 37°C and actin filaments were simultaneously counterstained with CytoPainter Phalloidin-iFluor 488 Reagent (Abcam - #ab176753). To estimate the background staining in each experiment control slides were treated with only one primary antibody. After primary incubation coverslips were washed with PBS, and cells were treated with the PLA reagents according to the manufacturer's protocol. Cells were mounted in DAKO with DAPI fluorescent mounting medium and analysed using a LSM 510-Meta confocal microscope, oil immersion objective 63x/1.3 (Carl Zeiss MicroImaging, Inc.). LSM image Browser software (Carl Zeiss MicroImaging, Inc.) was used to processed the images and subsequently dots were quantified using the Duolink ImageTool (Sigma-Aldrich) (see section 2.2.4.2.).

2.2.4. Microscopy techniques

2.2.4.1. Confocal microscopy

Immunofluorescence and PLA images were acquired with Zeiss LSM 510 meta confocal microscope. Images were taken with the objective LCI Plan-Neofluar 63x/1.3 Imm Corr DIC M27. This objective required the use of water-based Immersol W 2010 immersion oil. Another important component is the X-cite 120 mercury lamp, which has the excitation light source necessary to visualize the cells at the microscope. For immunofluorescence experiments was used different fluorophores with the respective wavelengths was used to visualize in the corresponding channel. For DAPI, a Diode-laser that excite molecules at

405 nm wavelength was used. Secondary antibodies were detected at 488, 594 or 647 nm wavelengths.

To adjust all samples with same conditions, cells were first focused with DAPI (nucleus) using LSM software. In the case of PLA samples after focusing with DAPI, a small re-focusing was done using the channel 594 for the PLA dots to make sure that the dots were in the right plane. Finally, samples were adjusted with the detector gain and amplifier offset (to reduce background), which were settled in control cells to be able to compare with silenced cells. Images were saved as lsm format and exported in jpg format. Analysis of the images was done in FiJi image J software.

2.2.4.2. PLA analysis

Analysis of PLA dots was done with Duolink Image tool (Sigma-Aldrich) software. This software allows to adjust the size of the nucleus and cytoplasm of the cells of the study to be able to quantify as many cells as possible from the images. Once this was defined, the next step was to determine the size of the PLA dots and make a preview run to check the accuracy of the quantification. Finally, all samples from same experiment were analyzed under these conditions and the values were processed in excel. The number of dots in the nucleus or the total number of dots in each image was divided by the total number of cells of the same image. These values were then plotted in a graph in prism software and each dot represented the mean of dots per cell of each image.

3. Results

3.1. Localization of DPP9 after DNA damage induction.

DPP9 is known to localize intracellularly, in the cytosol (Ajami *et al*., 2004) as well as in the nucleus (Justa-Schuch *et al*., 2014). Moreover, DPP9 was found to associate with plasma membrane components and be involved in cell migration and cell adhesion (Zhang *et al*., 2015). To understand better the role of DPP9 in the nucleus, we followed the localization of DPP9 upon different stresses in HeLa wild-type (WT) cells. In this search, we used mitomycin C (MMC), an interstrand crosslinker which creates double-strand breaks (DSBs) in the DNA. Surprisingly, after MMC exposure, cells displayed changes in the localization of the endogenous DPP9 as seen by immunofluorescence (Figure 6A) where endogenous DPP9, in red, changed its distribution after different concentrations of MMC (0 or control, 75, 150 and 300 nM). In untreated or control cells, DPP9, in red, localized all around the cell, with higher intensities in the cytosol and in the leading edge, whereas after MMC treatment, the localization of DPP9 was stronger in and around the nucleus. We used γH2AX, in purple, as DNA damage marker control, since γH2AX is one of the first signals after DSB and represents the phosphorylation of the Histone 2A-X (H2AX) in the serine 139 (γH2AX) by the kinases ATM and ATR (Rogakou *et al*., 1998). γH2AX is required for the binding of proteins involved in the repair of the DNA which makes it a good marker to test DNA damage (reviewed in Turinetto and Giachino, 2015). In addition, we used phalloidin, in green, which stains actin filaments and helps to visualize the cytoplasm and to compare the redistribution of DPP9 through the cell. The cells were quantified according to two groups, either more nuclear or more cytoplasmic, thereby establishing a comparison between nuclear (N) and cytoplasm (C). The quantification emphasized the increase in the nuclear signal of DPP9, which was significantly higher when comparing to the DPP9 cytoplasm signal after MMC treatment (N>C) (Figure 6B). This redistribution of DPP9 upon MMC could implicate a role of DPP9 in DNA damage repair.

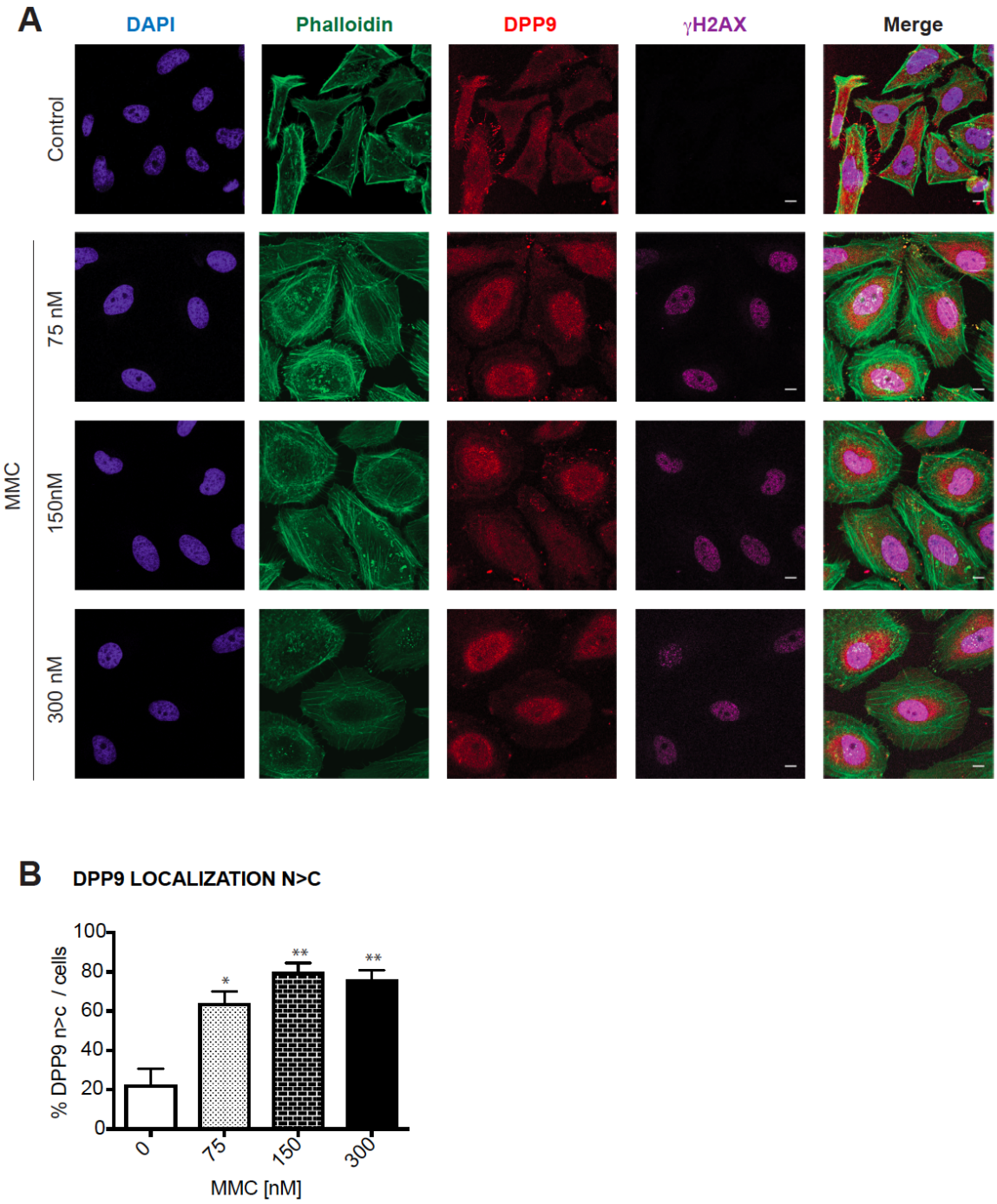

Figure 6. DPP9 localization changes upon MMC treatment.
(A) Immunofluorescence of endogenous DPP9 (in red) in HeLa cells upon different concentrations of MMC (0, 75, 150 and 300 nM) after 24 h. Control channels: Phalloidin (green) stains actin filaments, DAPI (blue) for nucleus and γH2AX (purple) to test the effect of MMC. Scale bar 10μm.
(B) Quantification from (A) comparing the signal of DPP9 in the nucleus to the cytoplasm. Positive cells for N>C present stronger signal in the nucleus and weaker in the leading edge. More than 50 cells were quantified for each condition respectively. Data are represented as the mean ± SEM from three independent experiments. Statistical analysis was carried out by an unpaired two-tailed t-test ($p<0.05$).

3.2. Recruitment of DPP9 to the Chromatin

The change in DPP9 localization upon MMC treatment suggests a possible function of DPP9 in the DDR, which will require that DPP9 localizes in close proximity to the DNA and moreover to the DNA damaged sites. To test that, we analyzed DPP9 in chromatin fractions from HeLa cells after DSB induction with MMC. HeLa WT cells and HeLa DPP9 knock-down (KD) stable cell line, which has a 50% reduction of endogenous DPP9, were treated with MMC for 8 and 24 h followed by isolation of the chromatin (Figure 7A and 7B). Surprisingly, for the first time we found that DPP9 was recruited to the chromatin and more importantly, the levels of DPP9 in the chromatin were increased upon MMC treatment to almost two-fold the amount found in the untreated cells (Figure 7B), thereby confirming that DPP9 senses DNA damage and localizes to chromatin fractions upon DSBs.

This increased found of DPP9 upon MMC correlated with a higher presence of DNA damaged sites as seen by the increased levels of γH2AX. However, the chromatin fractionation assay did not allow us to distinguish between the different sites of the chromatin. Thereby, we applied proximity ligation assay (PLA) to test if the endogenous DPP9 localizes near to the damaged sites, which are known to be positive for γH2AX. PLA is a microscopy method which detects proteins in close proximity, less than 40 nm distance, and represents each interaction event as a dot. PLA was done for endogenous DPP9 and endogenous γH2AX, and interestingly the results showed that DPP9 was in close proximity to the DNA damaged sites upon MMC. Untreated cells had no interaction between the two proteins, which it was expected since H2AX is not strongly phosphorylated in normal cells. To control that the signals were specific for DPP9 we used the stable DPP9 KD cell line (Figure 7C), which showed a significant reduction in the interaction after MMC treatment (Figure 7D).

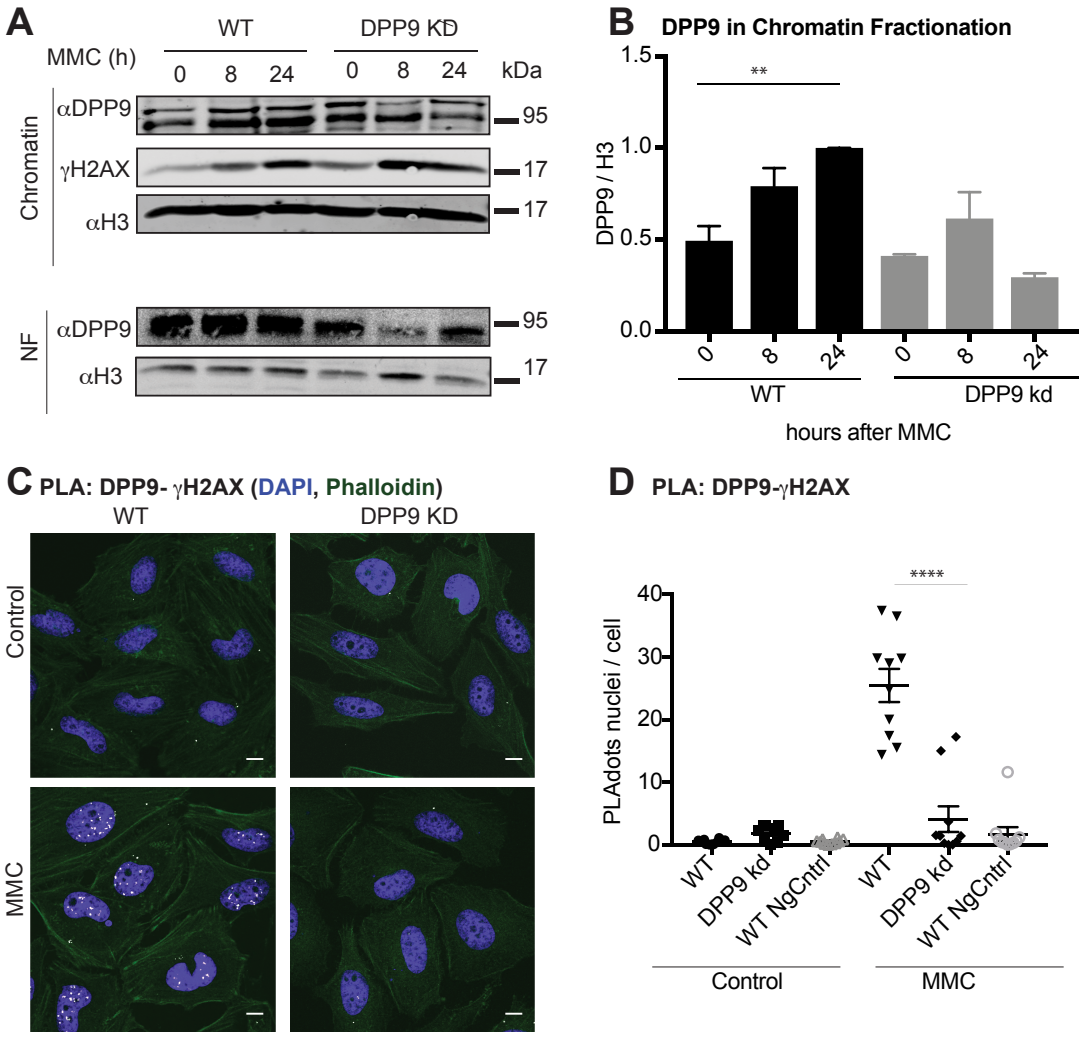

Figure 7. DPP9 localizes to chromatin and is in close proximity to γH2AX.
(A) Chromatin extracts of HeLa cells (WT and DPP9 KD) were obtained after 0, 8 and 24 h of MMC (300 nM) treatment and compared to the Nuclear Fraction (NF) from the same extracts. Samples were analyzed with antibodies against endogenous DPP9 (lower band), γH2AX and Histone 3 (H3). H3 was used as the loading control. Showing one of three independent experiments. Chromatin fractionation was performed by Dr. Vijaya Kari (Prof. Dr. Steven Johnsen, Clinic for General, Visceral and Pediatric Surgery, University of Göttingen) and analyzed by Maria Silva-Garcia (Dr. Ruth Geiss-Friedlander; Molecular Biology, University of Göttingen).
(B) Quantification of endogenous DPP9 signal from chromatin extracts related to endogenous H3 from three independent experiments. Statistical analysis was carried out by an unpaired two-tailed t-test ($p<0.05$).
(C) Proximity ligation assay (PLA) of endogenous DPP9-γH2AX in HeLa WT cells and DPP9 knock-down (KD) cells with MMC (300 nM) shown in white. Phalloidin (actin filaments in green), DAPI (nucleus in blue). Scale bar 10 µm.
(D) PLA dots quantification from (C). Each point represents the mean obtained from one image containing between five to eight cells approximately. In total, more than 50 cells were quantified for each condition respectively. Data are represented as the mean ± SEM and statistical analysis was carried out by an unpaired two-tailed t-test ($p<0.05$).

3.3. DPP9 deficiency leads to DNA damage accumulation after DSBs induction.

As shown before, DSBs induce the recruitment of DPP9 to the DNA, thus suggesting a possible role of DPP9 in DNA damage repair. Surprisingly in the chromatin experiment, we found that DPP9 KD cells displayed higher intensity bands of γH2AX compare to WT cells (Figure 7A and 7B). To further explore whether DPP9 KD cells accumulate more DNA damage, we measured the levels of γH2AX in WT and DPP9 KD cells after DNA damage induction with MMC. Cells were harvested at different time points, before MMC, after 24 h MMC and after a recovery step, which involved a washing step and replacement of the DMEM medium free of MMC, for 2, 4 and 8 h (Figure 8A). Samples were run in SDS-PAGE gels and blot against the endogenous proteins. The intensities of the γH2AX signals were quantified and related to the corresponding loading control, tubulin.

Interestingly, in untreated DPP9 KD cells, time 0, the levels of γH2AX were higher compared to WT cells (Figure 8B upper panel). Upon MMC treatment the difference between HeLa WT and HeLa KD increased significantly, times 24 h to 32 h, suggesting that DPP9 KD cells accumulate more DNA damage. Accumulation of DNA damage in DPP9 KD cells suggests that their repair is slower (Figure 8B upper panel, and 8C). Furthermore, γH2AX was measured in mice embryonic fibroblast, MEF WT, and MEF expressing the inactive mutated form of DPP9, MEF $DPP9^{S729A}$ or MEF DPP9 gki. Inactive DPP9 resulted in stronger levels of γH2AX in non-treated cells, time 0 h, compared to the corresponding WT. In addition, after MMC the levels of γH2AX were also significantly higher in the MEFs DPP9 gki (Figure 8B lower panel, and 8D). Those results suggest that DPP9 enzymatic activity is involved in the repair of DSBs, since inactivation of DPP9 leads to accumulation of DNA damage. Studying the recovery of those cells could be also measure by the levels of γH2AX but using longer time points.

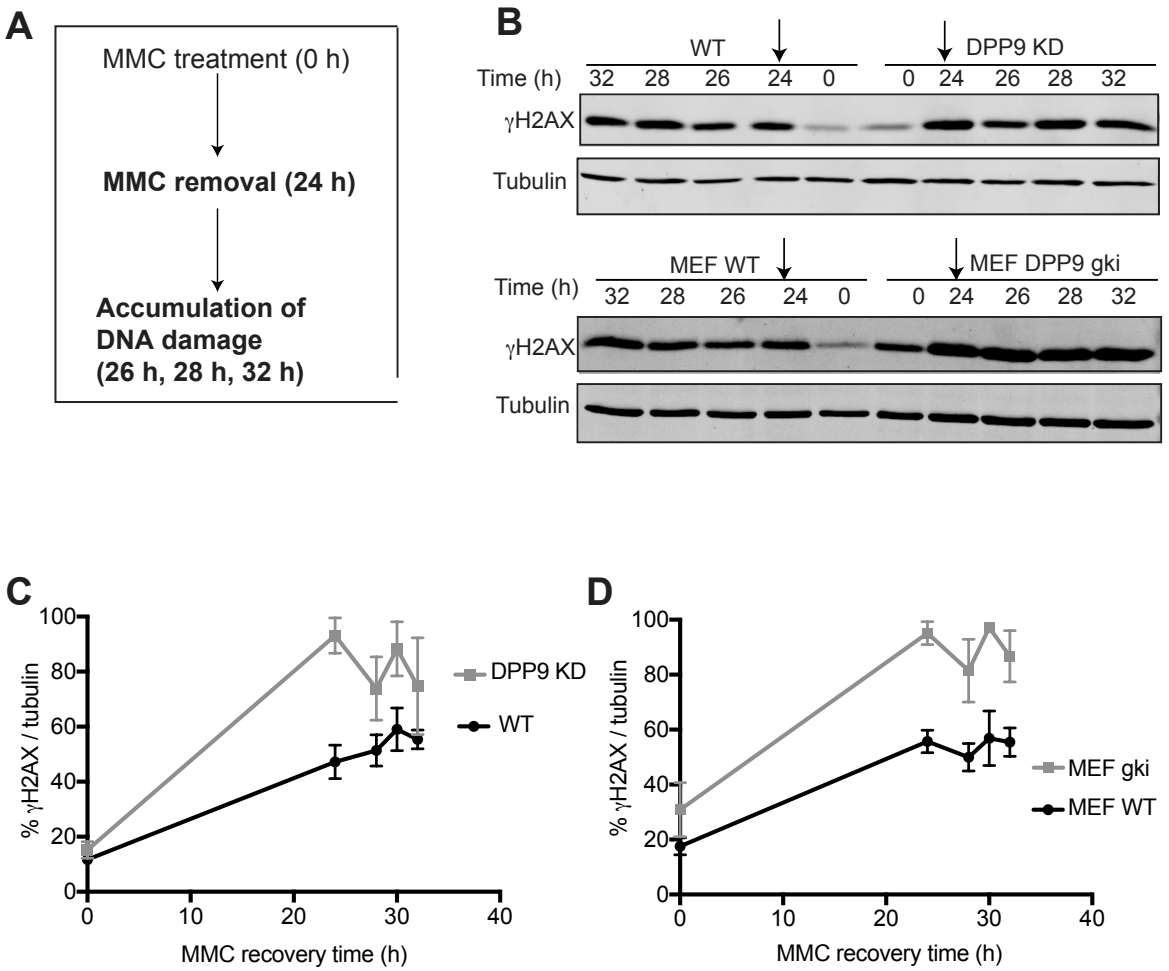

Figure 8. DPP9 deficiency cells accumulate more DNA damage.

(A) Schematic diagram of the MMC accumulation assay. MMC was added for 24 h and the removed from the cells. Cells were harvested after 2 h (26 h), 4 h (28 h) and 8 h (32 h) of MMC removal.

(B) Upper part: γH2AX signals from HeLa WT and DPP9 KD cells harvested at 0, after 24 hours (h) of MMC, and 26 h, 28 h, and 32 h of recovery. Tubulin was used as the loading control. Lower part: same as above but with MEF WT and MEF DPP9 gki. Showing one out of three independent experiments.

(C) Percentage of γH2AX signal divided by tubulin (loading control) in (B) in HeLa cells. Data are represented as the mean ± SEM from three independent experiments. Statistical analysis was carried out by an unpaired two-tailed t-test ($p<0.05$).

(D) Percentage of γH2AX signal divided by tubulin (loading control) in (B) in MEF WT and MEF DPP9 gki. Data are represented as the mean ± SEM from three independent experiments. Statistical analysis was carried out by an unpaired two-tailed t-test ($p<0.05$).

3.4. Decreased cell survival in DPP9 KD cells after DSBs induction.

Accumulation of DNA damaged together with deficient DNA damage repair leads to defects in cell survival (Lord and Ashworth, 2012), thereby cells lacking DPP9 might display survival problems since they accumulate more DNA damage. To accomplish whether DPP9 affects cell survival, we used two different approaches, colony formation assay, and viability assay.

Colony Formation Assay measures the capacity of forming colonies from seeded single cells. Here, we tested the formation of colonies after applying a DNA damage source, either gamma radiation (Gγ) or MMC. The results showed that MEF DPP9 gki cells exhibited fewer colonies compared to MEF WT cells after applying Gγ and more importantly this reduction in survival increased in a dose-dependent manner (Figure 9A). Moreover, similar results were obtained when applying MMC in MEF cells (Figure 9B). MEF DPP9 gki reached half of the survival fraction at a concentration below 40 ng/ml of MMC compared to MEF WT which reached it at 60 ng/ml (Figure 9B).

Additionally, we performed viability assay, which defines the cell survival by measuring the metabolic activity (ATP levels) of the cells. The viability of HeLa WT and HeLa DPP9 KD cells was tested after MMC or after olaparib treatment (Figure 9C and 9D). Olaparib is known to reduce cell survival in cells deficient for BRCA1 or BRCA2 (Zimmer *et al*., 2016, Foo *et al*., 2017) and it is used for the treatment of breast and ovarian cancer (see point 1.2.3.). Interestingly DPP9 KD cells displayed a strong reduction in survival compared to WT cells when treated with MMC or olaparib (Figure 9C and 9D). The half-life of HeLa DPP9 KD cells was reached at 150 nM of MMC compared to the HeLa WT that reached the half-life at 2400 nM of MMC (Figure 9C). Olaparib treatment also manifested a delayed in the half-life of WT cells (10 μM) compared to DPP9 KD which reached at 1 μM of olaparib.

Colony formation assay and viability assay suggest that DPP9 is essential for cell survival. Those results together with the accumulation of DNA damage in DPP9 KD cells and the change in the localization of DPP9, raised the question whether DPP9 targets a regulator of DNA damage repair.

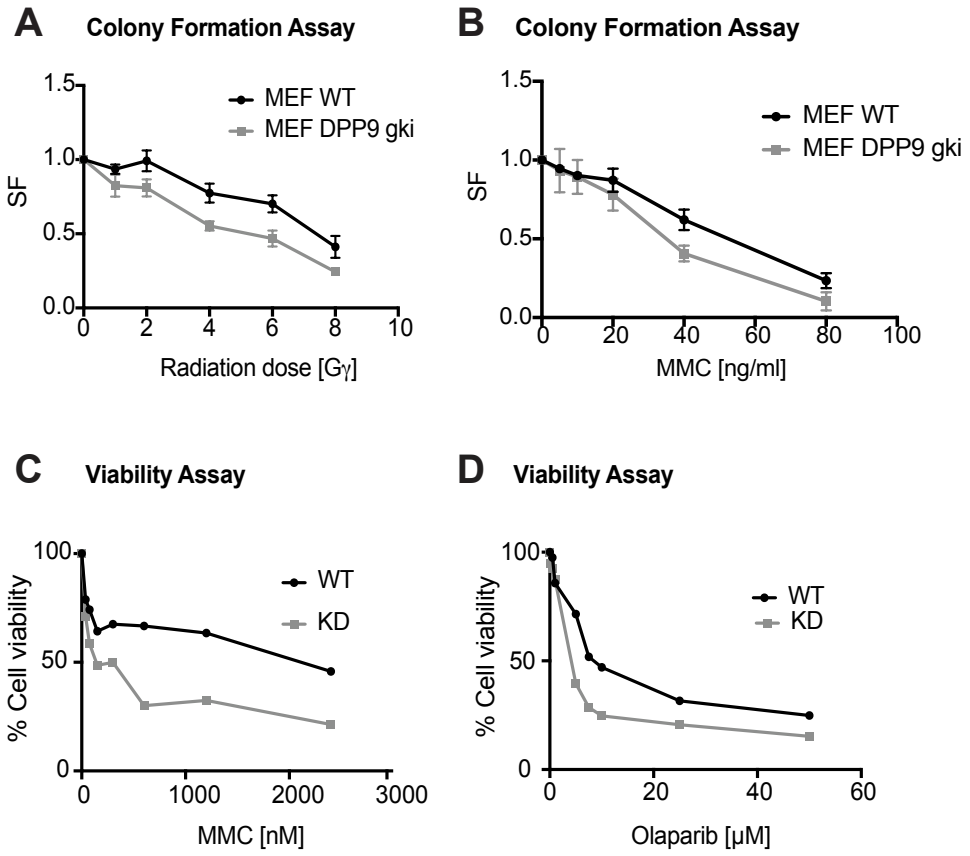

Figure 9. Deficiency of DPP9 activity is sensitive to DSB and reduce survival.
(A) Colony formation after Gγ radiation (0, 1, 2, 4, 8 Gγ) of MEF WT and MEF DPP9 gki showing the mean ± SEM of the survival fraction (SF) from three independent experiments.
(B) Colony formation of MEF WT and MEF DPP9 gki after MMC treatment showing the mean ± SEM of the survival fraction (SF) from three independent experiments. CFAs from (A) and (B) were performed in collaboration with Dr. Spitzner (Clinic for General, Visceral and Pediatric Surgery, Univerisity of Göttingen).
(C) Dose-dependent viability assay of HeLa cells upon 24 h of MMC (0, 37.5, 75, 150, 300, 600, 1200 and 2400 nM) followed by 72 h incubation and measured by luminometer after incubation from 10 min with CellTiter-Glo solution. Showing the mean ± SEM of one out of 3 independent biological replicates where each experiment was performed with three measurements per condition.
(D) Dose-dependent viability assay of HeLa cells upon Olaparib (0, 0.2, 0.5, 1, 5, 7.5, 10, 25 and 50 µM) treatment for 96 h and measured by luminometer after incubation from 10 min with CellTiter-Glo solution. Showing the mean ± SEM of one out of 3 independent biological replicates where each experiment was performed with three measurements per condition. Viability assays from (C) and (D) were performed in collaboration with Nadine Stark (Prof. Dr. Dobbelstein, Molecular Oncology, University of Göttingen).

3.5. DPP9 is in close proximity to BRCA2 and this interaction increases upon MMC treatment

In a recent publication, we showed that DPP9 binds FLNA and through this binding DPP9 can recruit its substrate Syk (Justa-Schuch *et al*., 2016). Until date, FLNA has been reported to bind around 90 proteins (Shao *et al*., 2015) among which we can find the breast cancer type 2 protein (BRCA2), a key regulator of HR, which binds in the C-terminal region of FLNA (Yuan and Shen, 2001). BRCA2 contains a Met-Pro (MP) in the N-terminal, which makes it a putative substrate of DPP9. Preliminary PLA approach performed by a previous student in the lab (Dr. Esther Pilla) showed close proximity between endogenous BRCA2 and DPP9. We speculate that this interaction of BRCA2 and DPP9 involves the N-terminal of BRCA2 since the N-terminal of BRCA2 contains a potential DPP9 cleavage site (Met-Pro). Thereby, proteins binding in the N-terminal of BRCA2 raised the interest of the study concerning DPP9 binding and function. One of the proteins that binds in the N-terminal of BRCA2 is PALB2, which binds between amino acids 21 to 39, (Xia *et al*., 2006).

The interaction between BRCA2 and PALB2 is known to be stable and to increase upon DSBs (Xia *et al*., 2006). In our studies by PLA, we induce DSBs in cells by using different doses of MMC (0, 75, 150, and 300nM for 24 h). We found that BRCA2 and PALB2 interaction manifested a significant increase upon 300 nM of MMC treatment but not in lower doses (Figure 10A third column and 10D).

Next, we explored whether DPP9 and BRCA2 are affected upon MMC. Curiously, the interaction between DPP9 and BRCA2 increased significantly upon MMC treatment (Figure 10A first column and 10B) and more surprisingly, this increase in the interaction was shown at lower doses (75 nM) of MMC.

Since BRCA2 and PALB2 are in close proximity and this increases upon DNA damage we also look for the proximity of DPP9 to PALB2. As seen with BRCA2, DPP9 increases its proximity to PALB2 significantly upon MMC treatment (Figure 10A second column and 10C).

This increased found in the DPP9 proximity to either BRCA2 and PALB2 after DNA damage induction suggests that DPP9 may form part of the complex of BRCA2 and PALB2 and probably be involved in the HR repair.

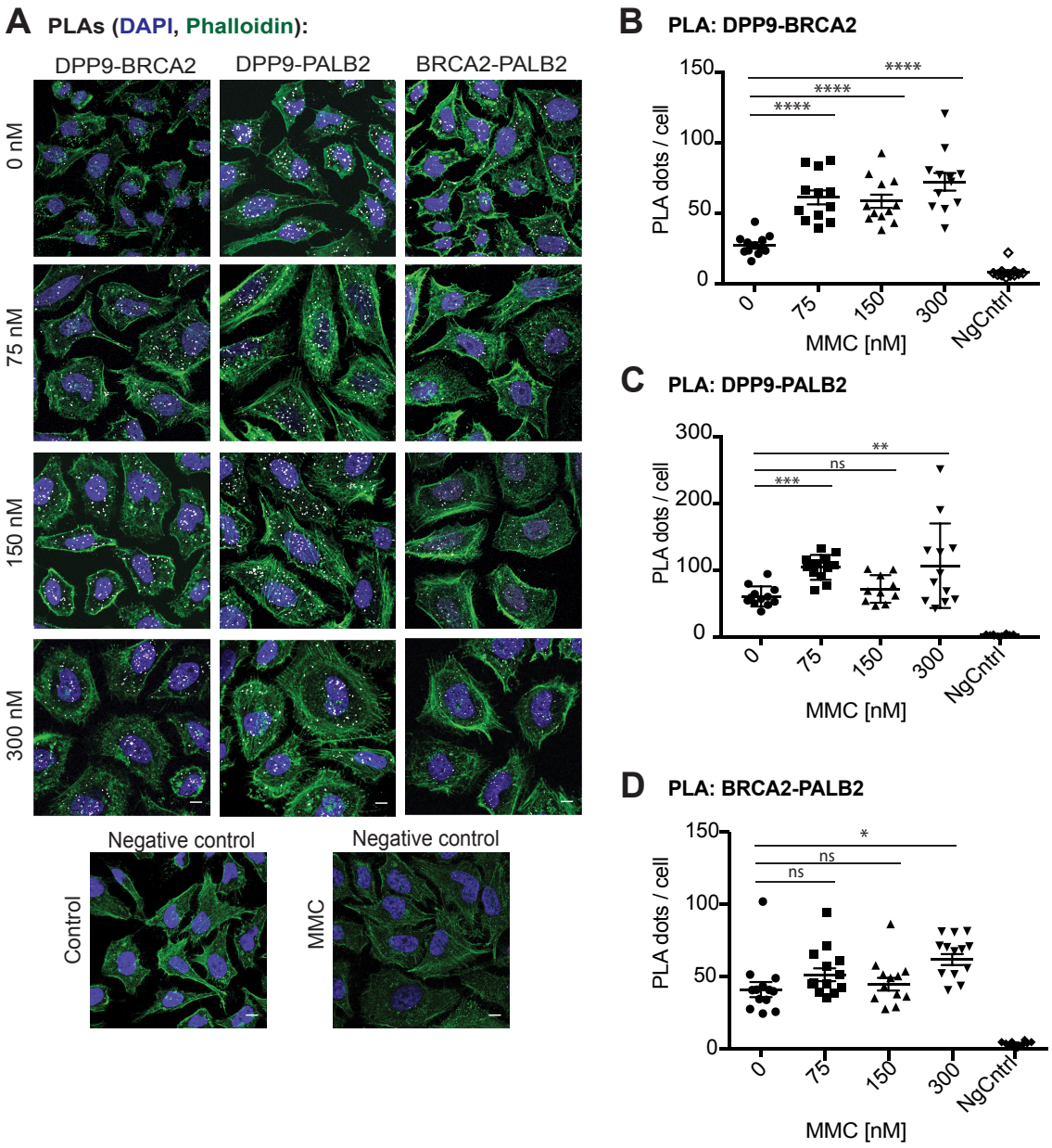

Figure 10. DPP9 increases its interaction with BRCA2 after MMC treatment.
(A) PLA of endogenous BRCA2-PALB2, endogenous DPP9-BRCA2 and endogenous BRCA2-PALB2 after 24 h of MMC (0, 75, 150 and 300 nM) in HeLa WT. Negative controls were done using only anti-BRCA2 as primary antibodies in WT control and WT with MMC treatment. Phalloidin (actin filaments in green), DAPI (nucleus in blue). Scale bar 10µm.
(B) Quantification of PLA from DPP9-BRCA2 upon MMC treatment showing dots per cell (>50 cells per condition) of one of 3 independent experiments. Statistical analysis was carried out by an unpaired two-tailed t-test ($p<0.05$).
(C) As in (B) quantification of PLA from endogenous DPP9-PALB2 interaction.
(D) As in (B) quantification of PLA from BRCA2-PALB2.

3.6. FLNA silencing reduces DPP9 binding to BRCA2 in MMC treated cells

As shown in our previous study, FLNA acts as a platform to recruit Syk to DPP9 (Justa-Schuch *et al.*, 2016). Here, we tested whether FLNA is also involved in the interaction of DPP9 and BRCA2. We tested the interaction of BRCA2 and DPP9 upon DNA damage induction in cells lacking FLNA. Surprisingly, BRCA2 and DPP9 interaction was significantly reduced after MMC in siFLNA cells compared to non-targeted silenced (siNT) cells with MMC (Figure 11A and 11B). The number of interactions found in control cells (without MMC) was similar in both cells, siNT and siFLNA. Upon MMC treatment, siNT cells experienced a significant increased that was not observed in siFLNA cells with MMC (Figure 11B).

This result, together with our previous publication, strongly suggests that FLNA acts as a platform for recruitment of substrates to DPP9.

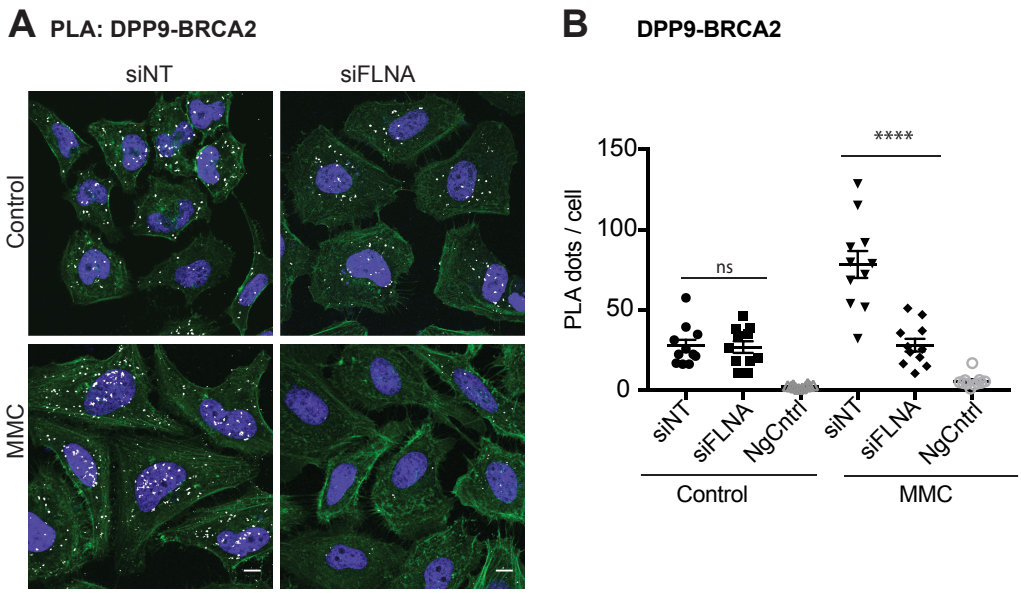

Figure 11. FLNA silencing reduces DPP9 binding to BRCA2 in MMC treated cells.
(A) PLA of endogenous DPP9-BRCA2 (white dots) in HeLa cells treated with a control (siNT) or a FLNA siRNA (siFLNA) for 48 h followed by 24 h of MMC (300 nM). The negative control for the method was done using one single primary antibody, anti BRCA2. Phalloidin (actin filaments in green), DAPI (nucleus in blue). Scale bar 10 µm. Showing one of 3 independent experiments.
(B) Quantification of PLA from (A) DPP9-BRCA2 showing dots per cell. Data are represented as the mean ± SEM. Showing one of 3 independent experiments. Signals of more than 50 cells were quantified for each condition respectively. Statistical analysis was carried out by an unpaired two-tailed t-test ($p<0.05$).

3.7. DPP9 interacts directly with BRCA2 peptide *in vitro*

In the previous assays, we found that DPP9 and BRCA2 are in close proximity by PLA, however, we did not prove a direct interaction between the two proteins. To accomplish whether the interaction is direct, we used Surface Plasmon Resonance (SPR), which allows us to measure direct binding between proteins and also to calculate the affinity of the binding *in vitro*. For that, we used recombinant DPP9, which was purified from insect cells and two peptides of the N-terminal of BRCA2 (Figure 12A-C).

Recombinant DPP9, obtained from insect cells (Figure 12A and 12B) was immobilized in the surface of the chip of the SPR, followed by the measurement of the binding to the peptide of BRCA2 containing the first 40 amino acids. SPR results showed a direct interaction between recombinant DPP9 and the N-terminal of BRCA2, with a high binding affinity of K_D 16.8 ± 0.7 μM (Figure 12C). Interestingly the affinities obtained in this experiment for DPP9 and $BRCA2_{1-40}$ peptide were higher than the affinity to DPP9 and $BRCA2_{3-40}$ peptide, which was of K_D 75.3 ± 4.8 μM. SPR analysis suggested that the Met-Pro in the N-terminal of BRCA2 increases the binding to DPP9 protein.

Moreover, we purified PALB2 from insect cells in order to use it for *in vitro* assays. However, the purification was not efficient enough. The expected peak of PALB2 after purification in the S-200 size exclusion column was in the first fractions, which correspond with the molecular weight of 170 kDa. The A1-A4 fractions were selected for concentration of the protein. As seen in the graph (Figure 12D), there were extra peaks of lower molecular weight products. Those peaks were seen in coomassie staining gel (Figure 12E) as side bands of lower molecular weight. To control that we purified PALB2 protein we performed immunoblotting using PALB2 antibody (Figure 12F). Immunoblot showed the band corresponding with the specific PALB2 protein band as well as side bands of lower molecular weight. Recognition of those side bands with PALB2 antibody indicates that those bands are degradation products from PALB2. To optimize the purification of the protein we could add additional protease inhibitors or increase their concentration to reduce the degradation, as well as, use a C-terminal end tag in PALB2, besides the N-terminal end tag, to capture the full-length protein.

A Coomassie staining for purified DPP9

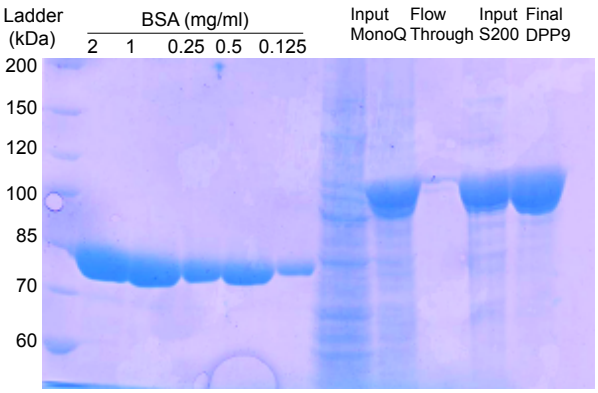

B Cromatograph of purified DPP9 after S200 column

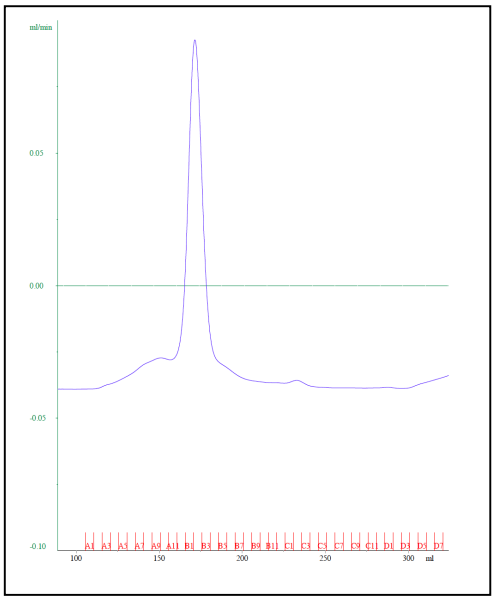

C SPR of DPP9 purified protein with BRCA2 peptides

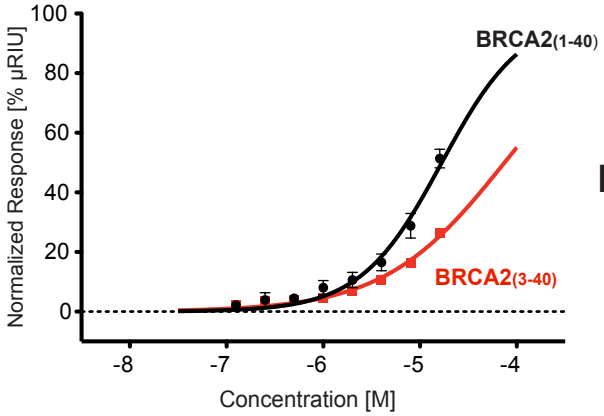

D Cromatograph of purified PALB2 after S200 column

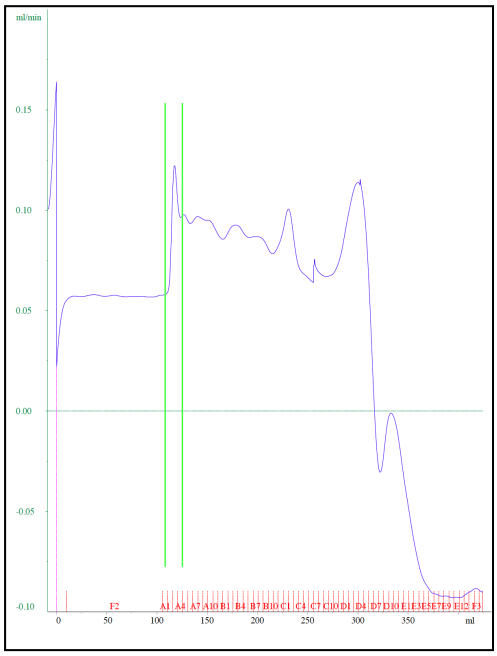

E

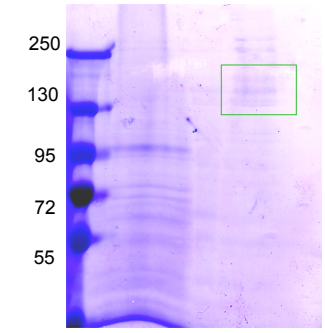

F

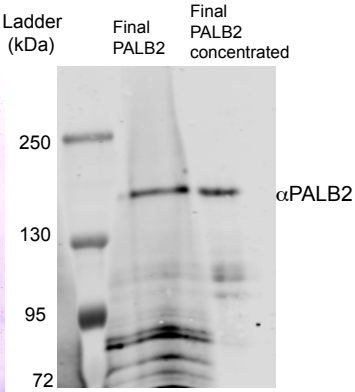

Figure 12. DPP9 shows direct interaction with BRCA2$_{1-40}$ peptide.
(A) Coomassie staining from DPP9 purification fractions showing inputs loaded into column monoQ and S200 of Äkta, and the final DPP9 protein (6 mg/ml).
(B) Chromatograph obtained for DPP9 after purification with Superdex S200 size exclusion column from ÄKTA.
(C) Surface plasmon resonance (SPR) from DPP9-BRCA2$_{1-40}$ peptide (black) and DPP9-BRCA2$_{3-40}$ peptide (red) from three independent experiments. Performed by Dr. Markus Killisch (Prof. Dr. Schwappach, Molecular Biology, University of Göttingen).
(D) Chromatograph obtained for PALB2 after Superdex S200 size exclusion column from ÄKTA. Fractions A1-A4 were selected for concentration and further analysis in coomassie (E) and blot (F) for PALB2.
(E) Coomassie staining of PALB2 samples showing the input of the S-200 size exclusion column and the final PALB2 obtained after the S-200 column. Bands corresponding with PALB2 protein were weak and some side band were observed.
(F) Blot of purified PALB2 before and after concentration. Developed with anti-PALB2 antibody. Side bands were detected with PALB2 antibody suggesting that those bands are degradation products from PALB2.

3.8. Inactive DPP9 shows reduce interaction with BRCA2

We showed that the interaction between DPP9 and BRCA2 occurs in the N-terminal of BRCA2 by SPR analysis. As DPP9 is an aminodipeptidase, we expected that the binding site of DPP9 to BRCA2 involves the active site of DPP9. A previous study in our group, performed by Dr. Esther Pilla and Dr. Christoph Lenz, found that the BRCA2$_{1-40}$ peptide was cleaved by recombinant DPP9 after *in vitro* incubation and Mass Spectrometry analysis.

To test whether DPP9 required the active site for BRCA2 binding in cells, we used the 1G244 inhibitor, which was designed as a competitive inhibitor of DPP9 and DPP8 (Wu *et al*., 2009). 1G244 (10 μM) was applied to the cells for 30 min, untreated or previously treated with MMC, and followed by PLA analysis of endogenous DPP9 and BRCA2. Remarkably, cells treated with 1G244 showed a reduction in the interaction events of endogenous DPP9 and BRCA2 (Figure 13A and 13B) and more importantly, after MMC treatment plus 1G244 inhibitor, cells had a significant decreased in DPP9-BRCA2 interaction (Figure 13A and13B). This decreased in DPP9 and BRCA2 interaction after 1G244 treatment together with the SPR results strongly suggest that the active site of DPP9 is important for the binding of BRCA2 and that BRCA2 might be a substrate of DPP9.

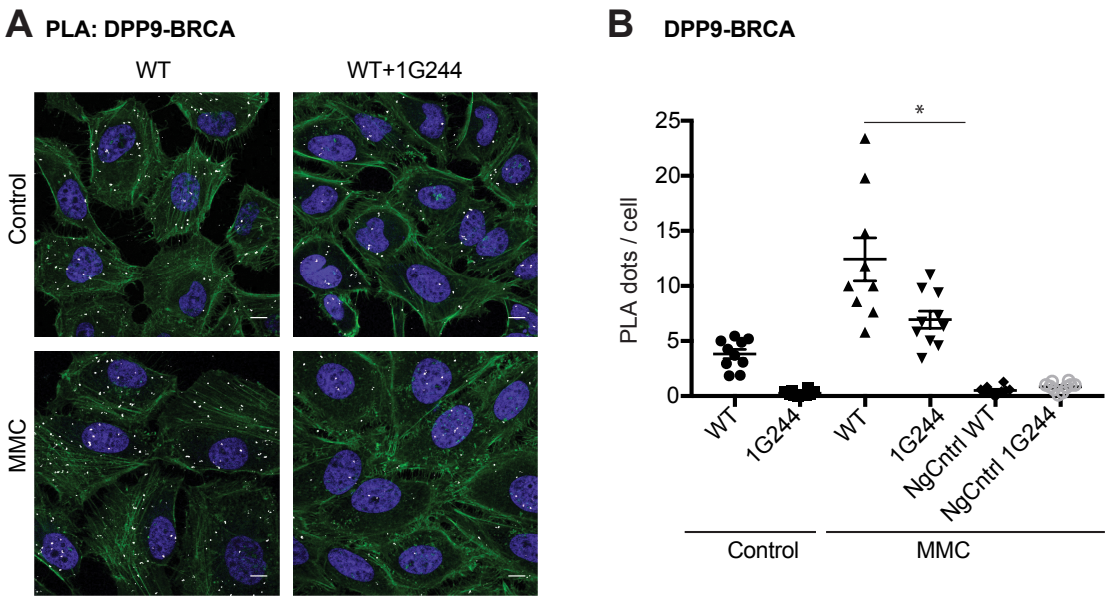

Figure 13. 1G244 inhibitor of DPP9 reduces its interaction with BRCA2.
(A) PLA of endogenous DPP9-BRCA2 (white) in HeLa cells treated with MMC for 24 h followed by treatment of 1G244 inhibitor or DMSO as mock for 30 min. Phalloidin (actin filaments in green), DAPI (nucleus in blue). Scale bar 10µm.
(B) Quantification of PLA (A) showing dots per cell (>50 cells per condition) of one of 3 independent experiments. Statistical analysis was carried out by an unpaired two-tailed t-test ($p<0.05$).

3.9. DPP9 silencing stabilizes BRCA2 protein

In our previous study, we showed that DPP9 can regulate the stability of Syk protein by the cleavage of the first two amino acids, which exposes the third amino acid in the N-terminal and targets the protein for degradation (Justa-Schuch *et al.*, 2016). This was the first time to connect DPP9 with the N-end rule pathway, which defines that the N-terminal end of proteins presents degradation signals or N-degrons, which are recognized by E3 ligases and targeted to the proteasome (see point 1.3.2.; Varshavsky, 2011). In BRCA2, the third amino acid after the Met-Pro, is isoleucine, which is classified as a destabilizing residue (see poing 1.3.2.). We studied the stability of BRCA2 in WT cells and cells deficient or inactive for DPP9 using CHX, which blocks translation of proteins and helps to analyze the half-life of a protein.

First, we tested the antibodies against endogenous BRCA2 and DPP9 after silencing the proteins followed by WB analysis (Figure 14A), which showed specific signals for BRCA2 at around 384 kDa.

Due to the little information about BRCA2 half-life, we started measuring the stability of BRCA2 by CHX chases in untreated WT cells and in cells treated with MMC (300 nM for 24 h), which induces DSBs. Quantification of BRCA2 bands intensities was related to the corresponding bands of the loading control, vinculin. Interestingly the results showed that the half-life of BRCA2 in control WT cells was between 7 to 8 h, meanwhile in WT cells treated with MMC, the half-life of BRCA2 was drastically reduced to 2 h (Figure 14B and 15C). Next, we tested the effect of DPP9 in BRCA2 stability using MMC in WT cells and DPP9 KD stable cell line, as well as in transiently silenced cells for DPP9 (siDPP9) with the corresponding siNT control. BRCA2 half-life increased up to 6 h in cells silenced for DPP9 (80 % DPP9 silencing) with MMC compared to siNT cells with MMC, which half-life was around 2 h, as seen in Figure 14B. Similar results were observed in the stable cell lines, where DPP9 is 50% knock-down (Figure 14F and 14G).

Compellingly, the results from these CHX chases showed stabilization of BRCA2 in cells lacking DPP9 compared to WT cells after MMC treatment (Figure 14D-G), thereby, involving DPP9 in the degradation of BRCA2.

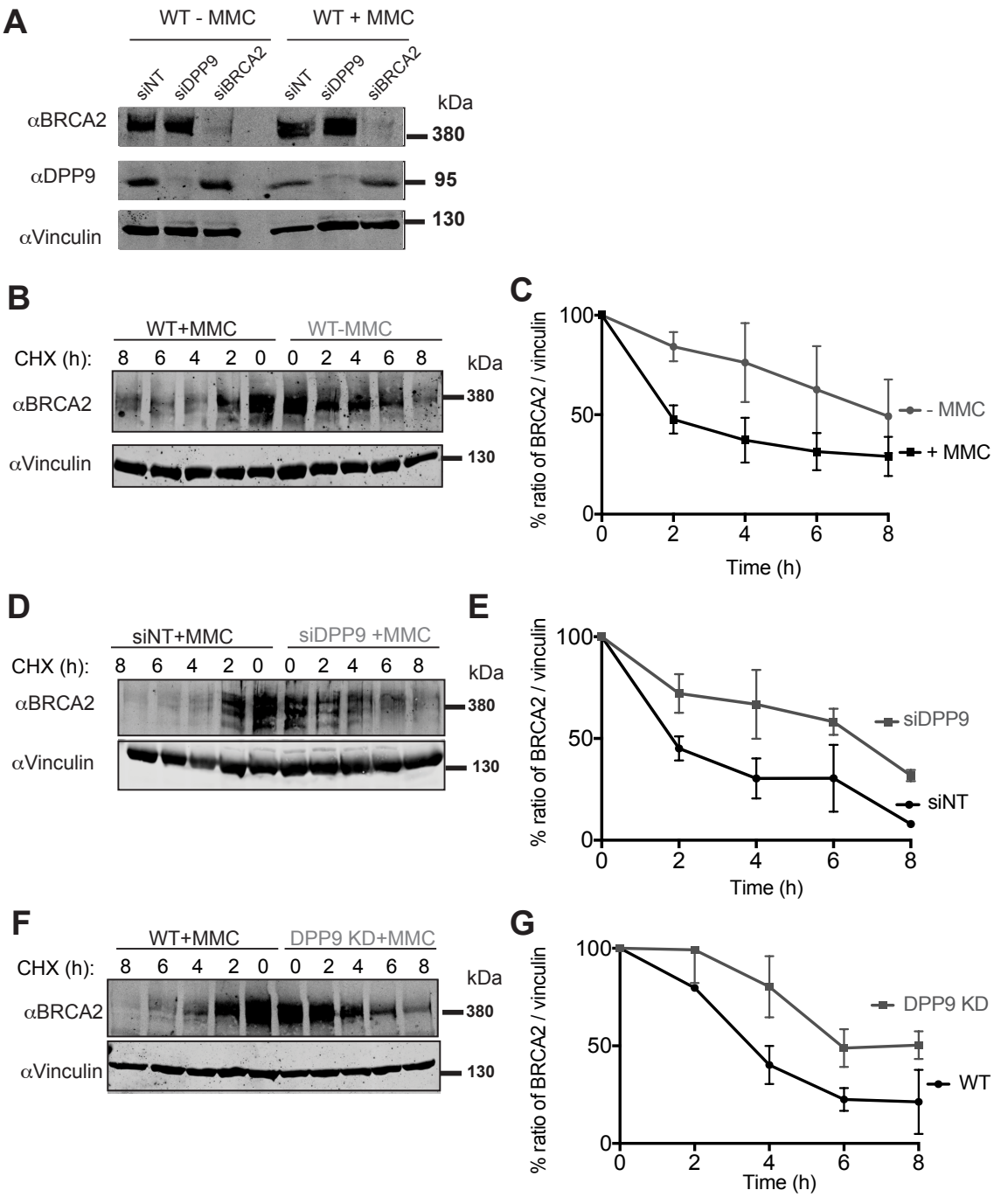
A
WT - MMC
WT + MMC
siNT
siDPP9
siBRCA2
siNT
siDPP9
siBRCA2
kDa
αBRCA2
380
αDPP9
95
αVinculin
130
B
WT+MMC
WT-MMC
CHX (h):
8 6 4 2 0 0 2 4 6 8
kDa
αBRCA2
380
αVinculin
130
C
% ratio of BRCA2 / vinculin
100
50
0
0 2 4 6 8
Time (h)
- MMC
+ MMC
D
siNT+MMC
siDPP9 +MMC
CHX (h):
8 6 4 2 0 0 2 4 6 8
kDa
αBRCA2
380
αVinculin
130
E
% ratio of BRCA2 / vinculin
100
50
0
0 2 4 6 8
Time (h)
siDPP9
siNT
F
WT+MMC
DPP9 KD+MMC
CHX (h):
8 6 4 2 0 0 2 4 6 8
kDa
αBRCA2
380
αVinculin
130
G
% ratio of BRCA2 / vinculin
100
50
0
0 2 4 6 8
Time (h)
DPP9 KD
WT

Figure 14. BRCA2 stability decreases upon MMC treatment, and DPP9 silenced cells compensate the decreased in the half-life of BRCA2 after MMC treatment.
(A) Immunoblot of endogenous BRCA2 and DPP9 upon DPP9 silencing in HeLa cells. Vinculin was used as the loading control.
(B) CHX chase of HeLa WT -/+ MMC (300 nM for 24 h) harvested after 0, 2, 4, 6, and 8 h of CHX (125 µg/ml) and immunoblotted against BRCA2 and Vinculin as the loading control.
(C) Percentage of BRCA2 signals related to Vinculin signals of CHX in HeLa WT -/+ MMC (300 nM for 24 h). Data are represented as the mean ± SEM from three independent experiments.
(D) CHX chase of HeLa WT + MMC (300 nM for 24 h) in NT cells (siNT) and DPP9 silenced cells (siDPP9) harvested after 0, 2, 4, 6, and 8 h of CHX (125 µg/ml) and immunoblotted against BRCA2 and Vinculin as the loading control.
(E) Percentage of BRCA2 signals related to Vinculin signals from CHX in HeLa WT + MMC (300 nM for 24 h) in NT cells (siNT) and DPP9 silenced cells (siDPP9). Data are represented as the mean ± SEM from three independent experiments.
(F) CHX chase of HeLa WT and HeLa DPP9 KD stable cell line + MMC (300 nM for 24 h) harvested after 0, 2, 4, 6, and 8 h of CHX (125 µg/ml) and immunoblotted against BRCA2 and Vinculin as the loading control.
(G) Percentage of BRCA2 signals related to Vinculin signals from CHX chase of HeLa WT and HeLa DPP9 KD stable cell line + MMC (300 nM for 24 h). Data are represented as the mean ± SEM from two independent experiments.

A previous study, inhibition of the proteasome results in higher levels of the nuclear BRCA2 in cells lacking PALB2 (Xia *et al*., 2006). To test whether the proteasome is involved in the process, we performed CHX chases in cells treated with the proteasome inhibitor MG132. Accordingly, we showed that after blocking translation of proteins with CHX, BRCA2 is stabilized in MG132 treated cells in the same manner as after DPP9 silencing (Figure 15A and 15B). All together shows for the first time that BRCA2 stability is regulated by DPP9 and by the proteasome.

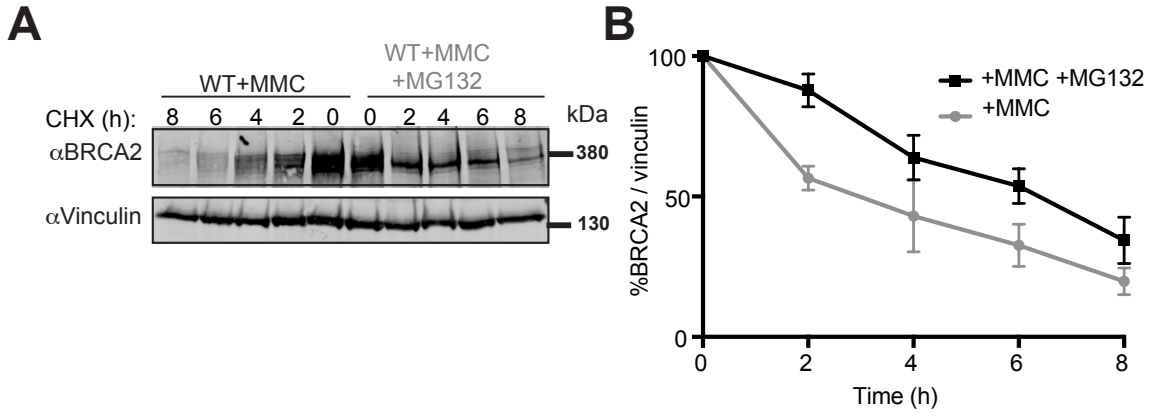

Figure 15. The proteasome is involved in BRCA2 degradation.
(A) CHX chase of HeLa WT + MMC (300 nM for 24 h) in WT cells -/+ MG132 harvested after 0, 2, 4, 6, and 8 h of CHX (125 µg/ml) and immunoblotted against BRCA2 and Vinculin as the loading control.
(B) Percentage of BRCA2 signals related to Vinculin signals from (A). Data are represented as the mean ± SEM from three independent experiments.

3.10. DPP9 silenced cells do not affect the formation of BRCA1 foci

In our results, we found that DPP9 is involved in DNA damage repair (Figure 7 and 8). We also found that DPP9 binds to BRCA2 and this binding increases after DNA damage (Figure 10). Importantly, BRCA2 is necessary for HR repair and its recruitment to the DSBs sites it is BRCA1-PALB2 dependent. More specifically, BRCA1 binding to the DNA occurs upstream to the recruitment of PALB2 and BRCA2 complex to the DNA damage sites. The binding of BRCA1 to the DSBs can be visualized as foci at the microscopy.

To test if DPP9 is involved in early HR steps we looked at BRCA1 foci by immunofluorescence against endogenous BRCA1. We used DPP9 silenced (siDPP9) HeLa cells and treated with MMC. Immunofluorescence results showed that BRCA1 foci (green) formation is not affected after DNA damaged induction with MMC in DPP9 silenced cells (Figure 16A-C). To control the DNA damage induction by MMC, we used antibody against endogenous γH2AX (red) as a marker. DPP9 silencing was controlled using antibody against endogenous DPP9 (purple). Notably, control cells (without DNA damage induction) showed a small increased in BRCA1 foci formation in DPP9 silenced cells (siDPP9; Figure 16C) compared to control cells siNT. Thus, suggesting that siDPP9 cells have activated the repair mechanisms. The DNA damage repair pathways are activated upon DNA damage. siDPP9 cells have higher levels of DNA damage compared to siNT cells, which correlates with the increased of DNA damaged found before in the stable DPP9 KD cells (Figure 8B and 8C) and in cells inactive for DPP9 (Figure 8B and 8D).

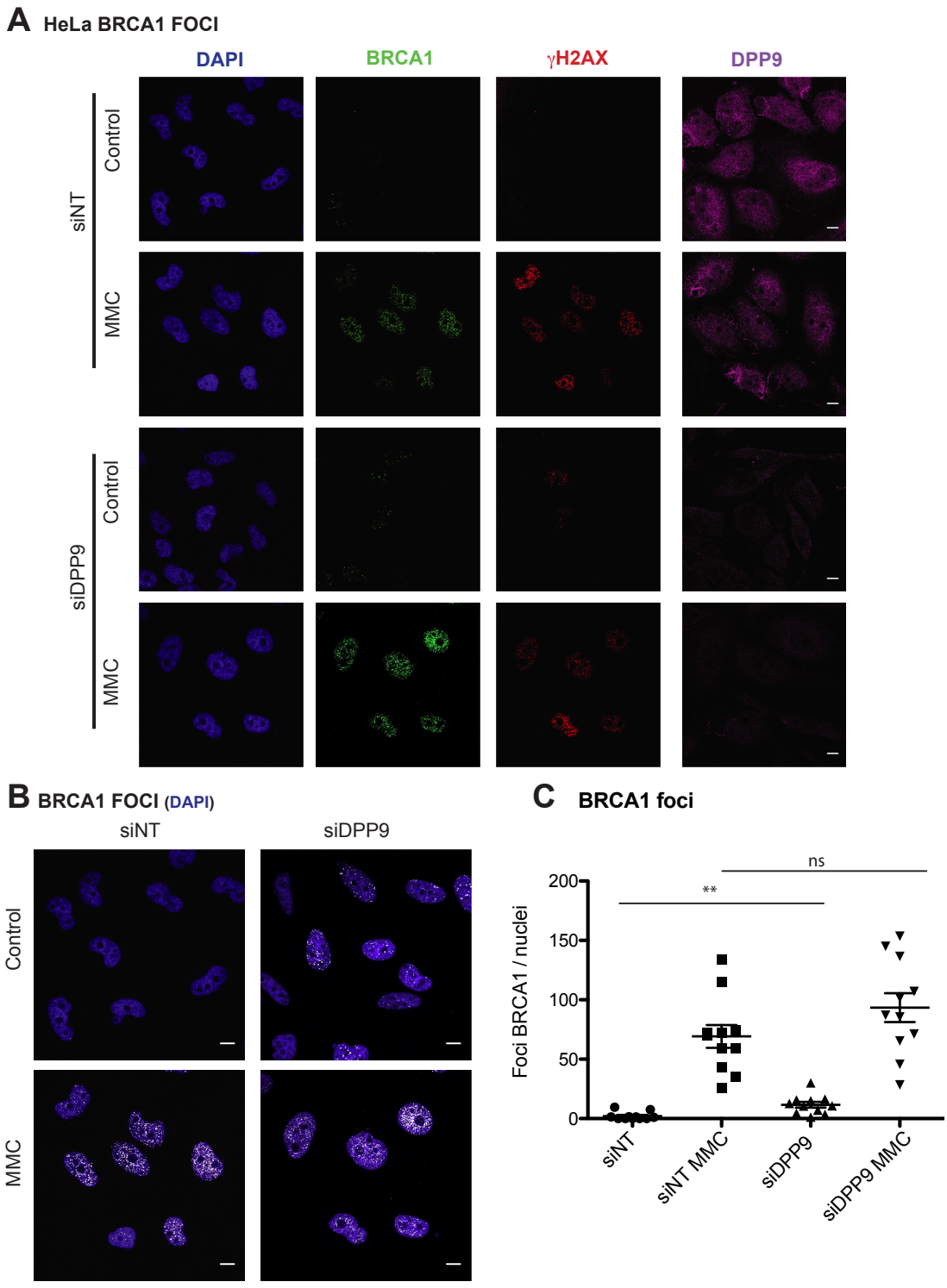

Figure 16. HeLa siDPP9 cells have no effect in BRCA1 foci formation after MMC treatment.

(A) IF of endogenous BRCA1 in HeLa siNT and siDPP9 cells showing BRCA1 foci (green) after 24 h of MMC (300 nM) treatment, γH2AX (red) as a DNA damage control, DPP9 (purple) and nucleus in DAPI (blue), scale bar 10 μm.
(B) Merge images from (A). BRCA1 foci (white) nucleus (blue). Scale bar 10 μm.
(C) Quantification of BRCA1 foci from (B) showing the number of dots per nucleus of one out of three independent experiments. Data are represented as the mean ± SEM. Signals of more than 50 cells were quantified for each condition respectively. Statistical analysis was carried out by an unpaired two-tailed t-test ($p<0.05$).

3.11. Defects in DPP9 results in lower BRCA2-BRCA1 binding

Defects on DPP9 expression did not have an effect in BRCA1 recruitment. At the same time, we found more damages in cells lacking DPP9. Next step, after BRCA1 has bound to the DNA, is the recruitment of PALB2-BRCA2 complex (Xia *et al*., 2006). PALB2 binds directly to BRCA1 and essential for recruitment of BRCA2 to the DSB sites (Xia *et al*., 2006; Figure 2). To define the step of HR repair in which DPP9 is involved we look at BRCA1 and PALB2 interaction in cells lacking DPP9. We tested whether silencing of DPP9 influence the binding of PALB2 to BRCA1 by PLA assay (Figure 17A and 17B). PLA results show that BRCA1 and PALB2 interaction is not affected upon DPP9 silencing.

Next, we look at BRCA2 recruitment to the DSB sites by measuring the proximity to BRCA1 in DPP9 silenced cells and after MMC treatment. In contrast to PALB2, the binding of BRCA2 to BRCA1 was reduced in cells lacking DPP9 expression (Figure 17C and 17D), suggesting that DPP9 regulates BRCA2 localization.

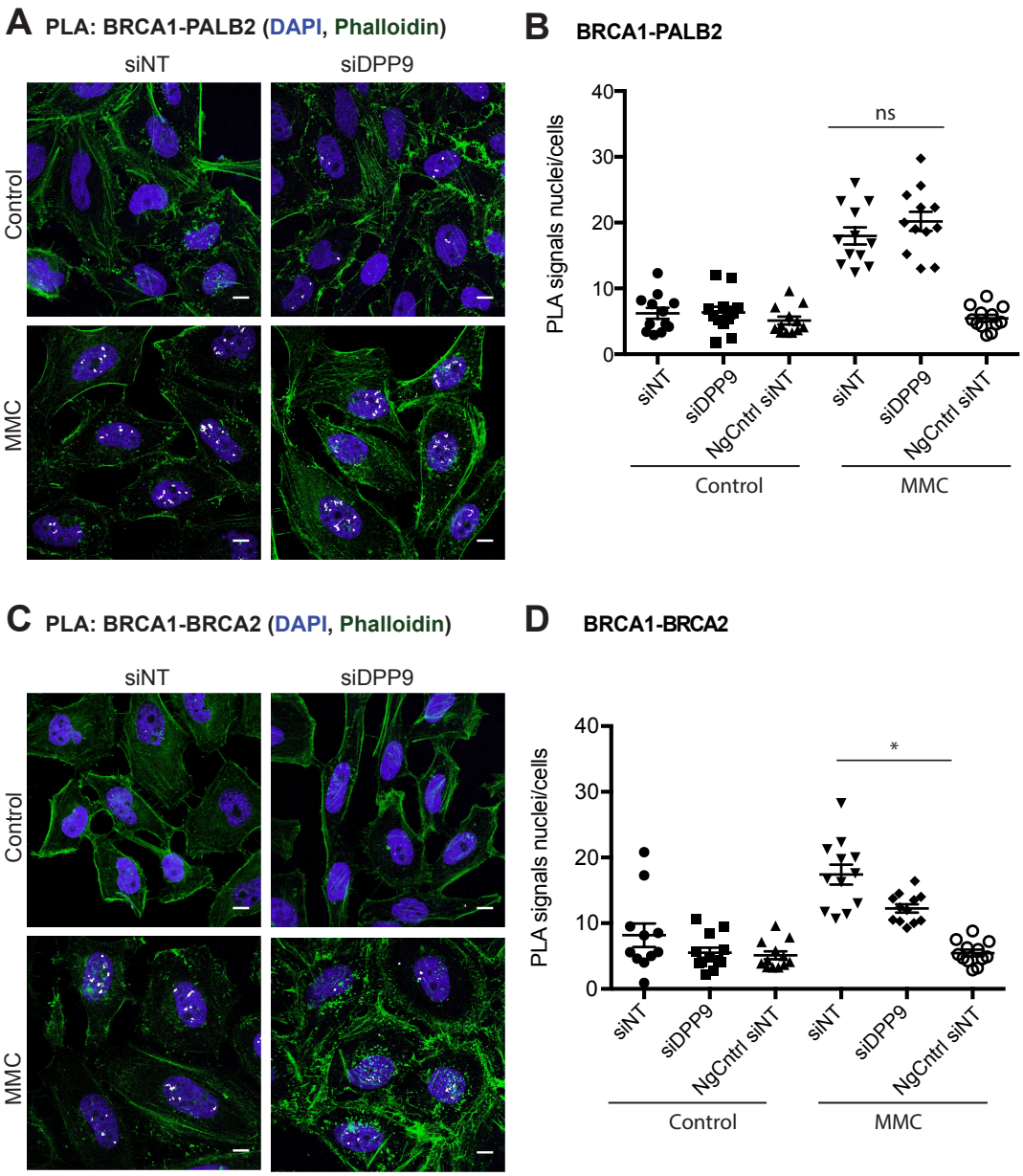

Figure 17. BRCA1 and PALB2 are not affected upon DPP9 silencing in contrast to BRCA1 and BRCA2 interaction which was significant reduced after MMC treatment.
(A) PLA (white) of endogenous BRCA1-PALB2 in HeLa siNT and HeLa siDPP9 cells upon MMC (300nM) treatment for 24 h. Phalloidin (actin filaments in green), DAPI (nucleus in blue). Scale bar 10 µm.
(B) Quantification of PLA from (A) showing the number of dots per cell (>50 cells per condition) of one of 3 independent experiments. Statistical analysis was carried out by an unpaired two-tailed t-test ($p<0.05$).
(C) PLA (white) of endogenous BRCA1-BRCA2 in HeLa siNT and HeLa siDPP9 cells upon MMC (300nM) treatment for 24 h. Phalloidin (actin filaments in green), DAPI (nucleus in blue). Scale bar 10 µm.
(D) Quantification of PLA from (C) showing the number of dots per cell (>50 cells per condition) of one of 3 independent experiments. Statistical analysis was carried out by an unpaired two-tailed t-test ($p<0.05$).

3.12. Inhibition of DPP9 reduces BRCA2 recruitment to the DNA damage sites

Collectively, we found that DPP9 regulates BRCA2 stability and affects its binding to BRCA1. To confirm that BRCA2 has defects in its recruitment to the DNA damage sites, we tested the proximity to its partner localizer, PALB2, which recruits BRCA2 to the DSB sites (Xia *et al*., 2006). We measured the interaction between BRCA2 and PALB2 by PLA in siNT cells and DPP9 transiently silenced cells (siDPP9). Interestingly the BRCA2 and PALB2 interaction exhibited a significant reduction in cells silenced for DPP9 after DNA damage induction by MMC treatment (Figure 18A and 18B). This correlates with the previous observation where BRCA2 and BRCA1 proximity was reduced in DPP9 silenced cells.

Low interaction of BRCA2 with PALB2 is known to affect the localization of BRCA2 to the DNA damage sites. To test that the reduction in the interaction of BRCA2 and PALB2 leads to a mis-localization of BRCA2 from the DNA damage sites, we measured the proximity of BRCA2 to γH2AX by PLA. Extraordinarily, DPP9 silenced cells showed that BRCA2 proximity to γH2AX was significantly reduced (Figure 18C and 18D) after MMC treatment. All together indicates that DPP9 regulates not only the stability of BRCA2 but also its localization. One explanation could be that DPP9 enzymatic activity occurs upstream the recruitment of BRCA2 to the DNA damage sites. Moreover, cells lacking DPP9 have defects in DNA damage repair due to the mis-localization of BRCA2, which could explain the increased of DNA damage found in cells lacking DPP9 in our previous experiments (Figure 7 and Figure 8).

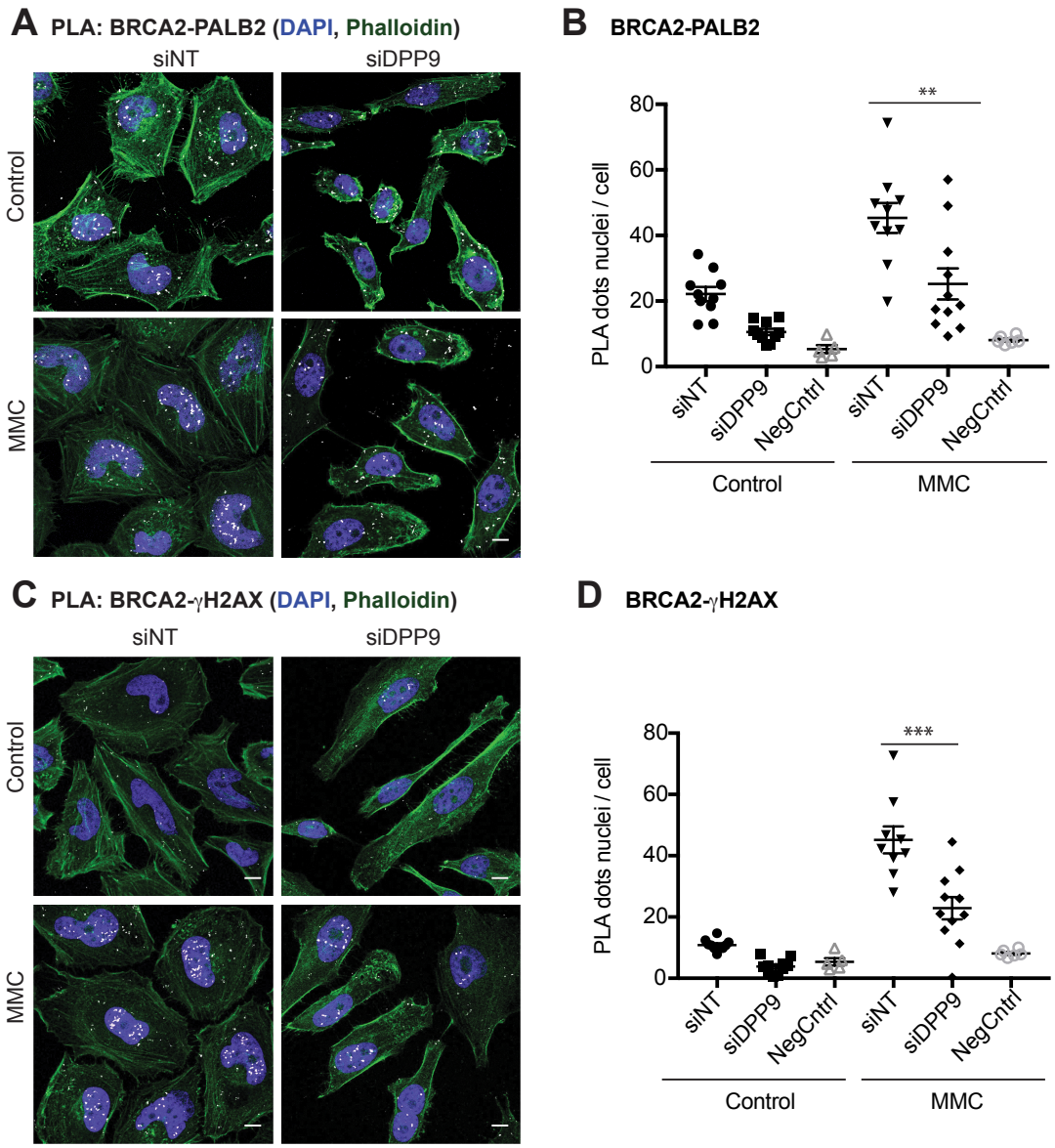

Figure 18. Defects in BRCA2 localization in DPP9 silenced cells upon DSB.
(A) PLA (white) of endogenous BRCA2-PALB2 in HeLa siNT and HeLa siDPP9 cells upon MMC (300nM) treatment for 24 h. Phalloidin (actin filaments in green), DAPI (nucleus in blue). Scale bar 10 µm.
(B) Quantification of PLA from (A) showing the number of dots per cell (>50 cells per condition) of one of 3 independent experiments. Statistical analysis was carried out by an unpaired two-tailed t-test ($p<0.05$).
(C) PLA (white) of endogenous BRCA2-γH2AX in HeLa siNT and HeLa siDPP9 cells upon MMC (300nM) treatment for 24 h. Phalloidin (actin) and DAPI (nucleus), scale bar 10 µm.
(D) Quantification of PLA from (C) showing the number of dots per cell (>50 cells per condition) of one of 3 independent experiments. Statistical analysis was carried out by an unpaired two-tailed t-test ($p<0.05$).

3.13. RAD51 levels are reduced in the chromatin fractions from HeLa DPP9 KD cells after MMC treatment.

In addition to the PLA assays, we measured the levels of BRCA2 in chromatin fractions after MMC treatment in HeLa WT and DPP9 KD cells. The cells were treated for 8 and 24 hours with MMC (300 nM), followed by chromatin fractionation. Analysis of the proteins was performed by WB. The levels of DPP9 were clearly lower in DPP9 KD cells. Importantly the levels of BRCA2 after 24 h of MMC treatment were reduced in the HeLa DPP9 KD cells compared to the HeLa WT cells (Figure 19), confirming the results found in the different PLAs for BRCA2 (Figure 16-18). Moreover, we additionally tested the levels of RAD51, protein necessary for the last step of HR repair (Figure 2). The levels of RAD51 protein were reduced in the HeLa DPP9 KD cells compared to the WT cells after 24 h MMC treatment. This reduction in RAD51 levels suggests that the mis-localization of BRCA2 has a direct effect in its function of loading RAD51 to the DNA damage sites.

Surprisingly RPA2 also showed lower values in DPP9 KD cells after 24 h of MMC treatment (Figure 19), RPA2 is known to act upstream to RAD51, as well as, during the D-loop formation (last step of HR repair). Since BRCA1 foci showed no defects after DPP9 silencing, we hypothesis that the reduction of RPA2 in the chromatin is not due to its first binding to the DNA, during end-resection process (first step of HR repair; Figure 2), but due to the second binding to the DNA, during the D-loop formation. The formation of the D-loop requires the binding of RAD51, thereby we suggest that cells lacking DPP9 have HR defects by the lack of RAD51 protein.

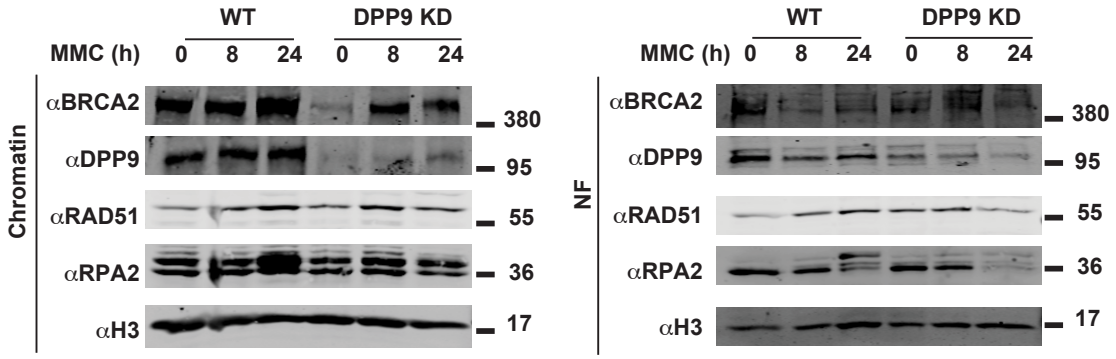

Figure 19. BRCA2 and RAD51 levels are reduced in the chromatin fractions of HeLa DPP9 KD cells after MMC treatment.

Chromatin Fractions (left) and Nuclear Fractions (right) of HeLa WT and HeLa DPP9 KD cells after MMC treatment. Samples analyzed by WB and developed with antibodies against endogenous BRCA2, DPP9, RAD51, RPA2 and H3 proteins. H3 was used as the loading control. Showing one of three independent experiments. Chromatin fractionation was performed by Dr. Vijaya Kari (Prof. Dr. Steven Johnsen, Clinic for General, Visceral and Pediatric Surgery, University of Göttingen) and analyzed by Maria Silva-Garcia (Dr. Ruth Geiss-Friedlander; Molecular Biology, University of Göttingen).

3.14. DPP9 silenced cells have defects in RAD51 foci formation

The recruitment of BRCA2 to the DNA damage sites is essential for the formation of RAD51 filaments, which coat the ssDNA overhangs of DSBs and promote the strand invasion into the homology DNA for HR completion (Jensen *et al*., 2010; Figure 2). These filaments are visualized in the microscope as dots, also known as foci, which can be quantified and analyzed. As seen in the chromatin fractionation assay, DPP9 KD cells have lower values of RAD51 after MMC treatment when compared to WT cells. To test whether RAD51 is able to form filaments we performed immunofluorescence to test the formation of RAD51 foci in siDPP9 cells compared to siNT cells (Figure 20A and 20B). Remarkably, the number of RAD51 foci in siDPP9 cells was significantly lower in comparison to siNT cells, which support the previous results found (Figure 17B).

All together, we found cells deficient in DPP9 have defects in BRCA2 localization as well as in its function, thereby accumulating more DNA damage.

To connect the enzymatic activity of DPP9 with BRCA2, we also tested the foci formation of RAD51 in cells expressing the inactive mutant of DPP9, MEF DPP9 gki cells. Compellingly, the MEF DPP9 gki showed a significant reduction in RAD51 foci formation after MMC treatment (Figure 21A and 21B), which confirmed that the enzymatic activity of DPP9 is regulating BRCA2 function, probably by the control of the stability of the protein and the localization to the DNA damage sites.

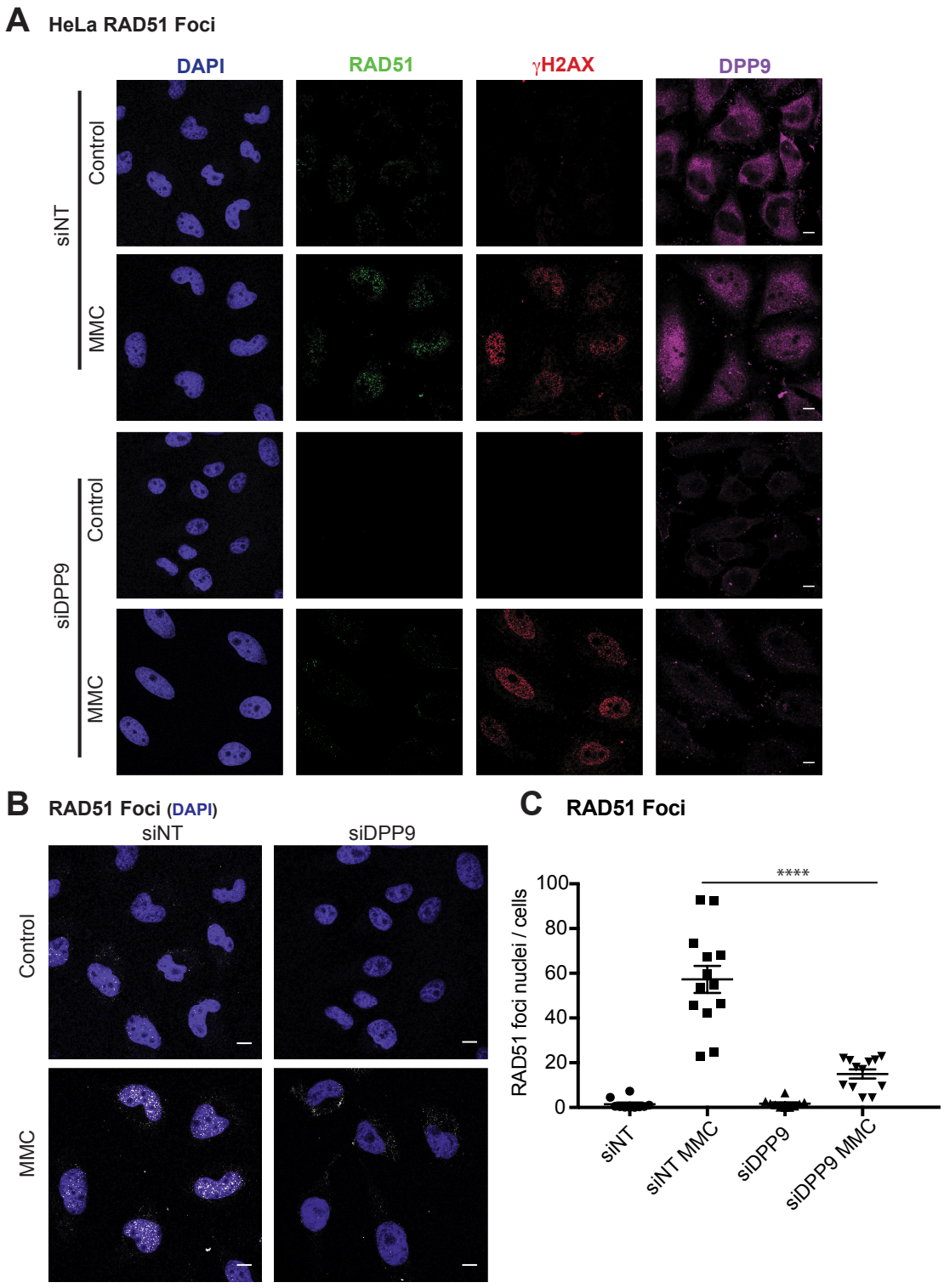

Figure 20. HeLa DPP9 silenced cells present deficient RAD51 foci formation.

(A) IF of endogenous RAD51 (green) in HeLa siNT and siDPP9 cells after 300 nM MMC (24 h). γH2AX (red) as DNA damage marker, DPP9 (purple) and nucleus, DAPI (blue). Scale bar 10 μm.
(B) Merge images of IF of endogenous RAD51 in HeLa siNT and siDPP9 cells showing RAD51 foci (white) after 24 h of MMC (300 nM) treatment. DAPI (nucleus in blue), scale bar 10 μm.
(C) Quantification of RAD51 foci from (B) showing the number of dots per nucleus of one out of three independent experiments. Data are represented as the mean ± SEM. Signals of more than

50 cells were quantified for each condition respectively. Statistical analysis was carried out by an unpaired two-tailed t-test ($p<0.05$).

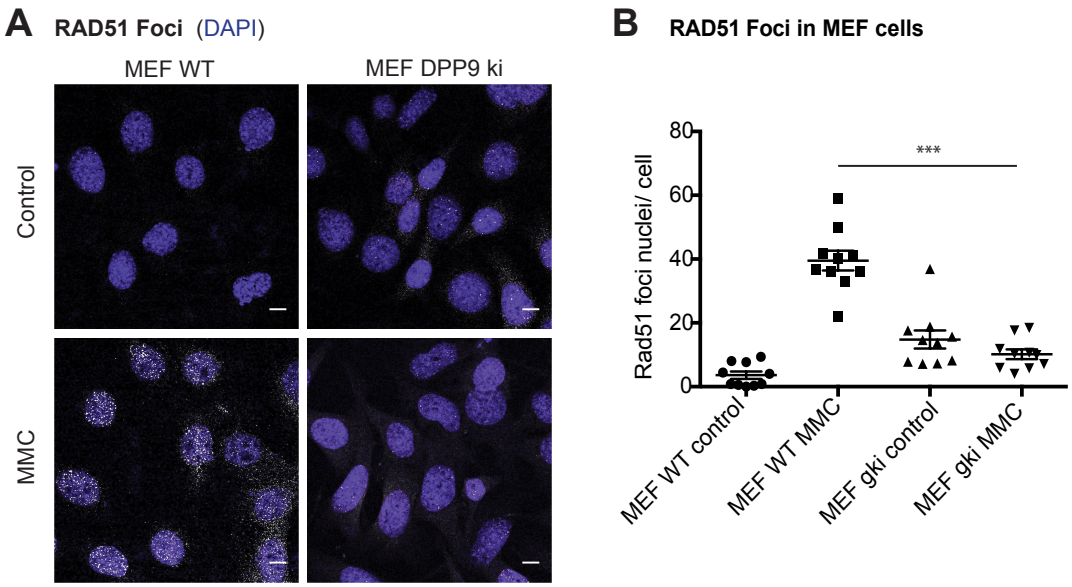

Figure 21. MEF DPP9 gki cells present deficient RAD51 foci formation.

(A) IF of endogenous RAD51 in MEF WT and MEF DPP9 gki cells showing RAD51 foci in white after 24 h of MMC (300nM) treatment. DAPI (nucleus in blue). Scale bar 10 µm.
(B) Quantification of RAD51 foci from (A) showing the number of dots per nucleus of one out of 3 independent experiments. Data are represented as the mean ± SEM. Signals of more than 50 cells were quantified for each condition respectively. Statistical analysis was carried out by an unpaired two-tailed t-test ($p<0.05$).

4. Discussion

4.1. Model of DPP9 and BRCA function in HR repair

Collectively our study identified a new function of DPP9 in cells connected to DNA damage repair protein, involving the regulation of BRCA2. Lack of DPP9 enzymatic activity results low in deficient DNA damage repair and less survival in cells. Moreover, the binding of DPP9 and BRCA2 is affected upon inhibition of DPP9 active site with 1G244, suggesting that DPP9 requires of the active site for proper BRCA2 binding. Importantly, silencing of DPP9 resulted in stabilization and mislocalization of BRCA2 protein and consequently, loss of BRCA2 function of loading RAD51 into the DNA damaged sites (Figure 22). Low RAD51 foci was observed not only in cells silenced for DPP9 but also in cells expressing the DPP9 inactive mutant, MEF DPP9 gki. Here, we propose a model in which lack of DPP9 activity stabilizes BRCA2 and reduces the loading of RAD51 protein to the DNA damaged sites.

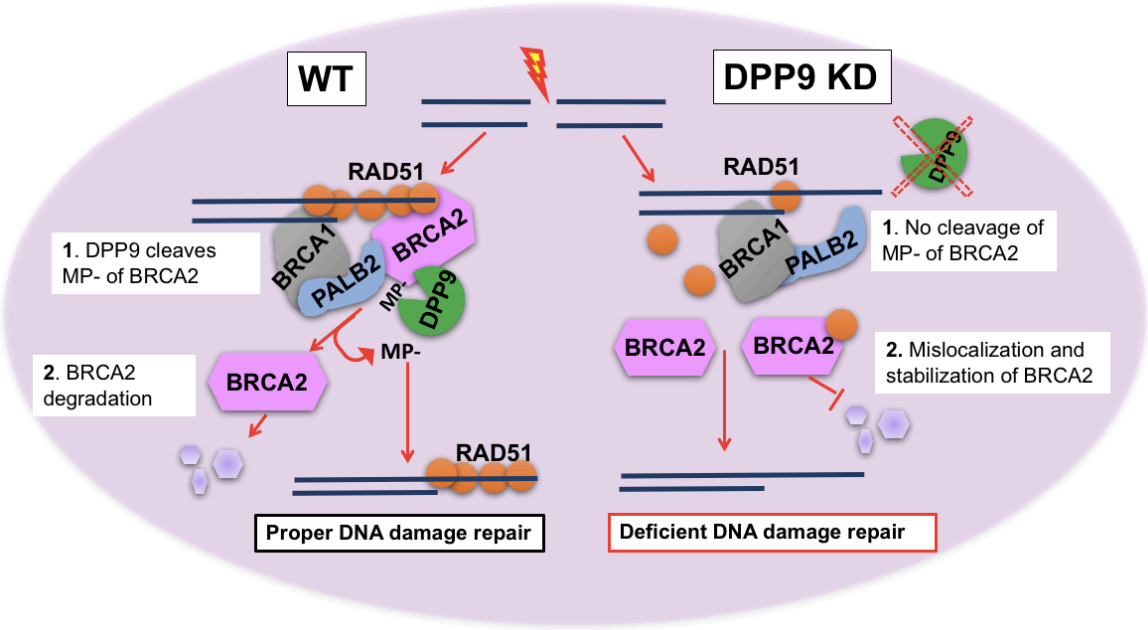

Figure 22. Model of DPP9 and BRCA2 function in HR repair of DSBs
Upon DSBs cells undergo into DDR either NHEJ or HR depending on cell cycle. HR repair requires the binding of the BRCA1-PALB2-BRCA2 complex for loading RAD51 into the ssDNA overhangs formed after end-resection. Cells lacking DPP9 activity are hypersensitive to DNA damaging agents and their survival is reduced compare to WT cells. In the absence of DPP9 the Met-Pro (MP) in the N-terminal of BRCA2 protein is not cleaved, thus stabilizing BRCA2 protein. Uncleaved BRCA2 is not able to localize to DSB sites and presents reduce PALB2 binding, thereby affecting BRCA2 function of loading RAD51 into the ssDNA overhangs for completion of the HR.

Reduced RAD51 filament formation implies reduce DNA damage repair and increases the accumulation of DNA damage, which we found in our results with the high values of γH2AX in cells lacking DPP9 (Figure 22).

Further studies are needed to define the molecular mechanism of the binding and cleavage of DPP9 towards BRCA2, which may help in developing new therapies to treat cancer.

4.2. DPP9 expression and localization

DPP9 is ubiquitously expressed in lymphoid, neuronal, epithelial and muscle cells of different organs in humans. In lymphoid cells from colon, lung, small intestine, stomach, and cirrhotic liver, the mRNA levels of DPP9 were reported to be high (Yu *et al*., 2009). DPP9 protein expression has also been found in human and murine macrophages (Okondo *et al*., 2016; Waumans *et al*., 2015; Zapletal *et al*., 2017), emphasizing the role of DPP9 in the immune system, which is one of the main studied functions of DPP9 until today (see point 1.4.4.5.). Besides the lymphoid cells, the epithelial cells also manifest DPP9 expression in organs such as lung, liver, and intestine. DPP9 is also expressed in brain tissues from baboon and mouse and DPP9 was also reported to be expressed in skeletal muscle, heart and uterus of baboon and mouse samples (Yu *et al*., 2009; reviewed in Gorrell *et al*., 2014). Furthermore, DPP9 and DPP8 enzyme activity has been detected in pancreas, adipose tissues, adrenal gland, and mouse testis. More importantly, DPP9 distribution in testis seemed to be dependent on the differentiation stage (Yu *et al*., 2009).

In the present study, we used human epithelial cells (HeLa) and mouse embryonic fibroblast (MEF) cell lines, both of which express DPP9 and more importantly, the levels of DPP9 were higher when comparing to the other cytosolic member of the family, DPP8 (Geiss-Friedlander *et al*., 2009). In lymphocytes, the DPP9 mRNA and/or protein levels did not change after stimulation by mitogen PHA in Jurkat cells by stimulation of the BCR receptor in DG-75 B cells (Tang *et al*., 2009; Justa-Schuch *et al*., 2016). Conversely, a previous report, also in lymphocytes (Raji cells), showed a mild protein increased of DPP9 after MMC treatment, however, the dose used for MMC was 500 times higher than the one used in our study (Chowdhury *et al*., 2013). In contrast, in our study, DPP9 levels did not change upon MMC (300 nM or 24 h) induction in HeLa cells. However, disruption of DPP9 basal levels is common in tumors and inflamed cells, emphasizing the importance of proper regulation of DPP9, which also involves the precise localization of the protein in the cell to carry out its enzymatic activity.

Moreover, during cell differentiation, inflammation and tumorigenesis, DPP9 protein levels and its enzymatic activity have been reported to increase in cells. Some examples involve differentiation processes such as the differentiation of monocytes into macrophages where DPP9 was found to exhibit a time-dependent increased (Matheeussen *et al*., 2013) and during spermatogenesis, in which the mRNA levels of DPP9 were shown to be higher, compared to DPP8, in pachytene spermatocytes and spermatids (Yu *et al*., 2009). In tumorigenesis DPP9 expression was reported to be higher in acute myeloid leukemia stem cells compared to normal hematopoietic cells (Spagnuolo *et al*., 2013) and moreover, the mRNA levels of DPP9 were found highly elevated in human testicular cancer cells (Yu *et al*., 2009).

Regarding DPP9 localization is known to be very broad in cells. First studies localized transfected DPP9 in the cytosol using flow cytometry and immunofluorescence (Ajami *et al*., 2004). This localization pattern was similar to the one seen in our microscopy results of normal cells without any stimuli (Figure 7). Moreover, prior studies from Geiss-Friedlander group found a nuclear localization of DPP9 which corresponded to the long isoform of DPP9, which contains an NLS in the N-terminal of the protein (Justa-Schuch *et al.*, 2014). Here, we showed that upon DNA damage, DPP9 changed the cellular distribution and it localized more into the nucleus and around the nucleus. In our previous study, we also found a change in the localization of DPP9, where DPP9 increased its nuclear staining after silencing FLNA in cells (Justa-Schuch *et al*., 2016). Importantly, FLNA is known to affect DNA damage repair, and lack of FLNA in cells was related to low survival and repair deficiencies in cells (Yue *et al*., 2009). Thereby, the nuclear localization of DPP9 in FLNA silenced cells found in our previous study may have imitated, to some extent, the effects of MMC seen in the present study, by promoting DNA damage in the cells and probably activating DPP9 and its localization into the nucleus.

In addition to the nuclear localization, we proved that DPP9 is recruited to the chromatin and that this binding increases upon DNA damage induced by MMC. MMC acts forming DSBs in the DNA, which repair requires a complex regulatory machinery of key proteins that are recruited to the DSB sites, which are marked by the phosphorylated H2AX (γH2AX; Turinetto and Giachino, 2015). The increased of DPP9 in the chromatin upon MMC raised the question whether the protein is recruited to the DSB sites. To approach this, we looked at the proximity between DPP9 and γH2AX using the PLA method. Surprisingly, we found that cells treated with MMC were positive for DPP9-γH2AX interaction, suggesting recruitment of DPP9 to the DNA damaged sites.

Altogether, these results showed, for the first time, that DPP9 is recruited to the chromatin and more specifically to the DNA damage sites, pointing into the direction of a possible role of DPP9 in the DNA damage repair.

Two other studies have also shown a change in DPP9 localization upon stimuli using the epidermal growth factor or Phorbol 12-myristate 13- acetate to induce cell migration and cell adhesion processes. After stimulation, DPP9 was partially re-localized to the surrounds of the ruffling membrane, which is the region of the plasma membrane involved in cell adhesion and cell migration processes and it is formed by a complex of proteins englobed as the focal adhesion complex (Yu *et al*., 2006; Zhang *et al*., 2015). Cells with inactive or silenced DPP9 had impaired cell adhesion and cell migration mechanisms, involving DPP9 in such processes (Yu *et al*., 2006; Zhang *et al*., 2015). It is important to highlight that FLNA has been also connected to focal adhesion complexes (Xu *et al*., 2010), however, it is unclear whether FLNA promotes or inhibits cell migration. The presence of FLNA in the ruffling membrane could explain the recruitment of DPP9 in those sites, which suggests again a role of FLNA in the localization of DPP9 to specific sites in the cell after induction, either cell migration or DNA damage repair.

Despite those findings, it is still unclear whether DPP9 short isoform or DPP9 long isoform confer different localization. Our results do not discriminate between the two DPP9 isoforms, but it is probable that both forms are localized into the nucleus after MMC treatment. One hypothesis we consider is that the long isoform may reside in the nucleus in normal cells while the short isoform is in the cytosol and upon MMC stimuli the DPP9 short form is then imported into the nucleus. This could suggest two different roles for the short and the long isoforms of DPP9 where DPP9 short responds upon stimuli and DPP9 long maintains the basal regulation in the nucleus. To clarify this will be necessary to develop antibodies capable of recognizing the different endogenous DPP9 isoforms by immunofluorescence.

4.3. DPP9 and cell survival

Previous studies have connected DPP9 to cell death, where inhibition of DPP9 increased the apoptosis in human macrophages (Matheeusen *et al*., 2013), mice macrophages (Waumans *et al*., 2015) and Ewing sarcoma cells (Lu *et al*., 2011). In addition to those studies, DPP9 silencing was also found to increase the expression of apoptotic markers in non-small cell lung cancer cells (NSCLC; Tang *et al*., 2017) and the specific inhibition of DPP8/9 resulted in mortality in rats (Lankas *et al*., 2005). Lately, two

studies has raised the interest of DPP9 and its relation to pyroptosis, a type of cell death (Okondo *et al*., 2016; Johnson *et al*., 2018; see section 1.4.4.6.).

However, the mechanisms by which DPP9 controls cell survival are still unknown. Here, we showed that DPP9 KD cells accumulate more DNA damage as seen by the high levels of γH2AX after MMC treatment. More importantly, we observed stronger accumulation of DNA damage in MEF DPP9 gki, which express the inactive form of DPP9. Accumulation of DNA damage repair suggests that those cells have defects in the DDR. Increase DNA damage is related to cell death, as seen in the colony formation assays where MEF DPP9 gki cells have lower colonies compared to MEF WT after DNA damage induction with gamma radiation or MMC treatment. Moreover, HeLa DPP9 KD cells also presented defects in viability when measuring the ATP levels after DNA damage induction with MMC or with olaparib (Figure 8). The increased of γH2AX in cells lacking DPP9 (Figure 7) together with the survival assays suggests that DPP9 is regulating DNA damage repair and its essential for proper DNA damage repair.

DNA damage is one of the characteristic features of cancer cells, thereby Ewing sarcoma cells and NSCLC cells are prone to DNA lesions. Inactivation of DPP9 in those cells leads to apoptosis, which, based in our results, could be explained by the accumulation of unrepaired DNA measured by the high levels γH2AX after MMC treatment in DPP9 deficient cells. However, not only DPP9 inhibition results in cell death but also overexpression of DPP9 seems to induce apoptosis in epithelial cells (Yao *et al*., 2011) and lymphocytes (Chowdhury *et al*., 2013) suggesting that the right balance of endogenous DPP9 levels is crucial for maintaining survival in cells.

Here we proved that DPP9 activity is essential for DNA damage repair since as seen in our results, lack of DPP9 or inactive form of DPP9 increased the accumulation of DNA damage measured by the levels of γH2AX and reduce cell survival.

4.4. DPP9 in the DNA damage response

Understanding the mechanism by which DPP9 regulates apoptosis has been one of the main paradigms to elucidate over the last years. In our study, we suggest a possible role of DPP9 in the repair of the DNA since after MMC treatment we found a sharp increase in the levels of γH2AX in DPP9 KD or inactive DPP9. As a protease, DPP9 might target different substrates, thereby regulating many processes in the cells.

A previous analysis in our group found that a short peptide of BRCA2, a key player of HR repair, was cleaved after incubation with recombinant DPP9 *in vitro* (Dr. Esther Pilla, Dr. Christoph Lenz, unpublished data). This, together with preliminary data, which

suggested interaction of DPP9 and BRCA2 by PLA, we studied the connection of DPP9 and BRCA2. First, we achieved this by looking at the proximity between BRCA2 and DPP9 in cells using the PLA method. We found positive PLA signals for endogenous DPP9 and BRCA2 using the different silencing controls for each of the proteins. Moreover, DPP9 was also found in close proximity to PALB2, an essential protein for BRCA2 localization to the DNA damage sites, suggesting that DPP9 is forming part of the complex of BRCA2 and PALB2.

Furthermore, our *in vitro* studies proved that DPP9 and short peptides from the N-terminal end of BRCA2 directly interact as seen by SPR. The N-terminal end of BRCA2 since contains the putative cleavage site of DPP9, Met-Pro. Notably, the short peptide of BRCA2, $BRCA2_{3-40}$, lacking the Met-Pro had less affinity compared to the peptide $BRCA2_{1-40}$, suggesting that the binding of DPP9 and BRCA2 might require the active site of DPP9. We analyzed this by studying the binding of DPP9 to BRCA2 after DPP9 inhibition with 1G244 inhibitor, which blocks the active site of DPP9. We found that the binding of endogenous DPP9 and BRCA2 is reduced when DPP9 active site is blocked.

In addition to this, we found that DPP9 and BRCA2 interaction increases after DSBs induction using MMC. Not only DPP9 and BRCA2 interaction was increased, but also DPP9 and PALB2 had higher amount of PLA signals after MMC treatment. This suggests that DPP9 is forming part of the complex of BRCA2 and PALB2, which interaction is known to increase after DNA damage (Figure 22).

To understand better the binding between DPP9 and BRCA2 we looked at FLNA protein. From our previous publication, FLNA was shown to be necessary for the interaction between DPP9 and its substrate Syk (Justa-Schuch *et al*., 2016). We tested the involvement of FLNA in DPP9 and BRCA2 interaction. First approach showed no difference on DPP9 and BRCA2 interaction after FLNA silencing. However, when cells were treated with MMC, there was a significant reduction in the binding of DPP9 and BRCA2. Thereby, we can strongly confirm that FLNA acts as a scaffold for recruitment of substrates to DPP9.

Taken together our results suggest that BRCA2 is a novel substrate of DPP9 and their binding is induced upon DNA damage. However, BRCA2 might not be the only cleaved protein by DPP9 in the DNA damaged sites and it remains to be shown whether DPP9 targets additional proteins.

4.5. BRCA2 regulation

The endogenous levels of BRCA2 have to be strictly regulated to achieve proper HR repair and reduce the tumorigenesis risk. BRCA2 loss of function carriers have a high chance of developing breast cancer (Wu *et al*., 2017; Petrovic *et al*., 2017). In sporadic prostate cancer, mutations in BRCA2 are rare and it is the loss of BRCA2 the major caused of those (Arbini *et al.*, 2011). Furthermore, the endogenous levels of BRCA2 were shown to be required for correct HR repair and that BRCA2 and RAD51 protein levels depend on each other since they are synergically regulated (Magwood *et al.,* 2013). However, the regulation and degradation of BRCA2 is still unknown. The stability of BRCA2 was shown to be maintained by DSS1 binding since DSS1 deficiency led to a reduction on BRCA2 protein levels after CHX chase analysis (Li *et al.,* 2005). The degradation of BRCA2 has been suggested to be mediated by the ubiquitin proteasome pathway where inhibition of the proteasome in PALB2 silenced cells led to stabilization of the nuclear BRCA2 (Xia *et al*., 2006).

In this work, we found a novel regulator of BRCA2 stability, DPP9. First, we described that the half-life of BRCA2 decreased upon MMC treatment followed by silencing of DPP9 studies, which reversed the MMC effect in BRCA2 stability and increased BRCA2 half-life. In our previous study, we showed that DPP9 cleavage reduced the stability of Syk and targeted the protein to the proteasome (Justa-Schuch *et al*., 2016). Here, we hypothesize that BRCA2 stability is also dependent on the first two amino acids, Met-Pro, in the N-terminus. The removal of the Met-Pro exposes the third amino acid of BRCA2, isoleucine, which is known to be a destabilizing residue, thereby after the cleavage BRCA2 is probably recognized by an E3 ligase.

Prior studies found that BRCA2 is ubiquitinated after MMC treatment, although the E3 ligase involved in this process is still unknown (Schoenfeld *et al*., 2004). The only E3 ligase reported to bind BRCA2 is SKP2, which overexpression resulted in loss of BRCA2 in prostate cancer cells, suggesting a possible connection to BRCA2 degradation (Arbini *et al*., 2011). Another possible E3 ligase for BRCA2 is RFWD3, which has emerged as an HR regulator since it is required for the removal and degradation of RPA2 and RAD51 proteins from the ssDNA during HR repair (Inano *et al*., 2017). Due to the proximity of BRCA2 with RPA2 and RAD51, one could hypothesize that BRCA2 is also targeted by RFWD3, promoting BRCA2 removal from the DSBs sites, but a deeper analysis is required to define accurately the E3 ligase involved in the recognition and further poly-ubiquitination of BRCA2 protein.

After poly-ubiquitination, proteins are targeted to the proteasome in where they are degraded. Previous studies showed that inhibition of the proteasome by MG132 resulted in BRCA2 stability (Schoenfeld *et al.*,2004; Xia *et al.*, 2006). In our experiments, after DNA damage induction and MG132 treatment, cells had an increased in BRCA2 half-life compared to cells without proteasome inhibitor. Thus, confirming that BRCA2 is degraded via the UPS.

Summarizing all together, we hypothesize that DPP9 cleaves the Met-Pro in BRCA2 N-terminal end, exposing the third residue, which may be recognized, poly-ubiquitinated and targeted to the proteasome by an E3 ligase.

Nonetheless, ubiquitination does not always imply degradation and can also be used for signaling purposes, thereby not only ubiquitin ligases are essential but also DUBs which reverse this modification. Interestingly, DUBs have been connected to BRCA2 regulation and other regulators of the DDR. USP3 and USP44 proteases have been reported to target ubiquitinated substrates of the E3 ligase RNF168, which is involved in the NHEJ repair (Mosbech *et al.*, 2013). Furthermore, USP26 and USP37 have been shown to remove directly the ubiquitins from RNF168, preventing the sequestration to the DNA of RNF168 substrates, BRCA1 and RAP80, essential regulators of the NHEJ repair, and inducing HR repair (Typas *et al.*, 2016).

Regarding BRCA2, the first DUB interacting with the protein was the known USP11, but no direct evidence was found regarding the stabilization of BRCA2 (Schoenfeld *et al.*2004). In contrast, USP21 has been lately connected to BRCA2 stability by its binding to the C-terminal region of BRCA2, which involves the DNA binding domain. The knockdown of USP21 resulted in low RAD51 loading into the ssDNA, which is performed by BRCA2, affecting the HR repair in those cells (Liu *et al.*, 2017).

4.6. BRCA2 function

BRCA2 function, loading of RAD51 to ssDNA overhangs, is essential in HR repair (Jensen *et al.*, 2010; Zhao *et al.*, 2015). Little is known about the activation of BRCA2 during S and G2 phases of cell cycle. However, the inactivation of BRCA2 was found to be controlled by cyclin-dependent kinase (CDK) phosphorylation. The phosphorylation of BRCA2 on serine 3291 in late G2 phase reduced the interaction of BRCA2 with RAD51. Thus, resulting in low RAD51 loading into the ssDNA and reducing HR repair (Esashi *et*

al., 2005). CDKs have also been reported to phosphorylate BRCA2 and induced the binding of a protein named Plk1 kinase (Yata *et al*., 2014) which indirectly activates RAD51 by phosphorylation, inducing the binding to the ssDNA and promoting HR repair (Yata *et al*., 2012).

The recruitment of BRCA2 to the DSB sites requires the binding to PALB2 protein, which forms a complex with BRCA2 and recruits it to the DNA damaged sites by interacting with the previously bound to the DNA, BRCA1 protein (Xia *et al*., 2006). Here, we showed that cells silenced for DPP9 had no defects in BRCA1 binding to the DSB sites, however they displayed a significant reduction in the interaction between BRCA2 and PALB2 after MMC treatment. This reduction resulted in low recruitment of BRCA2 to the DNA damaged sites as seen in the PLAs of endogenous BRCA2 and BRCA1, and BRCA2 and γH2AX, as well as in the chromatin fractions. Mislocalization of BRCA2 in silenced DPP9 cells suggests that DPP9 regulates BRCA2 recruitment to the DNA damage sites.

BRCA2 localization to the DNA damage sites is essential to load RAD51 for HR repair. It is known that the loading of RAD51 is inefficient in cells lacking BRCA2 (Jensen *et al*., 2010; Zhao *et al*., 2015). In our cells, after DPP9 was silenced, we found low RAD51 filament formation, correlating with the mislocalization of BRCA2 to the DSBs sites. Moreover, chromatin fractions showed low levels of RAD51 in the chromatin after MMC treatment in HeLa DPP9 KD cells, thus confirming that DPP9 regulates the binding of RAD51 to the DNA damage sites through the action of BRCA2. Moreover, we proved that the enzymatic activity of DPP9 is necessary for BRCA2 function since cells expressing an inactive form of DPP9 also showed a significant reduction in RAD51 filament formation, seen as foci, after MMC treatment. In contrast to BRCA1, which was not affected by DPP9 silencing as seen by the BRCA1 foci by immunofluorence.

Taken together those approaches, we proved a direct effect of DPP9 towards BRCA2 function where lack of DPP9 enzymatic activity impairs RAD51 loading into the ssDNA and the repair of the DNA lesions.

The molecular mechanisms by which DPP9 controls BRCA2 are unknown but our data indicates that upon the cleavage, BRCA2 binds PALB2 with higher affinity and it is recruited to the DSBs sites. DPP9 was also found in close proximity to γH2AX and PALB2, suggesting that BRCA2, PALB2, and DPP9 might be forming a complex. This indicates that after the cleavage of the Met-Pro of BRCA2, DPP9 may remain bound to BRCA2, and

only when the proteins are removed from the chromatin, BRCA2 disassociates from DPP9. This complex network of interactions could be regulated by FLNA.

FLNA was found to be involved in HR repair by its binding to BRCA2. In that study, FLNA was proposed to act as a scaffold protein to anchor BRCA2 to the repair machinery complex, since upon knockdown of FLNA, cells had low HR repair and reduced survival, as well as low RAD51 foci formation (Yue *et al*., 2009). Further studies also showed that FLNA silenced cells are sensitive to radiation and to some DNA damage-inducing agents (Yue *et al*., 2012). As we published before, DPP9 also binds FLNA and in the results shown in here, silencing of FLNA reduced BRCA2-DPP9 interaction in MMC treated cells. This could suggest that the complex of BRCA2, DPP9, and PALB2 is recruited to the DSBs in the presence of FLNA, nonetheless, no studies have tested whether BRCA2 losses its localization to the DNA damaged sites after FLNA silencing. For DPP9 we know, as seen in our previous study, that has stronger nuclear staining in cells lacking FLNA, which might be due to the increased of DNA lesions caused by FLNA silencing. Localization of DPP9 into the nucleus seems to not required FLNA, however, the proper recruitment of DPP9 to the DSBs could be affected in cells lacking FLNA. Further studies are needed of DPP9 and BRCA2 localization after FLNA silencing in damaged cells to understand the role of FLNA within this complex which could also answer the lack of RAD51 foci found in FLNA silenced cells (Yue *et al*., 2009).

4.7. Regulation of DPP9 enzymatic activity

DPP9 is known to be regulated in an allosteric manner by SUMO1 binding, which induces the enzymatic activity of DPP9 (Pilla *et al*., 2012). SUMO molecules have been related to the DDR and the three isoforms SUMO1, SUMO2 and SUMO3 have been found in nuclear-damaged foci after DNA damage induction (Morris *et al*., 2009). Sumoylation regulates the DDR by recruiting the proper machinery proteins, such as BRCA1, RAP80 or RNF168, sumoylated mainly by PIAS1 or PIAS4, to the DNA lesions (Morris *et al*., 2009; Lombardi *et al.*, 2017). Despite the fact that no connection of BRCA2 and sumoylation has been reported, BRCA2 could be also sumoylated to promote its recruitment to the DSBs sites as other DNA damage repair proteins.

DPP9 structure, which was recently published, helps in understanding the binding mechanism of DPP9 to SUMO1 and to the substrates. Binding studies reveal that DPP8 and DPP9 bind SUMO1 in their unliganded form and that the binding of SUMO1 enables the recruitment of substrates by DPP8 and DPP9 (Ross *et al*., 2018). More specifically, the solved structure suggests that the substrates might bind the activated DPP9 right after SUMO1 is disassociated from the complex. After the cleavage of the substrate, DPP9 and

DPP8, return to the unliganded conformation where SUMO1 could bind again closing the cycle (Ross *et al*., 2018). Following this idea, the binding of DPP9 with BRCA2 could be induced after the binding of SUMO1 to DPP9.

One possibility could be that upon DNA damage, BRCA2 is activated by sumoylation, increasing the binding affinity to DPP9. After the cleavage of the Met-Pro in the N-terminal of BRCA2 by DPP9, BRCA2 may induce its binding to PALB2, which is known to bind to the N-terminus of BRCA2 (Xia *et al*., 2006) and thereby inducing its recruitment to the DSBs. In our results, silencing of DPP9 in MMC treated cells reduced the binding between BRCA2 and PALB2 which resulted in low BRCA2 recruitment to DSBs as seen in the PLA assays after measuring the proximity between BRCA2 and γH2AX. In MEF, those assays were not performed due to the lack of a proper antibody for endogenous BRCA2 in mice. Nonetheless, MEFs also shared same phenotypes as HeLa cells in the survival studies, showing that MEFs expressing inactive DPP9 manifest less survival upon DNA damage compared to the WT and in the DNA damage accumulation analysis which exhibited an increased in the levels of γH2AX in the inactive DPP9 MEFs compared to the WT MEFs. To further validate the mislocalization of BRCA2, we tested the formation of RAD51 foci in both cell lines, which requires the proper localization of BRCA2 to the DNA damaged sites. HeLa cells silenced for DPP9 exhibited a strong significant reduction in the formation of RAD51 filaments compared to the non-targeted (siNT) cells. In the same line, MEF DPP9 gki had significantly lower levels of RAD51 foci than the MEF WT cells. All together suggests that DPP9 regulates BRCA2 function by its enzymatic activity and it is essential for proper completion of the HR repair.

In addition to SUMO1 regulation, the enzymatic activity of DPP9 has been shown to experience a loss of 80% of DPP8/9 enzymatic activity after *in vitro* exposure to hydrogen peroxide (H_2O_2) treatment (Park *et al*., 2008). However, the concentration used for that study was really high, 400 μM H_2O_2, and toxic for the cells (Halliwell *et al*., 2000). The reduction in the DPP9 enzymatic activity was attributed to the oxidation of cysteines residues, which might reduce the flexibility of DPP9 structure, probably making more difficult the binding to substrates (Park *et al*., 2008).

In our study, we used MMC and gamma radiation to induce DNA damage in cells, which are known to increase the presence of reactive oxygen species (ROS) in the cells. ROS englobes a group of molecules such as superoxide, H_2O_2 and hydroxyl radical (H+) that are formed by the incomplete reduction of oxygen. High levels of ROS are toxic in the cells, inducing oxidative stress, which can result in carcinogenesis, neurodegeneration, atherosclerosis, diabetes or aging. Cells have developed mechanisms to balance the

presence of ROS by the use of antioxidant molecules, which reduce ROS, however, at the same time these antioxidants get also oxidized, thereby enzymes, such as reductases together with the cofactor NADPH, play an important role in this network (reviewed in Chio and Tuveson, 2017).

Another example where ROS has been connected to DPP9 is during spermatogenesis. As discussed before, the mRNA levels of DPP9 were higher compared to DPP8 during the spermatozoa formation and even more they increased in pachytene spermatocytes and spermatids (Yu *et al*., 2009). In spermatogenesis, the stem cell is divided by mitosis into the replenish stem cell and the differentiate spermatocyte. The spermatocyte is divided into two secondary spermatocytes in Meiosis I and by a second Meiosis II four spermatids are formed. The final step, known as spermiogenesis, forms the sperm cells or spermatozoa. It is important to emphasize that during this process there is a high rate of DSBs, part of them due to the formation of ROS. Spermatocytes are the cell stage with higher rates of DSBs and thereby with elevated HR repair (Srivastava and Raman, 2006). This raises the question whether the high mRNA levels of DPP9 found in pachytene spermatocytes are caused by the increased of DNA lesions. In our study, the levels of DPP9 were not affected upon MMC, but in differentiation processes together with high DNA damage lesions and elevated ROS, could lead to an increase of DPP9 levels in the cells.

One more aspect to mention regarding the biochemical studies is the pH in the cell. DPP9 and DPP8 are known to have an optimal enzymatic activity at neutral pH between 7 to 8,5 (Tang *et al*., 2009), which correlates with the fact that high levels of H_2O_2 shift the intracellular pH from neutral to acidic and inactivates the enzymes. DPP9 is ubiquitously expressed in cells, however, the pH in cells varies depending on the organelle. In acidic organelles such as Golgi, endosome vesicles or lysosomes, DPP9 may not be enzymatically active since they have acidic pH. In the case of our study, we focus in the nucleus, where the pH is neutral. However, we could not discriminate in which compartment DPP9 cleaves BRCA2 since both proteins localized to either cytoplasm and nucleus where DPP9 has optimal activity.

4.8. DPP9 and diseases

DPP9 protein levels were found upregulated in cirrhotic liver (Yu *et al*., 2009; Chowdhury *et al*., 2013), inflamed lungs (Schade *et al*., 2008) and leukemia cells (Spagnuolo *et al*., 2013). Furthermore, DPP9 has been indirectly related to cancer in different studies when screening for cancer markers. One example is the high levels of DPP9 mRNA found in human testicular cancer cells (Yu *et al*., 2009). Nonetheless, the first connection of DPP9 with tumor cells was raised in a study on Ewing sarcoma family of tumors (ESFT). ESFT is a rare disease manifested in young people and characterized by the growth of malignant cells in bones and soft tissues. The neuropeptide Y (NPY), a substrate of the DPP4 family, has been associated to reduce viability in cells derived from ESFT (Lu *et al*., 2011). NPY_{1-36} peptide induces cell death through the binding to its receptors, Y1 and Y5, in a caspase-independent manner by increasing the levels of PARP1 and the presence of the apoptosis-inducing factor (AIF) in the nucleus (Lu *et al*., 2011; Kitlinska *et al*., 2005). Previous to this study, DPP9 enzymatic activity, as well as DPP4 or DPP8, were found to cleave NPY (Kitlinska *et al*., 2005). In ESFT cells, overexpression of DPP4, DPP8 or DPP9 induced the cleavage of NPY_{1-36} into NPY_{3-36}, thereby inactivating the peptide and abolishing the NPY response (Lu *et al*., 2011). More importantly, silencing of DPP8 or DPP9 lead to apoptosis in ESFT cells, probably in an NPY dependent manner (Lu *et al*., 2011). Curiously, in those cells, DPP9 silencing increased the levels of PAR-polymerases (Lu *et al*., 2011), which are necessary for DNA damage repair, thus suggesting that DPP9 removal increased the DNA damage in cells.

In addition to ESFT, DPP9 has been related to lung cancer, which is the most common cause of cancer death worldwide. Lung cancer main types are small lung cancer and non-small lung cancer, being the last one the most present in patients and with poor prognosis as reported by the World Health Organization. Tissues extracted from non-small cell lung cancer (NSCLC) of different patients exhibited high DPP9 mRNA levels as well as high DPP9 protein levels compared to the non-tumorigenic ones. Upon DPP9 silencing in the NSCLC cells, processes such as cell proliferation, cell migration, and cell invasion were impaired and the expression of the apoptotic markers p53 and Bax were highly induced. Furthermore, silencing of DPP9 in tumors that were injected to nude mice, resulted in retardation of the tumor growth, confirming the importance of DPP9 during tumorigenesis in vivo (Tang *et al*., 2017).

Moreover, the last report of DPP9 to cancer has involved *DPP9* in serous ovarian carcinoma by the formation of fusion genes, which are hybrid genes formed by two independent genes. *DPP9* was found in combination with *PPP6R3*, *PLIN3*, and *PAX2* genes, leading to the formation of fusion genes, which final product was an aberrant and inactive DPP9 protein. This loss of function of DPP9 was suggested to induce the tumorigenesis of serous ovarian carcinoma (Smebye *et al*., 2017).

In our study, presented here, we showed that DPP9 is an essential regulator of the DDR and it requires its enzymatic activity for the right repair of DSBs. We found a novel interacting protein of DPP9, BRCA2, which we suggest can be a putative substrate of DPP9. BRCA2 stability, localization and interactome was affected by the activity of DPP9. Moreover, we proved that defects in DPP9 led to deficient DNA damage repair and reduced cell survival, which could explain the reported connections of DPP9 in cancer. Defects in the repair of DSBs constitute a significant cause for tumorigenesis. All of these studies point at DPP9 as an important regulator of tumorigenesis and thereby targeting DPP9 in tumor cells could be a potential therapeutic treatment of different cancers. Developing specific inhibitors for DPP9 is one of the remaining difficulties found in this field. Some studies have already proposed the inactivation of DPP9 as a possible therapeutic treatment. For example, in acute myeloid leukemia (AML) the combinational treatment of parthenolide, a drug with specific toxicity to AML cells, with vildagliptin, a commercial drug used for type 2 diabetes treatment, which inhibits DPP4 but also DPP8 and DPP9, was found to potentiate the cytotoxic effects of parthenolide. However, parthenolide in combination with sitagliptin, a more specific DPP4 inhibitor, did not have additive effects (Spagnuolo *et al*., 2013). Another possible treatment involving DPP9 was found in atherosclerosis cells (a chronic inflammatory disorder of the arterial wall) since DPP9 was upregulated in pro-inflammatory macrophages, the key players of atherosclerosis, and inhibition of DPP9 induced macrophages apoptosis (Matheeussen *et al*., 2013).

Specific inhibitors for DPP9 are needed to tackle the protein without modifying the other members of the DPP4 family and likewise, it is important to consider the commonly used DPP4 inhibitors for diabetes, which some have been shown to target not only DPP4 but also DPP8 and DPP9, leading to side effects.

5. References

Abbott, C.A., and Gorrell, M.D. (2012). Chapter 746 Dipeptidyl Peptidase 8 (Elsevier Ltd).

Ahlskog, J.K., Larsen, B.D., Achanta, K., and Sørensen, C.S. (2016). ATM/ATR-mediated phosphorylation of PALB2 promotes RAD51 function. EMBO Rep. *17*, 671–681.

Ajami, K., Abbott, C.A., McCaughan, G.W., and Gorrell, M.D. (2004). Dipeptidyl peptidase 9 has two forms, a broad tissue distribution, cytoplasmic localization and DPIV-like peptidase activity. Biochimica Et Biophysica Acta (BBA) - Gene Structure and Expression *1679*, 18–28.

Arbini, A.A., Greco, M., Yao, J.L., Bourne, P., Marra, E., Hsieh, J.-T., di Sant'Agnese, P.A., and Moro, L. (2011). Skp2 Overexpression Is Associated with Loss of BRCA2 Protein in Human Prostate Cancer. The American Journal of Pathology *178*, 2367–2376.

Bachmair, A., Finley, D., and Varshavsky, A. (1986). In vivo half-life of a protein is a function of its amino-terminal residue. Science *234*, 179–186.

Bakkenist, C.J., and Kastan, M.B. (2004). Initiating Cellular Stress Responses. Cell *118*, 9–17.

Baretti, M., and Le, D.T. (2018). DNA mismatch repair in cancer. Pharmacology & Therapeutics *189*, 45–62.

Bebenek, K., Pedersen, L.C., and Kunkel, T.A. (2014). Structure–Function Studies of DNA Polymerase λ. Biochemistry *53*, 2781–2792.

Bjornson, K.P., Blackwell, L.J., Sage, H., Baitinger, C., Allen, D., and Modrich, P. (2003). Assembly and Molecular Activities of the MutS Tetramer. J. Biol. Chem. *278*, 34667–34673.

Blunt, T., Finnie, N.J., Taccioli, G.E., Smith, G.C.M., Demengeot, J., Gottlieb, T.M., Mizuta, R., Varghese, A.J., Alt, F.W., Jeggo, P.A., et al. (1995). Defective DNA-dependent protein kinase activity is linked to V(D)J recombination and DNA repair defects associated with the murine scid mutation. Cell *80*, 813–823.

Bossis, G., and Melchior, F. (2006). Regulation of SUMOylation by Reversible Oxidation of SUMO Conjugating Enzymes. Molecular Cell *21*, 349–357.

Buisson, R., and Masson, J.-Y. (2012). PALB2 self-interaction controls homologous recombination. Nucleic Acids Research *40*, 10312–10323.

Buisson, R., Dion-Côté, A.-M., Coulombe, Y., Launay, H., Cai, H., Stasiak, A.Z., Stasiak, A., Xia, B., and Masson, J.-Y. (2010). Cooperation of breast cancer proteins PALB2 and piccolo BRCA2 in stimulating homologous recombination. Nat Struct Mol Biol *17*, 1247–1254.

Buisson, R., Niraj, J., Pauty, J., Maity, R., Zhao, W., Coulombe, Y., Sung, P., and Masson, J.-Y. (2014). Breast Cancer Proteins PALB2 and BRCA2 Stimulate Polymerase η in Recombination-Associated DNA Synthesis at Blocked Replication Forks. CellReports *6*, 553–564.

Bunting, S.F., CallEn, E., Wong, N., Chen, H.-T., Polato, F., Gunn, A., Bothmer, A., Feldhahn, N., Fernandez-Capetillo, O., Cao, L., et al. (2010). 53BP1 Inhibits Homologous Recombination in Brca1-Deficient Cells by Blocking Resection of DNA Breaks. Cell *141*, 243–254.

Cannavo, E., and Cejka, P. (2014). Sae2 promotes dsDNA endonuclease activity within Mre11–Rad50–Xrs2 to resect DNA breaks. Nature *514*, 122–125.

Chang, H.H.Y., Pannunzio, N.R., Adachi, N., and Lieber, M.R. (2017). Non-homologous DNA end joining and alternative pathways to double-strand break repair. Nature Publishing Group *18*, 495–506.

Chang, H.H.Y., Watanabe, G., Gerodimos, C.A., Ochi, T., Blundell, T.L., Jackson, S.P., and Lieber, M.R. (2016). Different DNA End Configurations Dictate Which NHEJ Components Are Most Important for Joining Efficiency. J. Biol. Chem. *291*, 24377–24389.

Chen P.L, Chen C.F, Chen Y.M, Xiao J, Sharp Z.D, Lee W.H. (1998). The BRC repeats in Brca2 are critical for Rad51 binding and resistance to methyl methanesulfonate treatment.*Proc. Natl. Acad. Sci. USA*; 95 (b): 5287-5292

Chen, S.-J., and Jiaang, W.-T. (2011). Current Advances and Therapeutic Potential of Agents Targeting Dipeptidyl Peptidases-IV, -II, 8/9 and Fibroblast Activation Protein. Current Topics in Medicinal Chemistry *11*, 1447–1463.

Chen, S.-J., Wu, X., Wadas, B., Oh, J.-H., and Varshavsky, A. (2017). An N-end rule pathway that recognizes proline and destroys gluconeogenic enzymes. Science *355*, eaal3655.

Chio, I.I.C., and Tuveson, D.A. (2017). ROS in Cancer: The Burning Question. Trends in Molecular Medicine *23*, 411–429.

Choi, H.J., Kim, J.Y., Lim, S.-C., Kim, G., Yun, H.J., and Choi, H.S. (2015). Dipeptidyl peptidase 4 promotes epithelial cell transformation and breast tumourigenesis via induction of PIN1 gene expression. British Journal of Pharmacology *172*, 5096–5109.

Chowdhury, S., Chen, Y., Yao, T.-W., Ajami, K., Wang, X.M., Popov, Y., Schuppan, D., Bertolino, P., McCaughan, G.W., Yu, D.M., et al. (2013). Regulation of dipeptidyl peptidase 8 and 9 expression in activated lymphocytes and injured liver. World Journal of Gastroenterology *19*, 2883–2893.

Cimprich, K.A., Shin, T.B., Keith, C.T., and Schreiber, S.L. (1996). cDNA cloning and gene mapping of a candidate human cell cycle checkpoint protein. Proc Natl Acad Sci USA *93*, 2850–2855.

Couch, G.M.M.R.L.G.J.W.V.P.F., Rowley, M., Guidugli, L., Wu, J., Pankratz, V.S., and Couch, F.J. (2012). BRCA2 Localization to the Midbody by Filamin A Regulates CEP55 Signaling and Completion of Cytokinesis. Developmental Cell *23*, 137–152.

Dove, K.K., and Klevit, R.E. (2017). RING-Between-RING E3 Ligases: Emerging Themes amid the Variations. Journal of Molecular Biology *429*, 3363–3375.

Economopoulou, P., Dimitriadis, G., and Psyrri, A. (2014). Beyond BRCA: New hereditary breast cancer susceptibility genes. Cancer Treatment Reviews 1–8.

Eggler, A.L., Inman, R.B., and Cox, M.M. (2002). The Rad51-dependent Pairing of Long DNA Substrates Is Stabilized by Replication Protein A. J. Biol. Chem. *277*, 39280–39288.

Esashi, F., Christ, N., Gannon, J., Liu, Y., Hunt, T., Jasin, M., and West, S.C. (2005). CDK-dependent phosphorylation of BRCA2 as a regulatory mechanism for recombinational repair. Nature *434*, 598–604.

Feeney, L., Muñoz, I.M., Lachaud, C., Toth, R., Appleton, P.L., Schindler, D., and Rouse, J. (2017). RPA-Mediated Recruitment of the E3 Ligase RFWD3 Is Vital for Interstrand Crosslink Repair and Human Health. Molecular Cell *66*, 610–621.e614.

Fernandez-Capetillo, O., Lee, A., Nussenzweig, M., and Nussenzweig, A. (2004). H2AX: the histone guardian of the genome. DNA Repair *3*, 959–967.

FISCHER, A. (1946). Mechanism of the Proteolytic Activity of Malignant Tissue Cells. Nature *157*, 442–442.

Flotho, A., and Melchior, F. (2013). Sumoylation: A Regulatory Protein Modification in Health and Disease. Annu. Rev. Biochem. *82*, 357–385.

Foo, T.K., Tischkowitz, M., Simhadri, S., Boshari, T., Zayed, N., Burke, K.A., Berman, S.H., Blecua, P., Riaz, N., Huo, Y., et al. (2017). Compromised BRCA1–PALB2 interaction is associated with breast cancer risk. Nature Publishing Group *36*, 4161–4170.

Fradet-Turcotte, A., Canny, M.D., Escribano-Díaz, C., Orthwein, A., Leung, C.C.Y., Huang, H., Landry, M.-C., Kitevski-LeBlanc, J., Noordermeer, S.M., Sicheri, F., et al. (2013). 53BP1 is a reader of the DNA-damage-induced H2A Lys 15 ubiquitin mark. Nature *499*, 50–54.

Frerker, N., Wagner, L., Wolf, R., Heiser, U., Hoffmann, T., Rahfeld, J.-U., Schade, J., Karl, T., Naim, H.Y., Alfalah, M., et al. (2007). Neuropeptide Y (NPY) cleaving enzymes: Structural and functional homologues of dipeptidyl peptidase 4. Peptides *28*, 257–268.

Gall, M.G., and Gorrell, M.D. (2017). The Multifunctional Post-proline Dipeptidyl Peptidase, DPP9, in Mice, Cell Biology and Immunity. In Pathophysiological Aspects of Proteases, (Singapore: Springer Singapore), pp. 23–45.

Gall, M.G., Chen, Y., Vieira de Ribeiro, A.J., Zhang, H., Bailey, C.G., Spielman, D.S., Yu, D.M.T., and Gorrell, M.D. (2013). Targeted Inactivation of Dipeptidyl Peptidase 9 Enzymatic Activity Causes Mouse Neonate Lethality. PLoS ONE *8*, e78378–10.

Gallmeier, E., and Kern, S.E. (2007). Targeting Fanconi Anemia/BRCA2 Pathway Defects in Cancer: The Significance of Preclinical Pharmacogenomic Models. Clinical Cancer Research *13*, 4–10.

Geiss-Friedlander, R., and Melchior, F. (2007). Concepts in sumoylation: a decade on. Nature Reviews Molecular Cell Biology *8*, 947–956.

Geiss-Friedlander, R., Parmentier, N., Möller, U., Urlaub, H., Van den Eynde, B.J., and Melchior, F. (2009). The Cytoplasmic Peptidase DPP9 Is Rate-limiting for Degradation of Proline-containing Peptides. J. Biol. Chem. *284*, 27211–27219.

Gilberto, S., and Peter, M. (2017). Dynamic ubiquitin signaling in cell cycle regulation. J Cell Biol *216*, 2259–2271.

Goldberg, M., Stucki, M., Falck, J., D'Amours, D., Rahman, D., Pappin, D., Bartek, J., and Jackson, S.P. (2003). MDC1 is required for the intra-S-phase DNA damage checkpoint. Nature *421*, 952–956.

Gorrell, M.D. (2005). Dipeptidyl peptidase IV and related enzymes in cell biology and liver disorders. Clinical Science *108*, 277–292.

Gravel, S., Chapman, J.R., Magill, C., and Jackson, S.P. (2008). DNA helicases Sgs1 and BLM promote DNA double-strand break resection. Genes & Development *22*, 2767–2772.

Gumeni, S., Evangelakou, Z., Gorgoulis, V., and Trougakos, I. (2017). Proteome Stability as a Key Factor of Genome Integrity. Ijms *18*, 2036–26.

Halliwell, B., Clement, M.V., and Long, L.H. (2000). Hydrogen peroxide in the human body. FEBS Letters *486*, 10–13.

Han, J., Ruan, C., Huen, M.S.Y., Wang, J., Xie, A., Fu, C., Liu, T., and Huang, J. (2017). BRCA2 antagonizes classical and alternative nonhomologous end-joining to prevent gross genomic instability. Nature Communications *8*, 1071.

Han, R., Wang, X., Bachovchin, W., Zukowska, Z., and Osborn, J.W. (2015). Inhibition of dipeptidyl peptidase 8/9 impairs preadipocyte differentiation. Scientific Reports *5*, 1138.

Hoege, C., Pfander, B., Moldovan, G.-L., Pyrowolakis, G., and Jentsch, S. (2002). RAD6-dependent DNA repair is linked to modification of PCNA by ubiquitin and SUMO. Nature *419*, 135–141.

Hu, L.-Y., Chang, C.-C., Huang, Y.-S., Chou, W.-C., Lin, Y.-M., Ho, C.-C., Chen, W.-T., Shih, H.-M., Hsiung, C.-N., Wu, P.-E., et al. (2018). SUMOylation of XRCC1 activated by poly (ADP-ribosyl)ation regulates DNA repair. Human Molecular Genetics *27*, 2306–2317.

Huertas, P., Cortés-Ledesma, F., Sartori, A.A., Aguilera, A., and Jackson, S.P. (2008). CDK targets Sae2 to control DNA-end resection and homologous recombination. Nature *455*, 689–692.

Hughes-Davies, L., Huntsman, D., Ruas, M., Fuks, F., Bye, J., Chin, S.-F., Milner, J., Brown, L.A., Hsu, F., Gilks, B., et al. (2003). EMSY Links the BRCA2 Pathway to Sporadic Breast and Ovarian Cancer. Cell *115*, 523–535.

Inano, S., Sato, K., Katsuki, Y., Kobayashi, W., Tanaka, H., Nakajima, K., Nakada, S., Miyoshi, H., Knies, K., Takaori-Kondo, A., et al. (2017). RFWD3-Mediated Ubiquitination Promotes Timely Removal of Both RPA and RAD51 from DNA Damage Sites to Facilitate Homologous Recombination. Molecular Cell *66*, 622–634.e628.

Jelinic, P., Eccles, L.A., Tseng, J., Cybulska, P., Powell, S.N., and Levine, D.A. (2017). Abstract MIP-062: THE EMSY THREONINE 207 PHOSPHO–SITE IS REQUIRED FOR EMSY–DRIVEN SUPPRESSION OF DNA DAMAGE REPAIR. (American Association for Cancer Research), pp. MIP–062–MIP–062.

Jensen, R.B., Carreira, A., and Kowalczykowski, S.C. (2010). Purified human BRCA2 stimulates RAD51-mediated recombination. Nature *467*, 678–683.

Jeyasekharan, A.D., Liu, Y., Hattori, H., Pisupati, V., Jonsdottir, A.B., Rajendra, E., Lee, M., Sundaramoorthy, E., Schlachter, S., Kaminski, C.F., et al. (2013). A cancer-associated BRCA2 mutation reveals masked nuclear export signals controlling localization. Nat Struct Mol Biol *20*, 1191–1198.

Johnson, D.C., Taabazuing, C.Y., Okondo, M.C., Chui, A.J., Rao, S.D., Brown, F.C., Reed, C., Peguero, E., de Stanchina, E., Kentsis, A., et al. (2018). DPP8/DPP9 inhibitor-induced pyroptosis for treatment of acute myeloid leukemia. Nature Medicine *24*, 1151–1156

Justa-Schuch, D., Möller, U., and Geiss-Friedlander, R. (2014). The amino terminus extension in the long dipeptidyl peptidase 9 isoform contains a nuclear localization signal targeting the active peptidase to the nucleus. Cell. Mol. Life Sci. *71*, 3611–3626.

Justa-Schuch, D., Silva-Garcia, M., Pilla, E., Engelke, M., Kilisch, M., Lenz, C., Möller, U., Nakamura, F., Urlaub, H., and Geiss-Friedlander, R. (2016). DPP9 is a novel component of the N-end rule pathway targeting the tyrosine kinase Syk. eLife *5*, 14741.

Kakarougkas, A., Ismail, A., Katsuki, Y., Freire, R., Shibata, A., and Jeggo, P.A. (2013). Co-operation of BRCA1 and POH1 relieves the barriers posed by 53BP1 and RAP80 to resection. Nucleic Acids Research *41*, 10298–10311.

Kee, Y., and Huang, T.T. (2016). Role of Deubiquitinating Enzymes in DNA Repair. Molecular and Cellular Biology *36*, 524–544.

Kim, M., Minoux, M., Piaia, A., Kueng, B., Gapp, B., Weber, D., Haller, C., Barbieri, S., Namoto, K., Lorenz, T., et al. (2017). DPP9 enzyme activity controls survival of mouse migratory tongue muscle progenitors and its absence leads to neonatal lethality due to suckling defect. Developmental Biology *431*, 297–308.

Kitlinska, J., Abe, K., Kuo, L., Pons, J., Yu, M., Li, L., Tilan, J., Everhart, L., Lee, E.W., Zukowska, Z., et al. (2005). Differential Effects of Neuropeptide Y on the Growth and Vascularization of Neural Crest–Derived Tumors. Cancer Research *65*, 1719–1728.

Knies, K., Inano, S., Ramírez, M.J., Ishiai, M., Surrallés, J., Takata, M., and Schindler, D. (2017). Biallelic mutations in the ubiquitin ligase RFWD3 cause Fanconi anemia. Journal of Clinical Investigation *127*, 3013–3027.

Kragelund, B.B., Schenstrøm, S.M., Rebula, C.A., Panse, V.G., and Hartmann-Petersen, R. (2016). DSS1/Sem1, a Multifunctional and Intrinsically Disordered Protein. Trends in Biochemical Sciences *41*, 446–459.

Kunkel, T.A., and Erie, D.A. (2015). Eukaryotic Mismatch Repair in Relation to DNA Replication. Annu. Rev. Genet. *49*, 291–313.

Lankas, G.R., Leiting, B., Roy, R.S., Eiermann, G.J., Beconi, M.G., Biftu, T., Chan, C.C., Edmondson, S., Feeney, W.P., He, H., et al. (2005). Dipeptidyl Peptidase IV Inhibition for the Treatment of Type 2 Diabetes: Potential Importance of Selectivity Over Dipeptidyl Peptidases 8 and 9. Diabetes *54*, 2988–2994.

Lebedeva, N.A., Rechkunova, N.I., Dezhurov, S.V., Khodyreva, S.N., Favre, A., Blanco, L., and Lavrik, O.I. (2005). Comparison of functional properties of mammalian DNA polymerase λ and DNA polymerase β in reactions of DNA synthesis related to DNA repair. Biochimica Et Biophysica Acta (BBA) - Proteins and Proteomics *1751*, 150–158.

Levy, F., Burri, L., Morel, S., Peitrequin, A.L., Levy, N., Bachi, A., Hellman, U., Van den Eynde, B.J., and Servis, C. (2002). The Final N-Terminal Trimming of a Subaminoterminal Proline-Containing HLA Class I-Restricted Antigenic Peptide in the Cytosol Is Mediated by Two Peptidases. The Journal of Immunology *169*, 4161–4171.

Li, J., Zou, C., Bai, Y., Wazer, D.E., Band, V., and Gao, Q. (2005). DSS1 is required for the stability of BRCA2. Oncogene *25*, 1186–1194.

Li, M., Chen, D., Shiloh, A., Luo, J., Nikolaev, A.Y., Qin, J., and Gu, W. (2002). Deubiquitination of p53 by HAUSP is an important pathway for p53 stabilization. Nature *416*, 648–653.

Lieber, M.R., and Karanjawala, Z.E. (2004). Ageing, repetitive genomes and DNA damage. Nature Reviews Molecular Cell Biology *5*, 69–75.

Liu, D., Keijzers, G., and Rasmussen, L.J. (2017). DNA mismatch repair and its many roles in eukaryotic cells. Mutation Research/Reviews in Mutation Research *773*, 174–187.

Liu, Y., Beard, W.A., Shock, D.D., Prasad, R., Hou, E.W., and Wilson, S.H. (2005). DNA Polymerase β and Flap Endonuclease 1 Enzymatic Specificities Sustain DNA Synthesis for Long Patch Base Excision Repair. J. Biol. Chem. *280*, 3665–3674.

Lombardi, P.M., Matunis, M.J., and Wolberger, C. (2017). RAP80, ubiquitin and SUMO in the DNA damage response. J Mol Med *95*, 799–807..

Lord, C.J., and Ashworth, A. (2012). The DNA damage response and cancer therapy. Nature *481*, 287–294.

López-Otín, C., and Bond, J.S. (2008). Proteases: Multifunctional Enzymes in Life and Disease. J. Biol. Chem. *283*, 30433–30437.

López-Otín, C., and Matrisian, L.M. (2007). Emerging roles of proteases in tumour suppression. Nature Reviews Cancer *7*, 800–808.

Lu, C., Tilan, J.U., Everhart, L., Czarnecka, M., Soldin, S.J., Mendu, D.R., Jeha, D., Hanafy, J., Lee, C.K., Sun, J., et al. (2011). Dipeptidyl Peptidases as Survival Factors in Ewing Sarcoma Family of Tumors IMPLICATIONS FOR TUMOR BIOLOGY AND THERAPY. J. Biol. Chem. *286*, 27494–27505.

Lucas, X., and Ciulli, A. (2017). ScienceDirect Recognition of substrate degrons by E3 ubiquitin ligases and modulation by small-molecule mimicry strategies. 1–10.

Ludovic C J Gillet and and Orlando D Schärer (2006). Molecular Mechanisms of Mammalian Global Genome Nucleotide Excision Repair. 1–24.

Lupher, M.L., Jr., Rao, N., Lill, N.L., Andoniou, C.E., Miyake, S., Clark, E.A., Druker, B., and Band, H. (1998). Cbl-mediated Negative Regulation of the Syk Tyrosine Kinase. J. Biol. Chem. *273*, 35273–35281.

Magwood, A.C., Malysewich, M.J., Cealic, I., Mundia, M.M., Knapp, J., and Baker, M.D. (2013). Endogenous levels of Rad51 and Brca2 are required for homologous recombination and regulated by homeostatic re-balancing. DNA repair 12, 1122–1133.

Makvandi, M., Xu, K., Lieberman, B.P., Anderson, R.C., Effron, S.S., Winters, H.D., Zeng, C., McDonald, E.S., Pryma, D.A., Greenberg, R.A., et al. (2016). A Radiotracer Strategy to Quantify PARP-1 Expression In Vivo Provides a Biomarker That Can Enable Patient Selection for PARP Inhibitor Therapy. Cancer Research *76*, 4516–4524.

Matheeussen, V., Waumans, Y., Martinet, W., Goethem, S., Veken, P., Scharpé, S., Augustyns, K., Meyer, G.R.Y., and Meester, I. (2013). Dipeptidyl peptidases in atherosclerosis: expression and role in macrophage differentiation, activation and apoptosis. Basic Res Cardiol *108*, 6140–14.

Mimitou, E.P., and Symington, L.S. (2010). Ku prevents Exo1 and Sgs1-dependent resection of DNA ends in the absence of a functional MRX complex or Sae2. EMBO journal 29, 3358–69.

Mofers, A., Pellegrini, P., Linder, S., and D'Arcy, P. (2017). Proteasome-associated deubiquitinases and cancer. Cancer Metastasis Rev *36*, 635–653.

Moon, A.F., Pryor, J.M., Ramsden, D.A., Kunkel, T.A., Bebenek, K., and Pedersen, L.C. (2014). Sustained active site rigidity during synthesis by human DNA polymerase μ. Nat Struct Mol Biol *21*, 253–260.

Moor, N.A., and Lavrik, O.I. (2018). Protein–Protein Interactions in DNA Base Excision Repair. Biochemistry Moscow *83*, 411–422.

Morris, J.R., Boutell, C., Keppler, M., Densham, R., Weekes, D., Alamshah, A., Butler, L., Galanty, Y., Pangon, L., Kiuchi, T., et al. (2009b). The SUMO modification pathway is involved in the BRCA1 response to genotoxic stress. Nature *462*, 886–890.

Mosbech, A., Lukas, C., Bekker-Jensen, S., and Mailand, N. (2013). The Deubiquitylating Enzyme USP44 Counteracts the DNA Double-strand Break Response Mediated by the RNF8 and RNF168 Ubiquitin Ligases. J. Biol. Chem. *288*, 16579–16587.

Moudry, P., Lukas, C., Macurek, L., Hanzlikova, H., Hodny, Z., Lukas, J., and Bartek, J. (2014). Ubiquitin-activating enzyme UBA1 is required for cellular response to DNA damage. Cell Cycle *11*, 1573–1582.

Mulvihill, E.E. (2018). Dipeptidyl peptidase inhibitor therapy in type 2 diabetes: Control of the incretin axis and regulation of postprandial glucose and lipid metabolism. Peptides *100*, 158–164.

Nalepa, G., and Clapp, D.W. (2018). Fanconi anaemia and cancer: an intricate relationship. Nature reviews cancer 18, 168–185.

NEURATH, H., and WALSH, K.A. (1976). THE ROLE OF PROTEASES IN BIOLOGICAL REGULATION. In Proteolysis and Physiological Regulation, (Elsevier), pp. 29–42.

Ogi, T., and Lehmann, A.R. (2006). The Y-family DNA polymerase κ (pol κ) functions in mammalian nucleotide-excision repair. Nature Cell Biology *8*, 640–642.

Ogi, T., Limsirichaikul, S., Overmeer, R.M., Volker, M., Takenaka, K., Cloney, R., Nakazawa, Y., Niimi, A., Miki, Y., Jaspers, N.G., et al. (2010). Three DNA Polymerases, Recruited by Different Mechanisms, Carry Out NER Repair Synthesis in Human Cells. Molecular Cell *37*, 714–727.

Ojeda-Montes, M.J., Gimeno, A., Tomas-Hernández, S., Cereto-Massagué, A., Beltrán-Debón, R., Valls, C., Mulero, M., Pujadas, G., and Garcia-Vallvé, S. (2018). Activity and selectivity cliffs for DPP-IV inhibitors: Lessons we can learn from SAR studies and their application to virtual screening. Med Res Rev *31*, 1719.

Okondo, M.C., Johnson, D.C., Sridharan, R., Go, E.B., Chui, A.J., Wang, M.S., Poplawski, S.E., Wu, W., Liu, Y., Lai, J.H., et al. (2016). DPP8 and DPP9 inhibition induces pro-caspase-1-dependent monocyte and macrophage pyroptosis. Nature Chemical Biology *13*, 46–53.

Oliver, A.W., Swift, S., Lord, C.J., Ashworth, A., and Pearl, L.H. (2009). Structural basis for recruitment of BRCA2 by PALB2. EMBO Rep. *10*, 990–996.

Olsen, C., and Wagtmann, N. (2002). Identification and characterization of human DPP9 , a novel homologue of dipeptidyl peptidase IV. Gene *299*, 185–193.

Orthwein, A., Noordermeer, S.M., Wilson, M.D., Landry, S., Enchev, R.I., Sherker, A., Munro, M., Pinder, J., Salsman, J., Dellaire, G., et al. (2015). A mechanism for the suppression of homologous recombination in G1 cells. Nature *528*, 422–426.

Park, J., Knott, H.M., Nadvi, N.A., Collyer, C.A., Wang, X.M., Church, W.B., and Gorrell, M.D. (2008). Reversible Inactivation of Human Dipeptidyl Peptidases 8 and 9 by Oxidation. The Open Enzyme Inhibition Journal *1*, 52–60.

Park, S.E., Kim, J.M., Seok, O.H., Cho, H., Wadas, B., Kim, S.Y., Varshavsky, A., and Hwang, C.S. (2015). Control of mammalian G protein signaling by N-terminal acetylation and the N-end rule pathway. Science *347*, 1249–1252.

Parsons, J.L., Dianova, I.I., Finch, D., Tait, P.S., m, C.E.S., Helleday, T., and Dianov, G.L. (2010). XRCC1 phosphorylation by CK2 is required for its stability and efficient DNA repair. DNA Repair *9*, 835–841.

Parsons, J.L., Tait, P.S., Finch, D., Dianova, I.I., Allinson, S.L., and Dianov, G.L. (2008). CHIP-Mediated Degradation and DNA Damage-Dependent Stabilization Regulate Base Excision Repair Proteins. Molecular Cell *29*, 477–487.

Petrovic, N., Davidovic, R., Bajic, V., Obradovic, M., and Isenovic, R.E. (2017). MicroRNA in breast cancer: The association with BRCA1/2. Cbm *19*, 119–128.

Pilla, E., Kilisch, M., Lenz, C., Urlaub, H., and Geiss-Friedlander, R. (2013). The SUMO1-E67 Interacting Loop Peptide Is an Allosteric Inhibitor of the Dipeptidyl Peptidases 8 and 9. J. Biol. Chem. *288*, 32787–32796.

Pilla, E., Möller, U., Sauer, G., Mattiroli, F., Melchior, F., and Geiss-Friedlander, R. (2012). A Novel SUMO1-specific Interacting Motif in Dipeptidyl Peptidase 9 (DPP9) That Is Important for Enzymatic Regulation. J. Biol. Chem. *287*, 44320–44329.

Rajagopalan, S., Andreeva, A., Rutherford, T.J., and Fersht, A.R. (2010). Mapping the physical and functional interactions between the tumor suppressors p53 and BRCA2. Proc Natl Acad Sci USA *107*, 8587–8592.

Ramsden, D.A. (1998). Ku protein stimulates DNA end joining by mammalian DNA ligases: a direct role for Ku in repair of DNA double-strand breaks. The EMBO Journal *17*, 609–614.

Ranjha, L., Howard, S.M., and Cejka, P. (2018). Main steps in DNA double-strand break repair: an introduction to homologous recombination and related processes. Chromosoma *127*, 187–214.

Rawlings, N.D., Barrett, A.J., Thomas, P.D., Huang, X., Bateman, A., and Finn, R.D. (2017). The MEROPS database of proteolytic enzymes, their substrates and inhibitors in 2017 and a comparison with peptidases in the PANTHER database. Nucleic Acids Research *46*, D624–D632.

Reinhold, D., Goihl, A., Wrenger, S., Reinhold, A., Kühlmann, U.C., Faust, J., Neubert, K., Thielitz, A., Brocke, S., Täger, M., et al. (2009). Role of dipeptidyl peptidase IV (DP IV)-like enzymes in T lymphocyte activation: investigations in DP IV/CD26-knockout mice. Clinical Chemistry and Laboratory Medicine *47*, 3.

Renkawitz, J., Lademann, C.A., and Jentsch, S. (2014). Mechanisms and principles of homology search during recombination. Nature Reviews Molecular Cell Biology *15*, 369–383.

Rogakou, E.P., Pilch, D.R., Orr, A.H., Ivanova, V.S., and Bonner, W.M. (1998). DNA Double-stranded Breaks Induce Histone H2AX Phosphorylation on Serine 139. J. Biol. Chem. *273*, 5858–5868.

Ross, B., Krapp, S., Augustin, M., Kierfersauer, R., Arciniega, M., Geiss-Friedlander, R., and Huber, R. (2018). Structures and mechanism of dipeptidyl peptidases 8 and 9, important players in cellular homeostasis and cancer. Proc Natl Acad Sci USA *115*, E1437–E1445.

San Filippo, J., Sung, P., and Klein, H. (2008). Mechanism of Eukaryotic Homologous Recombination. Annu. Rev. Biochem. *77*, 229–257.

Savitsky, K., Bar-Shira, A., Gilad, S., Rotman, G., Ziv, Y., Vanagaite, L., Tagle, D., Smith, S., Uziel, T., Sfez, S., et al. (1995). A single ataxia telangiectasia gene with a product similar to PI-3 kinase. Science *268*, 1749–1753.

Schade, J., Stephan, M., Schmiedl, A., Wagner, L., Niestroj, A.J., Demuth, H.-U., Frerker, N., Klemann, C., Raber, K.A., Pabst, R., et al. (2007). Regulation of Expression and Function of Dipeptidyl Peptidase 4 (DP4), DP8/9, and DP10 in Allergic Responses of the Lung in Rats. J Histochem Cytochem. *56*, 147–155.

Schoenfeld, A.R., Apgar, S., Dolios, G., Wang, R., and Aaronson, S.A. (2004). BRCA2 Is Ubiquitinated In Vivo and Interacts with USP11, a Deubiquitinating Enzyme That Exhibits Prosurvival Function in the Cellular Response to DNA Damage. Molecular and Cellular Biology *24*, 7444–7455.

Shao, Q.-Q., Zhang, T.-P., Zhao, W.-J., Liu, Z.-W., You, L., Zhou, L., Guo, J.-C., and Zhao, Y.-P. (2015). Filamin A: Insights into its Exact Role in Cancers. Pathol. Oncol. Res. *22*, 245–252.

Shiloh, Y., and Ziv, Y. (2013). The ATM protein kinase: regulating the cellular response to genotoxic stress, and more. Nature Publishing Group *14*, 197–210.

Shin, S., and Verma, I.M. (2003). BRCA2 cooperates with histone acetyltransferases in androgen receptor-mediated transcription. Proc Natl Acad Sci USA *100*, 7201–7206.

Shrivastav, M., De Haro, L.P., and Nickoloff, J.A. (2007). Regulation of DNA double-strand break repair pathway choice. Cell Res *18*, 134–147.

Sigurdsson, S. (2001). Mediator function of the human Rad51B-Rad51C complex in Rad51/RPA-catalyzed DNA strand exchange. Genes & Development *15*, 3308–3318.

Smebye, M.L., Agostini, A., Johannessen, B., Thorsen, J., Davidson, B., Tropé, C.G., Heim, S., Skotheim, R.I., and Micci, F. (2017). Involvement of DPP9 in gene fusions in serous ovarian carcinoma. BMC Cancer *17*, 668.

Spagnuolo, P.A., Hurren, R., Gronda, M., MacLean, N., Datti, A., Basheer, A., Lin, F.-H., Wang, X., Wrana, J., and Schimmer, A.D. (2013). Inhibition of intracellular dipeptidyl peptidases 8 and 9 enhances parthenolide's anti-leukemic activity. Leukemia *27*, 1236–1244.

Srivastava, N., and Raman, M.J. (2006). Homologous recombination-mediated double-strand break repair in mouse testicular extracts and comparison with different germ cell stages. Cell Biochemistry and Function *25*, 75–86.

Summers, K.C., Shen, F., Sierra Potchanant, E.A., Phipps, E.A., Hickey, R.J., and Malkas, L.H. (2011). Phosphorylation: The Molecular Switch of Double-Strand Break Repair. International Journal of Proteomics *2011*, 1–8.

Tanaka, S., Murakami, T., Horikawa, H., Sugiura, M., Kawashima, K., and Sugita, T. (1997). Suppression of arthritis by the inhibitors of dipeptidyl peptidase IV. International Journal of Immunopharmacology *19*, 15–24.

Tang, H.-K., Tang, H.-Y., Hsu, S.-C., Chu, Y.-R., Chien, C.-H., Shu, C.-H., and Chen, X. (2009). Biochemical properties and expression profile of human prolyl dipeptidase DPP9. Archives of Biochemistry and Biophysics *485*, 120–127.

Tang, Z., Li, J., Shen, Q., Feng, J., Liu, H., Wang, W., Xu, L., Shi, G., Ye, X., Ge, M., et al. (2017). Contribution of upregulated dipeptidyl peptidase 9 (DPP9) in promoting tumoregenicity, metastasis and the prediction of poor prognosis in non-small cell lung cancer (NSCLC). Int. J. Cancer *140*, 1620–1632.

Telli, M.L., Stover, D.G., Loi, S., Aparicio, S., Carey, L.A., Domchek, S.M., Newman, L., Sledge, G.W., and Winer, E.P. (2018). Homologous recombination deficiency and host anti-tumor immunity in triple-negative breast cancer. Breast Cancer Res Treat *7*, 683–11.

Tinoco, A.D., Tagore, D.M., and Saghatelian, A. (2010). Expanding the Dipeptidyl Peptidase 4-Regulated Peptidome via an Optimized Peptidomics Platform. J. Am. Chem. Soc. *132*, 3819–3830.

Tkáč, J., Xu, G., Adhikary, H., Young, J.T.F., Gallo, D., Escribano-Díaz, C., Krietsch, J., Orthwein, A., Munro, M., Sol, W., et al. (2016). HELB Is a Feedback Inhibitor of DNA End Resection. Molecular Cell *61*, 405–418.

Turinetto, V., and Giachino, C. (2015a). Multiple facets of histone variant H2AX: a DNA double-strand-break marker with several biological functions. Nucleic Acids Research *43*, 2489–2498.

Turinetto, V., and Giachino, C. (2015b). Histone variants as emerging regulators of embryonic stem cell identity. Epigenetics *10*, 563–573.

Turk, B. (2006). Targeting proteases: successes, failures and future prospects. Nat Rev Drug Discov *5*, 785–799.

Typas, D., Luijsterburg, M.S., Wiegant, W.W., Diakatou, M., Helfricht, A., Thijssen, P.E., van den Broek, B., Mullenders, L.H., and van Attikum, H. (2016). The de-ubiquitylating enzymes USP26 and USP37 regulate homologous recombination by counteracting RAP80. Nucleic Acids Research *44*, 2976–2976.

Varshavsky, A. (1991). Naming a targeting signal. Cell *64*, 13–15.

Varshavsky, A. (1997). The N-end rule pathway of protein degradation. Genes to Cells *2*, 13–28.

Varshavsky, A. (2011). The N-end rule pathway and regulation by proteolysis. Protein Science *20*, 1298–1345.

Wang, B., and Elledge, S.J. (2007). Ubc13/Rnf8 ubiquitin ligases control foci formation of the Rap80/Abraxas/Brca1/Brcc36 complex in response to DNA damage. Proc Natl Acad Sci USA *104*, 20759–20763.

Waters, L.S., Minesinger, B.K., Wiltrout, M.E., D'Souza, S., Woodruff, R.V., and Walker, G.C. (2009). Eukaryotic Translesion Polymerases and Their Roles and Regulation in DNA Damage Tolerance. Microbiology and Molecular Biology Reviews *73*, 134–154.

Waumans, Y., Baerts, L., Kehoe, K., Lambeir, A.-M., and De Meester, I. (2015). The Dipeptidyl Peptidase Family, Prolyl Oligopeptidase, and Prolyl Carboxypeptidase in the Immune System and Inflammatory Disease, Including Atherosclerosis. Frontiers in Immunology *6*, 1786.

Wei, L., Nakajima, S., Hsieh, C.L., Kanno, S., Masutani, M., Levine, A.S., Yasui, A., and Lan, L. (2013). Damage response of XRCC1 at sites of DNA single strand breaks is regulated by phosphorylation and ubiquitylation after degradation of poly(ADP-ribose). Journal of Cell Science *126*, 4414–4423.

Weterings, E., and Chen, D.J. (2007). DNA-dependent protein kinase in nonhomologous end joining: a lock with multiple keys? J Cell Biol *179*, 183–186.

Wilson, C.H., Indarto, D., Doucet, A., Pogson, L.D., Pitman, M.R., McNicholas, K., Menz, R.I., Overall, C.M., and Abbott, C.A. (2013). Identifying Natural Substrates for Dipeptidyl Peptidases 8 and 9 Using Terminal Amine Isotopic Labeling of Substrates (TAILS) Reveals in VivoRoles in Cellular Homeostasis and Energy Metabolism. J. Biol. Chem. *288*, 13936–13949.

Wood, R. (1997). Which DNA polymerases are used for DNA-repair in eukaryotes? Carcinogenesis *18*, 605–610.

Wu, H., Wu, X., and Liang, Z. (2017). Impact of germline and somatic BRCA1/2 mutations: tumor spectrum and detection platforms. Gene Therapy *24*, 601–609.

Wu, J.-J., Tang, H.-K., Yeh, T.-K., Chen, C.-M., Shy, H.-S., Chu, Y.-R., Chien, C.-H., Tsai, T.-Y., Huang, Y.-C., Huang, Y.-L., et al. (2009). Biochemistry, pharmacokinetics, and toxicology of a potent and selective DPP8/9 inhibitor. Biochemical Pharmacology *78*, 203–210.

Xia, B., Sheng, Q., Nakanishi, K., Ohashi, A., Wu, J., Christ, N., Liu, X., Jasin, M., Couch, F.J., and Livingston, D.M. (2006). Control of BRCA2 Cellular and Clinical Functions by a Nuclear Partner, PALB2. Molecular Cell *22*, 719–729.

Xu, Y., Bismar, T.A., Su, J., Xu, B., Kristiansen, G., Varga, Z., Teng, L., Ingber, D.E., Mammoto, A., Kumar, R., et al. (2010). Filamin A regulates focal adhesion disassembly and suppresses breast cancer cell migration and invasion. The Journal of Experimental Medicine *207*, 2421–2437.

Yamamoto, H., and Imai, K. (2015). Microsatellite instability: an update. Archives of Toxicology *89*, 899–921.

Yang, H. (2002). BRCA2 Function in DNA Binding and Recombination from a BRCA2-DSS1-ssDNA Structure. Science *297*, 1837–1848.

Yao, T.W., Kim, W.S., Yu, D.M., Sharbeen, G., McCaughan, G.W., Choi, K.Y., Xia, P., and Gorrell, M.D. (2011). A Novel Role of Dipeptidyl Peptidase 9 in Epidermal Growth Factor Signaling. Molecular Cancer Research *9*, 948–959.

Yata, K., Bleuyard, J.-Y., Nakato, R., Ralf, C., Katou, Y., Schwab, R.A., Niedzwiedz, W., Shirahige, K., and Esashi, F. (2014). BRCA2 Coordinates the Activities of Cell-Cycle Kinases to Promote Genome Stability. Cell Reports *7*, 1547–1559.

Yata, K., Lloyd, J., Maslen, S., Bleuyard, J.-Y., Skehel, M., Smerdon, S.J., and Esashi, F. (2012). Plk1 and CK2 Act in Concert to Regulate Rad51 during DNA Double Strand Break Repair. Molecular Cell *45*, 371–383.

Yu, D.M.T., Ajami, K., Gall, M.G., Park, J., Lee, C.S., Evans, K.A., McLaughlin, E.A., Pitman, M.R., Abbott, C.A., McCaughan, G.W., et al. (2009). The In Vivo Expression of Dipeptidyl Peptidases 8 and 9. J Histochem Cytochem. *57*, 1025–1040.

Yu, D.M.T., Wang, X.M., McCaughan, G.W., and Gorrell, M.D. (2006). Extraenzymatic functions of the dipeptidyl peptidase IV-related proteins DP8 and DP9 in cell adhesion, migration and apoptosis. FEBS Journal *273*, 2447–2460.

Yu, D.M.T., Yao, T.-W., Chowdhury, S., Nadvi, N.A., Osborne, B., Church, W.B., McCaughan, G.W., and Gorrell, M.D. (2010). The dipeptidyl peptidase IV family in cancer and cell biology. FEBS Journal *277*, 1126–1144.

Yuan, Y., and Shen, Z. (2001). Interaction with BRCA2 Suggests a Role for Filamin-1 (hsFLNa) in DNA Damage Response. J. Biol. Chem. *276*, 48318–48324.

Yue, J., Wang, Q., Lu, H., Brenneman, M., Fan, F., and Shen, Z. (2009). The Cytoskeleton Protein Filamin-A Is Required for an Efficient Recombinational DNA Double Strand Break Repair. Cancer Research *69*, 7978–7985.

Yue, J., Lu, H., Liu, J., Berwick, M., and Shen, Z. (2012). Filamin-A as a marker and target for DNA damage based cancer therapy. DNA Repair *11*, 192–200.

Zapletal, E., Cupic, B., and Gabrilovac, J. (2017). Expression, subcellular localisation, and possible roles of dipeptidyl peptidase 9 (DPP9) in murine macrophages. Cell Biochemistry and Function *35*, 124–137.

Zhang, F., Fan, Q., Ren, K., and Andreassen, P.R. (2009). PALB2 Functionally Connects the Breast Cancer Susceptibility Proteins BRCA1 and BRCA2. Molecular Cancer Research *7*, 1110–1118.

Zhang, H., Chen, Y., Wadham, C., McCaughan, G.W., Keane, F.M., and Gorrell, M.D. (2015). Dipeptidyl peptidase 9 subcellular localization and a role in cell adhesion involving focal adhesion kinase and paxillin. Biochimica Et Biophysica Acta (BBA) - Molecular Cell Research *1853*, 470–480.

Zhang, H., Maqsudi, S., Rainczuk, A., Duffield, N., Lawrence, J., Keane, F.M., Justa-Schuch, D., Geiss-Friedlander, R., Gorrell, M.D., and Stephens, A.N. (2015). Identification of novel dipeptidyl peptidase 9 substrates by two-dimensional differential in-gel electrophoresis. Febs J *282*, 3737–3757

Zhao, W., Vaithiyalingam, S., Filippo, J.S., Maranon, D.G., Jimenez-Sainz, J., Fontenay, G.V., Kwon, Y., Leung, S.G., Lu, L., Jensen, R.B., et al. (2015). Promotion of BRCA2-Dependent Homologous Recombination by DSS1 via RPA Targeting and DNA Mimicry. Molecular Cell *59*, 176–187.

Zhong, F.L., Robinson, K., Lim, C., Harapas, C.R., Yu, C.-H., Xie, W., Sobota, R.M., Au, V.B., Hopkins, R., Connolly, J.E., et al. (2018). DPP9 is an endogenous and direct inhibitor of the NLRP1 inflammasome that guards against human auto-inflammatory diseases. bioRxiv 260919.

Zhu, Z., Chung, W.-H., Shim, E.Y., Lee, S.E., and Ira, G. (2008). Sgs1 Helicase and Two Nucleases Dna2 and Exo1 Resect DNA Double-Strand Break Ends. Cell *134*, 981–994.

Zimmer, J., Tacconi, E.M.C., Folio, C., Badie, S., Porru, M., Klare, K., Tumiati, M., Markkanen, E., Halder, S., Ryan, A., et al. (2016). Targeting BRCA1 and BRCA2 Deficiencies with G-Quadruplex-Interacting Compounds. Molecular Cell *61*, 449–460.